Acta Numerica (2022), pp. 415–489 Printed in the United Kingdom
doi:10.1017/S0962492922000010

Asymptotic-preserving schemes for multiscale physical problems

Shi Jin*
School of Mathematical Sciences, Institute of Natural Sciences and MOE-LSC, Shanghai Jiao Tong University, Shanghai 200240, China
E-mail: shijin-m@sjtu.edu.cn

We present the asymptotic transitions from microscopic to macroscopic physics, their computational challenges and the asymptotic-preserving (AP) strategies to compute multiscale physical problems efficiently. Specifically, we will first study the asymptotic transition from quantum to classical mechanics, from classical mechanics to kinetic theory, and then from kinetic theory to hydrodynamics. We then review some representative AP schemes that mimic these asymptotic transitions at the discrete level, and hence can be used crossing scales and, in particular, capture the macroscopic behaviour without resolving the microscopic physical scale numerically.

CONTENTS

* S. Jin was partially supported by National Key R&D Program of China Project no. 2020YFA0712000, NSFC grant no. 12031013, Strategic Priority Research Program of Chinese Academy of Sciences XDA25010401, and Shanghai Municipal Science and Technology Major Project 2021SHZDZX0102.

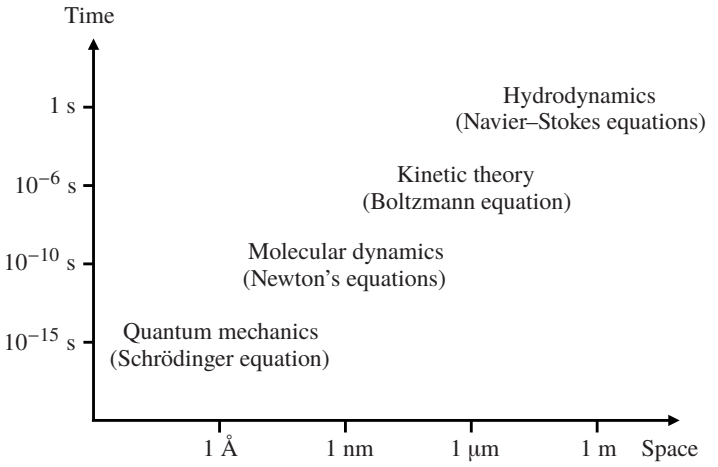

Figure 1.1. Multiscale diagram.

1. Introduction

Ignoring relativistic effects, quantum mechanics is considered to be enough for us to understand the physical properties of matter. Since solving the Schrödinger equation analytically is impossible, we rely upon computer simulations to solve the equation. However, there are essential computational bottlenecks in simulation at the quantum level. First is the curse of dimensionality. For common molecules such as carbon dioxide CO_2, which consists of 3 nuclei and 22 electrons, the full time-dependent Schrödinger equation is defined in 75 space dimensions! The benzene molecule consists of 12 nuclei and 42 electrons, so we need to solve the Schrödinger equation in 162 dimensions. Another challenge is that quantum mechanics is valid at spatial scales of Angstroms, *i.e.* 10^{-10} m, and time scales of femtoseconds, *i.e.* 10^{-15} s. To simulate such a small-scale system on any physical scales of interest, *e.g.* micrometres to millimetres or microseconds to milliseconds, is computationally formidable for today's computers.

Physical models at larger scales, such as classical mechanics, statistical mechanics and hydrodynamics, are computationally much less expensive compared to a quantum simulation, but they are valid in certain time and spatial scales; see Figure 1.1. When we deal with problems that go across different scales, either due to the nature of the problems or computational needs, multiscale computation becomes a viable tool when we cannot afford to resolve the smallest scales.

Understanding transitions from one scale to another is a central topic in mathematical physics and partial differential equations. This is related to Hilbert's sixth problem (Corry 2004). These asymptotic transitions are not only of great mathematical interest: they also guide the design of multiscale computational methods, as will be reflected in this survey.

https://doi.org/10.1017/S0962492922000010 Published online by Cambridge University Press

If the asymptotic or macroscopic equations are uniformly valid in the entire domain of interest, it is much more efficient just to solve the problem at the macroscopic level, which is computationally more economical. However, there are many problems where the macroscopic models break down in part of the domain, or we lack information or data on the macro models, so microscopic models are needed, at least locally. Therefore a multiscale and multiphysics approach becomes necessary, for example by hybridizing the microscopic and the macroscopic models in a domain-decomposition or heterogeneous multiscale framework; see *e.g.* Bourgat, Le Tallec, Perthame and Qiu (1994), Klar, Neunzert and Struckmeier (2000) and Degond, Jin and Mieussens (2005) for multiscale kinetic problems, and E and Engquist (2003), Abdulle, E, Engquist and Vanden-Eijnden (2012) and Kevrekidis, Gear and Hummer (2004) for broader areas of multiscale modelling and simulation.

Central to the design of multiscale computational methods is to identify the critical physical scales in the system and the connections between microscopic and macroscopic models. The Schrödinger equation is valid at the Angstrom scale, which is exceedingly small compared to the scale of interest. The Newton equations in classical mechanics often involve a number of particles that is simply too large. Kinetic equations often contain small mean-free paths or times, or the Knudsen number, the average distance or time between two collisions of particles. When the characteristic scales become small, tremendous computational challenges arise since we need to resolve these small scales numerically, which can be prohibitively expensive. A main difficulty in most multiscale and multiphysics methods is that we have to couple models at different scales via an interface or buffer zone where we have to match two different models. While it is often easy to generate macroscopic data from microscopic data via ensemble averages or taking moments, for example, it is difficult to convert macroscopic data to microscopic data, since most of the time this conversion is not unique. The coupling locations may also be difficult to determine in a dynamic problem.

On the other hand, asymptotic expansions on these small parameters for a microscopic model usually give rise to the macroscopic equations. We hope such a transition can not only guide the design of effective and efficient multiscale computational methods but also help to analyse them.

This paper surveys one multiscale framework: the *asymptotic-preserving (AP) schemes*. This approach has its origin in capturing steady-state solutions for neutron transport in the diffusive regime (Larsen, Morel and Miller Jr 1987, Larsen and Morel 1989). Since the 1990s, AP schemes have been developed for a wide range of time-dependent kinetic and hyperbolic equations, and far beyond. The basic idea is to develop numerical methods that *preserve the asymptotic limits from the microscopic to the macroscopic models, in the discrete setting*. Comparing with multiphysics domain decomposition methods, AP schemes solve one set of equations – the microscopic ones – and thus avoid the coupling of different models. An AP scheme switches from a microscopic solver to the macroscopic solver *automatically*. Specifically, if we resolve the small physical scales numerically,

https://doi.org/10.1017/S0962492922000010 Published online by Cambridge University Press

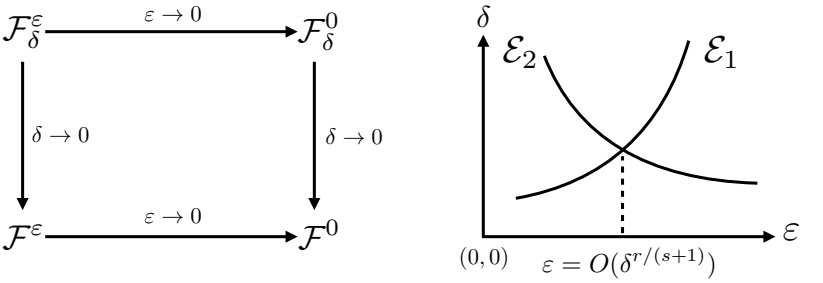

(a) (b)

Figure 1.2. Illustration of (a) AP schemes, (b) uniform convergence of AP schemes.

then the scheme is a micro solver. Otherwise it effectively becomes a macro solver, when the physically small scales are *not numerically resolved*.

The idea of AP can be illustrated by Figure 1.2(a). Assume we start with a microscopic model $\mathcal{F}^\varepsilon$, which depends on the scaling parameter ε. As $\varepsilon \to 0$, the model asymptotically approaches the macroscopic model $\mathcal{F}^0$, which is independent of ε. Denote the numerical discretization of $\mathcal{F}^\varepsilon$ by $\mathcal{F}_\delta^\varepsilon$, where δ is the numerical parameter (such as mesh size and/or time step). The asymptotic limit of $\mathcal{F}_\delta^\varepsilon$, as $\varepsilon \to 0$ (with δ fixed), if it exists, is denoted by $\mathcal{F}_\delta^0$. *Scheme $\mathcal{F}_\delta^\varepsilon$ is called AP if $\mathcal{F}_\delta^0$ is a good (consistent and stable) approximation of $\mathcal{F}^0$,*

Error estimates on an AP scheme can be obtained by the following argument (Golse, Jin and Levermore 1999). Typically,

$$\|\mathcal{F}^\varepsilon - \mathcal{F}^0\| = O(\varepsilon), \tag{1.1}$$

under some suitable problem-dependent norm. Assume $\mathcal{F}_\delta^\varepsilon$ is an rth-order approximation to $\mathcal{F}^\varepsilon$ for fixed ε. Due to the presence of the small parameter ε, a classical numerical analysis typically gives the following error estimate:

$$\mathcal{E}_1 = \|\mathcal{F}_\delta^\varepsilon - \mathcal{F}^\varepsilon\| = O(\delta^r/\varepsilon^s), \quad 1 \le s \le r. \tag{1.2}$$

The error is large when $\delta^r \gg \varepsilon^s$, namely when the small physical scales are not numerically resolved (if we use coarse meshes or large time steps relative to ε). An AP scheme usually requires

$$\|\mathcal{F}_\delta^\varepsilon - \mathcal{F}_\delta^0\| = O(\varepsilon) \quad \text{uniformly in } \delta, \tag{1.3}$$

and

$$\|\mathcal{F}_\delta^0 - \mathcal{F}^0\| = O(\delta^r). \tag{1.4}$$

Clearly, if we add up the errors in (1.1), (1.3) and (1.4), by the triangle inequality, the following error estimate can be obtained:

$$\mathcal{E}_2 = \|\mathcal{F}_\delta^\varepsilon - \mathcal{F}^\varepsilon\| \le \|\mathcal{F}_\delta^\varepsilon - \mathcal{F}_\delta^0\| + \|\mathcal{F}_\delta^0 - \mathcal{F}^0\| + \|\mathcal{F}^0 - \mathcal{F}^\varepsilon\| = O(\varepsilon + \delta^r). \tag{1.5}$$

https://doi.org/10.1017/S0962492922000010 Published online by Cambridge University Press

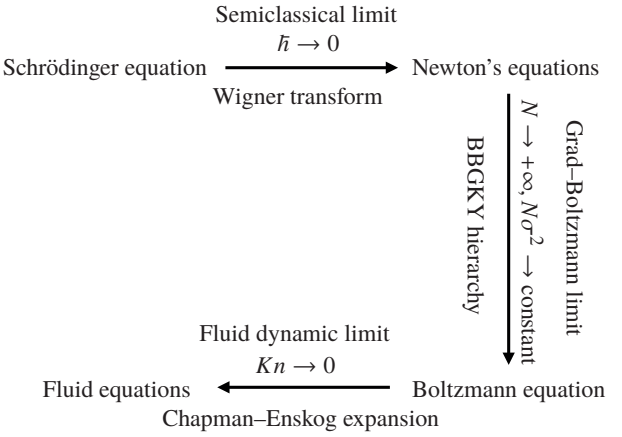

Figure 1.3. Scaling limits from microscopic to macroscopic models.

This error is small for $\varepsilon \ll 1$. Clearly both estimates on $\mathcal{E}_1$ (1.2) and $\mathcal{E}_2$ (1.5) are mathematically valid and can hold simultaneously. By comparing the two estimates,

$$\|\mathcal{F}_\delta^\varepsilon - \mathcal{F}^\varepsilon\| = \min(\mathcal{E}_1, \mathcal{E}_2),$$

which has an upper bound around $\varepsilon = O(\delta^{r/(s+1)})$, as shown by Figure 1.2(b). This gives

$$\|\mathcal{F}_\delta^\varepsilon - \mathcal{F}^\varepsilon\| = O(\delta^{r/(s+1)}) \quad \text{uniformly in } \varepsilon. \tag{1.6}$$

This argument shows that an AP scheme is *convergent uniformly in* ε. Indeed, if we resolve ε by δ (with $\delta = o(\varepsilon^{s/r})$), we get a good approximation to the microscopic model $\mathcal{F}^\varepsilon$, as shown by (1.2). If ε is not resolved by δ, then we obtain a good approximation to the macroscopic model $\mathcal{F}^0$. This transition is done *automatically* by the code.

There have been a few earlier reviews of AP schemes, *e.g.* for multiscale kinetic equations (Jin 2010, Degond and Deluzet 2017, Hu, Jin and Li 2017) and for semiclassical computation of the Schrödinger equation (Jin, Markowich and Sparber 2011, Lasser and Lubich 2020). This survey, however, is unique in that it covers the topics in essentially *all* important physical regimes in a more comprehensive way, from quantum to classical mechanics, from classical mechanics to kinetic theory, and then from kinetic theory to hydrodynamics. It also includes the most recent advances in this topic, including new directions.

Since the design of AP schemes relies upon a good understanding of the asymptotic transitions from the microscopic to the macroscopic models, in the next section we first review such transitions for some of the most fundamental physical equations and scalings shown in Figure 1.1. They are summarized in Figure 1.3.

https://doi.org/10.1017/S0962492922000010 Published online by Cambridge University Press

2. Asymptotic transitions from microscopic to macroscopic physics

2.1. From quantum mechanics to classical mechanics

Consider the dimensionless Schrödinger equation from quantum mechanics:

$$\mathrm{i}\varepsilon\partial_t u^\varepsilon = -\frac{\varepsilon^2}{2}\Delta u^\varepsilon + V(x)u^\varepsilon, \quad u^\varepsilon(0,x) = u^\varepsilon_{\mathrm{in}}(x). \tag{2.1}$$

Here $u^\varepsilon = u^\varepsilon(t,x) \in \mathbb{C}$ is a complex-valued quantum mechanical wave function, $(t,x) \in \mathbb{R}\times\mathbb{R}^d$, with $d \in \mathbb{N}$ denoting the spatial dimension. In addition, $\varepsilon > 0$ denotes the small *semiclassical parameter* (the scaled Planck's constant $\hbar$), describing the microscopic/macroscopic scale ratio. In quantum mechanics for N particles, $V(x)$ is the Coulomb potential, but here it is left as a general function of x.

The physical observables are real-valued quadratic quantities of u^ε. They include the *position density*

$$\rho^\varepsilon(t,x) := |u^\varepsilon(t,x)|^2, \tag{2.2}$$

the *current density*

$$j^\varepsilon(t,x) := \varepsilon\,\mathrm{Im}\big(\overline{u^\varepsilon}(t,x)\nabla u^\varepsilon(t,x)\big), \tag{2.3}$$

and the *energy density*

$$\mathrm{e}^\varepsilon(t,x) := \frac{1}{2}|\varepsilon\nabla u^\varepsilon(t,x)|^2 + V(x)\rho^\varepsilon(t,x). \tag{2.4}$$

Simple analysis shows that these observables are governed by the following dynamics:

$$\begin{aligned} \partial_t\rho^\varepsilon + \nabla\cdot j^\varepsilon &= 0,\\ \partial_t j^\varepsilon + \nabla\cdot\left[\frac{j^\varepsilon\otimes j^\varepsilon}{\rho^\varepsilon}\right] + \rho\nabla V &= \frac{\varepsilon^2}{2}\rho^\varepsilon\nabla\left(\frac{1}{\sqrt{\rho^\varepsilon}}\Delta\sqrt{\rho^\varepsilon}\right),\\ \partial_t\,\mathrm{e}^\varepsilon + \nabla\cdot\left(\frac{j^\varepsilon}{\rho^\varepsilon}(\mathrm{e}^\varepsilon + \rho^\varepsilon V - V\rho^\varepsilon)\right) &= \frac{\varepsilon^2}{4}\nabla\cdot\left[\frac{j^\varepsilon\Delta\rho^\varepsilon}{\rho^\varepsilon} - \frac{\nabla\cdot j^\varepsilon\nabla\rho^\varepsilon}{\rho^\varepsilon}\right]. \end{aligned} \tag{2.5}$$

From here we can easily deduce the conservation in time of total mass and energy:

$$\partial_t\int_{\mathbb{R}}\rho^\varepsilon\,\mathrm{d}x = 0, \quad \partial_t\int_{\mathbb{R}}\mathrm{e}^\varepsilon\,\mathrm{d}x = 0. \tag{2.6}$$

The two main computational challenges to the Schrödinger equation are as follows.

(i) *Small* ε. Here u^ε oscillates with frequency $1/\varepsilon$ in both space *and* time, so we need to numerically resolve these oscillations both spatially and temporarily.

(ii) *Large* d. For a system consisting of N particles, $d = 3N$. Typically N is large. For example, for the carbon dioxide molecule $d = 75$; for the benzene

https://doi.org/10.1017/S0962492922000010 Published online by Cambridge University Press

molecule $N = 162$. This incurs the curse of dimensionality. Totally different techniques need to be used for such high-dimensional problems and we shall not elaborate on these issues in this paper.

In this survey we focus on the first challenge, namely how one numerically deals with the small ε problem efficiently. To this end, we first review the so-called 'semiclassical' approximation.

2.1.1. The WKB analysis

Consider the initial data of the following form (the so-called WKB initial data):

$$u^\varepsilon(0, x) = A_0(x)\, \mathrm{e}^{\mathrm{i}S_0(x)/\varepsilon}. \tag{2.7}$$

The WKB analysis assumes that the solution remains of the same form at a later time:

$$u^\varepsilon(t, x) = A(t, x)\, \mathrm{e}^{\mathrm{i}S(t,x)/\varepsilon}. \tag{2.8}$$

Here A is the amplitude and S is the phase. Applying this *ansatz*, which is also called the Madelung transform, to the Schrödinger equation (2.1), and separating the real part from the imaginary part, we obtain

$$\begin{aligned} A\partial_t S &= \frac{\varepsilon^2}{2}\Delta A - \frac{1}{2}A|\nabla S|^2 - AV, \\ \partial_t A &= -\nabla A \cdot \nabla S - \frac{1}{2}A\Delta S. \end{aligned} \tag{2.9}$$

Ignoring the $O(\varepsilon^2)$-terms, we get

$$\begin{aligned} \partial_t |A|^2 + \nabla(|A|^2 \nabla S) &= 0, \\ \partial_t S + \frac{1}{2}|\nabla S|^2 + V &= 0. \end{aligned} \tag{2.10}$$

The first equation above is called the *transport equation* while the second is the *eikonal equation*. The eikonal equation is a Hamilton–Jacobi equation that admits solutions S with discontinuous derivatives. This can be easily seen once we take a gradient on the equation to get (by letting $u = \nabla S$)

$$\partial_t u + u \cdot \nabla u + \nabla V = 0. \tag{2.11}$$

This is the inviscid Burgers' equation (with forcing term $-\nabla V$), which admits discontinuous solutions (shocks) to u even if the initial data of u is smooth. Consequently the gradient of S becomes discontinuous, a point usually referred to as the *caustic*.

By defining $\rho = |A|^2$, system (2.10) can be written as

$$\begin{aligned} \partial_t \rho + \nabla \cdot (\rho u) &= 0, \\ \partial_t(\rho u) + \nabla \cdot (\rho u \otimes u) + \rho V &= 0. \end{aligned} \tag{2.12}$$

https://doi.org/10.1017/S0962492922000010 Published online by Cambridge University Press

This is the pressureless gas system. Clearly the system is decoupled. One can solve the second equation (which is actually (2.11)) for u and then obtain ρ from the first equation. When u becomes discontinuous, ρ becomes a Dirac delta function, usually called a *delta shock* (Tan, Zhang, Chang and Zheng 1994). Thus, at a caustic, the amplitude A blows up (becomes infinity).

Beyond the caustic, one notion of mathematical solution to the Hamilton–Jacobi equation is the *viscosity solution*, introduced by Crandall and Lions (1983). This notion, however, cannot be used here since system (2.12) is in fact the $\varepsilon \to 0$ limit of system (2.5), which is a *zero dispersion limit*. The zero dispersion limit is drastically different from the zero dissipation limit, as studied for the Korteweg–de Vries (KdV) equation (Lax and Levermore 1983). For the semiclassical limit of the defocusing non-linear Schrödinger equation, see Jin, Levermore and McLaughlin (1999)). Thus the WKB analysis is only valid up to the time when the first caustic forms. Beyond caustics, the solution becomes *multi-valued* (Sparber, Markowich and Mauser 2003).

In contrast, the Wigner transform technique, which we study next, yields the Liouville equation in *phase space*, in the semiclassical limit $\varepsilon \to 0$, whose solution does not exhibit caustics, hence is valid globally in time.

2.1.2. *Classical limit via the Wigner transform*

The *Wigner transform* of u^ε is defined as (Wigner 1932)

$$w^\varepsilon[u^\varepsilon](x,\xi) := \frac{1}{(2\pi)^d}\int_{\mathbb{R}^d} u^\varepsilon\left(x+\frac{\varepsilon}{2}\eta\right)\overline{u^\varepsilon}\left(x-\frac{\varepsilon}{2}\eta\right)\mathrm{e}^{\mathrm{i}\xi\cdot\eta}\,\mathrm{d}\eta, \tag{2.13}$$

which is the Fourier transform of the density matrix.

It is easy to see that the Wigner transform w^ε is real-valued but in general not necessarily positive. The moments of w^ε give the quantum mechanical physical observables. For example, the particle density (2.2) can be computed via

$$\rho^\varepsilon(t,x) = \int_{\mathbb{R}^d} w^\varepsilon(t,x,\xi)\,\mathrm{d}\xi,$$

the current density (2.3) can be obtained by

$$j^\varepsilon(t,x) = \int_{\mathbb{R}^d} \xi w^\varepsilon(t,x,\xi)\,\mathrm{d}\xi,$$

while the energy density (2.4) is just

$$\mathrm{e}^\varepsilon(t,x) = \int_{\mathbb{R}^d}\left(\frac{1}{2}|\xi|^2 + V(x)\right)w^\varepsilon(t,x,\xi)\,\mathrm{d}\xi.$$

Applying the Wigner transformation to the Schrödinger equation (2.1), we obtain the Wigner equation (also called the quantum Liouville equation)

$$\partial_t w^\varepsilon + \xi\cdot\nabla_x w^\varepsilon - \Theta^\varepsilon[V]w^\varepsilon = 0, \quad w^\varepsilon(0,x,\xi) = w^\varepsilon_{\mathrm{in}}(x,\xi), \tag{2.14}$$

https://doi.org/10.1017/S0962492922000010 Published online by Cambridge University Press

where $\Theta^\varepsilon[V]$ is given by

$$\Theta^\varepsilon[V]f(x,\xi) := \frac{\mathrm{i}}{(2\pi)^d}\iint_{\mathbb{R}^d\times\mathbb{R}^d} \delta V^\varepsilon(x,y) f(x,\xi')\,\mathrm{e}^{\mathrm{i}\eta(\xi-\xi')}\,\mathrm{d}\eta\,\mathrm{d}\xi', \tag{2.15}$$

with

$$\delta V^\varepsilon := \frac{1}{\varepsilon}\left(V\left(x-\frac{\varepsilon}{2}y\right) - V\left(x+\frac{\varepsilon}{2}y\right)\right).$$

When $\varepsilon \to 0$,

$$\delta V^\varepsilon \overset{\varepsilon\to 0}{\longrightarrow} y\cdot\nabla_x V,$$

then (2.14) formally becomes the classical *Liouville equation* in phase space:

$$\partial_t w + \xi\cdot\nabla_\xi w - \nabla_x V(x)\cdot\nabla_\xi w = 0. \tag{2.16}$$

This is the classical limit of the Schrödinger equation as $\varepsilon \to 0$, valid *globally* in time, even beyond the caustic (Lions and Paul 1993, Gérard, Markowich, Mauser and Poupaud 1997), in contrast to the WKB analysis. Note that the Liouville equation (2.16) is linear, which unfolds the singularity, and the linear superposition and time reversibility of the Schrödinger equation are also preserved.

The (bi)characteristic equations for (2.16) are given by

$$\dot{x} = \xi, \quad \dot{\xi} = -\nabla_x V(x),$$

which is exactly Newton's equation. This system can be written as a Hamiltonian system:

$$\begin{cases} \dot{x} = \nabla_\xi H(x,\xi), \\ \dot{\xi} = -\nabla_x H(x,\xi), \end{cases} \tag{2.17}$$

with the Hamiltonian H (in classical mechanics) given by

$$H(x,\xi) = \frac{1}{2}|\xi|^2 + V(x). \tag{2.18}$$

For $x,\xi \in \mathbb{R}^{dN}$, and V the potential for N-particles, (2.17) is the particle system to be studied in the next subsection.

2.2. *From classical mechanics to kinetic equations*

2.2.1. *From hard sphere particles to the Boltzmann equation*

Consider N hard spherical particles,

$$\dot{x}_i = v_i,$$
$$\dot{v}_i = 0,$$

where $(x_i, v_i) \in \mathbb{R}^d \times \mathbb{R}^d$ $(1 \le i \le N)$ denote the position and velocity of particle i. Assume each particle has the same diameter σ; then they satisfy the exclusion

https://doi.org/10.1017/S0962492922000010 Published online by Cambridge University Press

condition

$$|x_i(t) - x_j(t)| > \sigma. \tag{2.19}$$

Assume particles i and j collide elastically when $|x_i - x_j| = \sigma$; then the post-collisional velocities, denoted by v_i' and v_j' respectively, are given by

$$v_i' = v_i - [(v_i - v_j) \cdot \omega]\omega, \quad v_j' = v_j + [(v_i - v_j) \cdot \omega]\omega, \tag{2.20}$$

where $\omega = (x_j - x_i)/|x_j - x_i|$.

Define

$$Z_N = (z_1, \ldots, z_N) = (x_1, v_1, \ldots, x_N, v_N). \tag{2.21}$$

Let $W^N(t, Z_N)$ be the probability distribution of the particle system. Then it solves the N-body Liouville equation

$$\partial_t W^N(t) = \mathcal{L}_N W^N(t), \quad \mathcal{L}_N = -\sum_{i=1}^{N} (v_i \cdot \nabla_{x_i}), \tag{2.22}$$

which is defined on the domain

$$\mathcal{D}_N = \{Z_N \in \mathbb{R}^{2dN} : |x_i - x_j| > \sigma \text{ for } i \neq j\}.$$

At the boundary, where $|x_i - x_j| = \sigma$, we have $W^N(t, Z_N') = W^N(t, Z_N)$.

Assume all particles are *identical and indistinguishable*, namely

$$W^N(z_1, \ldots, z_N) = W^N(z_{\sigma_1}, \ldots, z_{\sigma_N})$$

for any $\{\sigma_1, \ldots, \sigma_N\}$, a random permutation of set $\{1, \ldots, N\}$. Furthermore, assume the so-called *molecular chaos* condition:

$$W^N(z_1, \cdots z_N) = W_1^N(x_1, v_1) \cdots W_N^N(x_n, v_N).$$

Under the above assumptions, the Grad–Boltzmann limit of classical particles can be derived by letting $\sigma \to 0$ and $N \to \infty$ under the assumption

$$N\sigma^2 \to \text{constant},$$

in which the one-particle distribution $W_1^N(x_1, v_1)$ formally approaches the Boltzmann equation for hard spheres (Bouchut, Golse and Pulvirenti 2000):

$$\partial_t f + v \cdot \nabla_x f = \int |(v - v_*) \cdot \omega| \{f(v')f(v_*') - (f(v)f(v_*)\} \, \mathrm{d}\omega \, \mathrm{d}v_*, \tag{2.23}$$

where v and v_* are pre-collisional velocities with corresponding post-collisional velocities v' and v_*' determined by (2.20) (with $v_i = v, v_j = v_*$).

The proof of the Grad–Boltzmann limit is extremely challenging. So far the only rigorous results are available for a very short duration of time – a fraction of a mean-free time; see Lanford (1975) and Gallagher, Saint-Raymond and Texier (2013).

https://doi.org/10.1017/S0962492922000010 Published online by Cambridge University Press

2.2.2. Mean-field limit of particle systems

The Newton-type equations also arise in microscopic modelling of a vast number of important phenomena in physical, social and biological sciences (Vicsek *et al.* 1995, Cucker and Smale 2007, Motsch and Tadmor 2014, Albi *et al.* 2019). These problems can all be modelled by interacting particle systems of first order,

$$\mathrm{d}X^i = b(X^i)\,\mathrm{d}t + \alpha_N \sum_{j:j\neq i} K_1(X^i - X^j)\,\mathrm{d}t + \eta\,\mathrm{d}W^i, \quad i = 1, 2, \ldots, N, \tag{2.24}$$

or second order,

$$\begin{aligned} \mathrm{d}X^i &= V^i\,\mathrm{d}t, \\ \mathrm{d}V^i &= \left[b(X^i) + \alpha_N \sum_{j:j\neq i} K(X^i - X^j) - \gamma V^i \right] \mathrm{d}t + \eta\,\mathrm{d}W^i. \end{aligned} \tag{2.25}$$

Here $(X^i, V^i) \in \mathbb{R}^d \times \mathbb{R}^d$, loosely speaking, represent the position and velocity of the ith particle, and $b(\cdot)$ is the external field. The stochastic processes $\{W^i\}_{i=1}^N$ are i.i.d. Wiener processes, or the standard Brownian motions. The function $K(\cdot)\colon \mathbb{R}^d \to \mathbb{R}^d$ is the interaction kernel. For the molecules in the heat bath, η and γ satisfy the so-called 'fluctuation–dissipation relation'

$$\eta = \sqrt{2\gamma/\beta}, \tag{2.26}$$

where β is the inverse of the temperature (we assume all the quantities are scaled and hence dimensionless so that the Boltzmann constant is absent). The first-order system (2.24) can be viewed as the over-damped limit of the second-order system (2.25), *i.e.* rescaling t to γt and letting $\gamma \to \infty$ (Stanley 1971, Georges, Kotliar, Krauth and Rozenberg 1996, Lelièvre and Stoltz 2016).

The mean-field limit is usually taken by choosing

$$\alpha_N = \frac{1}{N-1}. \tag{2.27}$$

Define the empirical distribution

$$\mu^{(N)} := \frac{1}{N} \sum_{i=1}^{N} \delta(x - X^i) \otimes \delta(v - V^i). \tag{2.28}$$

For the second-order system (2.25), as $N \to \infty$, $\mu^{(N)}$ converges almost surely in the weak topology to the solutions of the (mean-field) Fokker–Planck equation

$$\partial_t f = -\nabla_x \cdot (vf) - \nabla_v \cdot ((b(x) + K *_x f - \gamma v)f) + \frac{1}{2}\eta^2 \Delta_v f. \tag{2.29}$$

The mean-field limit corresponding to the first-order system (2.24) is (McKean 1967, Golse 2003, Jabin and Wang 2017)

$$\partial_t f = -\nabla \cdot ((b(x) + K_1 * f)f) + \frac{1}{2}\eta^2 \Delta f. \tag{2.30}$$

https://doi.org/10.1017/S0962492922000010 Published online by Cambridge University Press

These mean-field limits can also be derived from taking the limit $N \to \infty$ of the N-body distribution with molecular chaos assumptions, as in the derivation of the Boltzmann equation from the N-body Newton's equations described above.

2.3. From kinetic equations to hydrodynamics

2.3.1. Hydrodynamic limit of the Boltzmann equation

The Boltzmann equation describes the probability density function $f(t, x, v)$ of particles that undergo transport and binary collisions (Cercignani 1988),

$$\partial_t f + v \cdot \nabla_x f = \frac{1}{\varepsilon} \mathcal{Q}(f), \quad x, v \in \mathbb{R}^n, \tag{2.31}$$

where the collision term $\mathcal{Q}(f)$ is a non-linear integral operator:

$$\mathcal{Q}(f)(v) = \frac{1}{\varepsilon} \int_{\mathbb{R}^d} \int_{S^{d-1}} B(v - v_*, \omega) \left[f(v') f(v'_*) - f(v) f(v_*) \right] \mathrm{d}\omega \, \mathrm{d}v_*. \tag{2.32}$$

Here (v, v_*) and (v', v'_*) are the velocity pairs before and after an elastic collision, which conserve the momentum and energy. They are related by

$$v' = v - [(v - v_*) \cdot \omega]\omega, \quad v'_* = v_* + [(v - v_*) \cdot \omega]\omega,$$

with the parameter $\omega \in S^{d-1}$, the unit sphere in $\mathbb{R}^d$. Here $B(v - v_*, \omega)$ is the (non-negative) collision kernel depending only on $|v - v_*|$ and the cosine of the deviation angle $(\sigma \cdot (v - v_*))/|v - v_*|$, and ε is the Knudsen number, the dimensionless mean-free path.

The hydrodynamic quantities ρ, u and T, the density, macroscopic velocity and temperature respectively, are defined as the moments of f, that is,

$$\rho = \int_{\mathbb{R}^d} f \, \mathrm{d}v = \int_{\mathbb{R}^d} \mathcal{M} \, \mathrm{d}v, \quad u = \frac{1}{\rho} \int_{\mathbb{R}^d} v f \, \mathrm{d}v = \int_{\mathbb{R}^d} v \mathcal{M} \, \mathrm{d}v, \tag{2.33}$$

$$T = \frac{1}{\mathrm{d}\rho} \int_{\mathbb{R}^d} |v - u|^2 f \, \mathrm{d}v = \frac{1}{\mathrm{d}\rho} \int_{\mathbb{R}^d} |v - u|^2 \mathcal{M} \, \mathrm{d}v, \tag{2.34}$$

where the local Maxwellian

$$\mathcal{M} = \frac{\rho}{(2\pi T)^{d/2}} \exp\left(-\frac{|u - v|^2}{2T} \right). \tag{2.35}$$

The collision operator $\mathcal{Q}(f)$ conserves mass, momentum and energy:

$$\int_{\mathbb{R}^d} \mathcal{Q}(f) \phi(v) \, \mathrm{d}v = 0, \quad \phi(v) = (1, v, |v|^2/2)^T, \tag{2.36}$$

with the momentum $m = \rho u$ and the total energy $E = \frac{1}{2}\rho u^2 + \rho T$.

One of the most important properties of $\mathcal{Q}$ is Boltzmann's celebrated H-theorem:

$$\partial_t \int_{\mathbb{R}^d} f \log f \, \mathrm{d}v = \int_{\mathbb{R}^d} \mathcal{Q}(f) \ln f \, \mathrm{d}v \le 0.$$

The functional $f \log f$ is the entropy of the system. Boltzmann's H-theorem implies

https://doi.org/10.1017/S0962492922000010 Published online by Cambridge University Press

that any equilibrium distribution function, *i.e.* any function which is a maximum of the entropy, has the form of a local Maxwellian distribution:

$$\int_{\mathbb{R}^d} \mathcal{Q}(f) \ln f \, \mathrm{d}v = 0 \Longleftrightarrow \mathcal{Q}(f) = 0 \Longleftrightarrow f = \mathcal{M}. \tag{2.37}$$

When $\varepsilon \to 0$, $\mathcal{Q} \to 0$, (2.37) implies $f = \mathcal{M}$. Consequently the moments of f solve the compressible Euler equations:

$$\begin{cases} \partial_t \rho + \nabla_x \cdot (\rho u) = 0, \\ \partial_t (\rho u) + \nabla_x \cdot (\rho u \otimes u + pI) = 0, \\ \partial_t E + \nabla_x \cdot ((E + p)u) = 0. \end{cases} \tag{2.38}$$

Via the Chapman–Enskog expansion, we can derive the Navier–Stokes (NS) equations by retaining $O(\varepsilon)$-terms (Bouchut *et al.* 2000):

$$\begin{cases} \partial_t \rho + \nabla_x \cdot (\rho u) = 0, \\ \partial_t (\rho u) + \nabla_x \cdot (\rho u \otimes u + pI) = \varepsilon \nabla_x \cdot (\mu \sigma(u)), \\ \partial_t E + \nabla_x \cdot ((E + p)u) = \varepsilon \nabla_x \cdot (\mu \sigma(u) u + \kappa \nabla_x T), \end{cases} \tag{2.39}$$

where

$$\sigma(u) = \nabla_x u + \nabla_x u^T - \frac{2}{d} \nabla_x \cdot u I,$$

I is the identity matrix, and μ and κ are the viscosity and heat conductivity, determined via the linearized Boltzmann collision operator, and usually depend on T.

2.3.2. *Diffusion limit of transport equation*

In many applications, such as neutron transport and radiative transfer, the collision operator is linear. The interesting scaling is often the diffusive scaling, where the scattering rate is large. A typical such equation takes the form

$$\varepsilon \, \partial_t f + v \cdot \nabla_x f = \frac{1}{\varepsilon} \int b(v, w) \{ M(v) f(w) - M(w) f(v) \} \, \mathrm{d}w, \quad x, v \in \mathbb{R}^d, \tag{2.40}$$

with the normalized Maxwellian M defined by

$$M(v) = \frac{1}{(2\pi)^{d/2}} \exp(-|v|^2/2).$$

The (anisotropic) scattering kernel b is rotationally invariant, satisfying

$$b(v, w) = b(w, v) > 0.$$

Define the collision frequency λ as

$$\lambda(v) = \int b(v, w) M(w) \, \mathrm{d}w.$$

https://doi.org/10.1017/S0962492922000010 Published online by Cambridge University Press

As $\varepsilon \to 0$, $f \to \rho(x,t)M(v)$, where $\rho(t,x) = \int f(v)\,\mathrm{d}v$ satisfies the diffusion equation (Bardos, Santos and Sentis 1984, Markowich, Ringhofer and Schmeiser 1990)

$$\partial_t \rho = \nabla_x \cdot (D \nabla_x \rho), \tag{2.41}$$

with the diffusion coefficient matrix

$$D = \int \frac{M(v)}{\lambda(v)} v \otimes v \,\mathrm{d}v. \tag{2.42}$$

3. Numerical passages from quantum to classical mechanics

The highly oscillatory nature of the solution, in both space and time, to the Schrödinger equation (2.1) poses a huge challenge in numerical computations, especially in high dimensions, since we need to resolve numerically, in both space and time, the small wave length of $O(\varepsilon)$, which is computationally daunting. If we do not use a sufficiently small time step or mesh size, even if the numerical scheme is stable, we may get completely incorrect solutions (Markowich, Pietra and Pohl 1999, Bao, Jin and Markowich 2002). To understand the numerical behaviour in the semiclassical regime, in addition to standard consistency and stability – which implies convergence by Lax's equivalence theorem – we need a new semiclassical analysis to understand the correct behaviour of the numerical solutions.

Here we are interested in two questions.

- What kind of scheme best suits the highly oscillatory problems?
- How should we analyse the numerical performance when ε is small?

For the first question, when the solution is smooth but highly oscillatory, spectral or pseudo-spectral methods give the best performance in terms of numerical accuracy and resolution. It is worth pointing out that taking care of spatial discretization alone is not enough to achieve the best performance for the Schrödinger equation (2.1). It takes a good combination of both spatial *and* temporal discretizations to achieve the most favourable mesh strategies (the largest possible ratio between the mesh size and time steps over ε). In this regard, time-splitting spectral methods, as studied in Bao *et al.* (2002), offer the best mesh strategy, while finite difference schemes require very fine numerical resolution of the oscillations (Markowich *et al.* 1999).

3.1. Time-splitting spectral methods for the semiclassical Schrödinger equations

For the sake of notational clarity, we shall discuss the method in only one space dimension ($d = 1$). Generalizations to $d > 1$ are straightforward for tensor product grids and the same conclusions hold.

Consider the one-dimensional version of equation (2.1),

$$\mathrm{i}\varepsilon \partial_t u^\varepsilon = -\frac{\varepsilon^2}{2} \partial_{xx} u^\varepsilon + V(x) u^\varepsilon, \quad u^\varepsilon(0,x) = u^\varepsilon_{\mathrm{in}}(x), \tag{3.1}$$

https://doi.org/10.1017/S0962492922000010 Published online by Cambridge University Press

for $x \in [0,1]$, with periodic boundary conditions

$$u^\varepsilon(t,0) = u^\varepsilon(t,1), \quad \partial_x u^\varepsilon(t,0) = \partial_x u^\varepsilon(t,1) \quad \text{for all } t \in \mathbb{R}.$$

We choose the spatial mesh size $\Delta x = 1/M$ for some large positive integer M, and time step $\Delta t > 0$. The spatio-temporal grid-points are then given by

$$x_j := j\Delta x,\ j = 1,\dots,M, \quad t_n := n\Delta t,\ n \in \mathbb{N}.$$

Let $u_j^{\varepsilon,n}$ be the numerical approximation of $u^\varepsilon(x_j,t_n)$, for $j = 1,\dots,M$.

The Schrödinger equation (3.1) is solved by the following time-splitting method.

Step 1. From time $t = t_n$ to time $t = t_{n+1}$, first solve the free Schrödinger equation

$$\mathrm{i}\varepsilon\partial_t u^\varepsilon + \frac{\varepsilon^2}{2}\partial_{xx} u^\varepsilon = 0. \tag{3.2}$$

Step 2. Also on $t \in [t_n, t_{n+1}]$, solve the ordinary differential equation

$$\mathrm{i}\varepsilon\partial_t u^\varepsilon - V(x)u^\varepsilon = 0, \tag{3.3}$$

with the solution $u^{\varepsilon,*}$ obtained from Step 1 as initial data.

Note that (3.3) can be solved *exactly*:

$$u(t_{n+1},x) = u(t_n,x)\,\mathrm{e}^{-\mathrm{i}V(x)\Delta t/\varepsilon}.$$

In Step 1, equation (3.2) will be discretized by a (pseudo-) spectral method in space and consequently integrated in time *exactly* in the Fourier space. More precisely,

$$u_j^{\varepsilon,*} = \frac{1}{M}\sum_{\ell=-M/2}^{M/2-1} \mathrm{e}^{\mathrm{i}\varepsilon\Delta t\gamma_\ell^2/2}\,\widehat{u}_\ell^{\varepsilon,n}\,\mathrm{e}^{\mathrm{i}\gamma_\ell(x_j-a)},$$

where $\gamma_\ell = 2\pi l$ and $\widehat{u}_\ell^{\varepsilon,n}$ is the Fourier coefficients of $u^{\varepsilon,n}$, that is,

$$\widehat{u}_\ell^{\varepsilon,n} = \sum_{j=1}^{M} u_j^{\varepsilon,n}\,\mathrm{e}^{-\mathrm{i}\gamma_\ell x_j}, \quad \ell = -\frac{M}{2},\dots,\frac{M}{2}-1.$$

Note that in both steps the time integration is *exact*. The only time discretization error of this method is the splitting error, which is *first-order* in k, for any *fixed* $\varepsilon > 0$. We will refer to this method as TSSP.

The second order in time (for fixed $\varepsilon > 0$) can be obtained via the Strang splitting method. Extensions to higher-order (in time) splitting schemes can also be done; see *e.g.* Bao and Shen (2005). See also its extension to the case of vector potentials (Jin and Zhou 2013).

3.2. *Numerical analysis in the semiclassical regime*

Classical numerical analysis, based on consistency and stability, does not provide accurate assessment of the numerical performance when $\varepsilon \ll 1$. Wigner analysis,

https://doi.org/10.1017/S0962492922000010 Published online by Cambridge University Press

on the other hand, gives more insight into the behaviour of numerical solutions, for *physical observables*, in the semiclassical regime.

Assume that the potential $V(x)$ is periodic in domain $[0, 1]$, smooth, and satisfies

$$\left\| \frac{\mathrm{d}^m}{\mathrm{d}x^m} V \right\|_{L^\infty[a,b]} \leq C_m \tag{3.4}$$

for some constant $C_m > 0$, and furthermore

$$\left\| \frac{\partial^{m_1+m_2}}{\partial t^{m_1} \partial x^{m_2}} u^\varepsilon \right\|_{C([0,T];L^2[a,b])} \leq \frac{C_{m_1+m_2}}{\varepsilon^{m_1+m_2}} \tag{3.5}$$

for all $m, m_1, m_2 \in \mathbb{N} \cup \{0\}$, namely the solution oscillates in space and time with wavelength ε. The following estimate was given in Bao *et al.* (2002).

Theorem 3.1. Let $V(x)$ satisfy assumption (3.4) and let $u^\varepsilon(t, x)$ be a solution of (3.1) satisfying (3.5). Let $u_{\mathrm{int}}^{\varepsilon,n}$ denote the interpolation of the discrete approximation obtained via TSSP. Then, for $t_n \in [0, T]$,

$$\left\| u^\varepsilon(t_n) - u_{\mathrm{int}}^{\varepsilon,n} \right\|_{L^2(0,1)} \leq G_m \frac{T}{\Delta t} \left(\frac{\Delta x}{\varepsilon} \right)^m + \frac{CT\Delta t}{\varepsilon}, \tag{3.6}$$

where $C > 0$ is independent of ε and m and $G_m > 0$ is independent of ε, Δx, Δt.

Clearly, (3.6) implies that to get an accurate u^ε we need the following mesh strategy:

$$\Delta t = o(\varepsilon), \quad \Delta x = o(\varepsilon).$$

Hence the oscillations need to be resolved both spatially and temporally.

3.3. Accurate computation of physical observables

Bao *et al.* (2002) observed that if we are only interested in obtaining accurate physical observables, the time step can be greatly relaxed. This cannot be understood from the above classical numerical analysis; rather, the Wigner picture of quantum dynamics will offer the clue.

Let $u^\varepsilon(t, x)$ be the solution of (3.1) and let $w^\varepsilon(t, x, \xi)$ be the corresponding Wigner transform. It is easy to see that the splitting scheme (3.2)–(3.3) corresponds to the following time-splitting scheme for the Wigner equation (2.14).

Step 1. For $t \in [t_n, t_{n+1}]$, first solve the linear transport equation

$$\partial_t w^\varepsilon + \xi \, \partial_x w^\varepsilon = 0. \tag{3.7}$$

Step 2. On the same time interval, solve the scattering term

$$\partial_t w^\varepsilon - \Theta^\varepsilon[V] w^\varepsilon = 0, \tag{3.8}$$

with initial data obtained from Step 1.

https://doi.org/10.1017/S0962492922000010 Published online by Cambridge University Press

Since the time integration is *exact* in each step of the splitting, we can take the $\varepsilon \to 0$ limit in each step without any discretization error, and thus obtain the following limiting scheme.

Step 1. For $t \in [t_n, t_{n+1}]$, solve

$$\partial_t w + \xi\, \partial_x w^0 = 0. \tag{3.9}$$

Step 2. Using the outcome of Step 1 as initial data, solve, on the same time interval,

$$\partial_t w - \partial_x V\, \partial_\xi w^0 = 0. \tag{3.10}$$

This is *exactly* the time-splitting scheme for the limiting Liouville equation (2.16)! Since in the limiting process Δt was held fixed, hence independent of ε, thus when $\Delta t = O(1)$, and as $\varepsilon \to 0$, schemes (3.7) and (3.8) collapse to schemes (3.9) and (3.10), so the scheme is AP in time! Hence we can take $\Delta t = O(1)$, combined with the spectral mesh size $\Delta x = o(\varepsilon)$ to get accurate w^ε, and as a consequence, *all physical observables*!

Remark 3.2. While the above Wigner analysis is formal, a rigorous uniform-in-ε error estimate was obtained recently. Golse, Jin and Paul (2021), for both first- and second-order splittings, gave uniform-in-ε error estimates, with explicit constants, at least for the von Neumann equation – the density operator representation of the Schrödinger equation which is valid even for mixed states. The errors are measured by a pseudo-metric introduced in Golse and Paul (2017), which is an analogue of the Wasserstein distance of exponent 2 between a quantum density operator and a classical density in phase space. The regularity requirement for V is $V \in C^{1,1}$. Sharper uniform error estimates for physical observables were also obtained for the Strang splitting (Lasser and Lubich 2020), based on Egorov's theorem, with additional regularity requirements on V.

Example 3.3. We take one example from Bao *et al.* (2002). The Schrödinger equation (3.1) is solved with initial condition $u_0(x) = n_0(x) \exp(-\mathrm{i} S_0(x)/\varepsilon)$, where

$$n_0(x) = (\mathrm{e}^{-25(x-0.5)^2})^2, \quad S_0(x) = -\frac{1}{5} \ln(\mathrm{e}^{5(x-0.5)} + \mathrm{e}^{-5(x-0.5)}), \tag{3.11}$$

and $V(x) = 10$. Due to the compressive initial velocity $(\mathrm{d}/\mathrm{d}x)S_0(x)$, caustics will form. The weak limits $n^0(x,t)$, $J^0(x,t)$ of $n^\varepsilon(x,t)$, $J^\varepsilon(x,t)$, respectively, as $\varepsilon \to 0$ can be computed by evaluating the zeroth- and first-order velocity moments of the solution to the Liouville equation (2.16). As a reference we plot them at $t = 0.54$ (after the caustics formed) in Figure 3.1. We compare the solutions between CNSP (Crank–Nicolson in time and pseudo-spectral method in space) and TSSP2 (Strang's splitting in time and pseudo-spectral method in space). The mesh size Δx is taken in the same order as $\varepsilon = 10^{-3}$. One can see that for CNSP, even for $\Delta t = 0.0001$, the numerical solution cannot capture the correct weak limit. TSSP2 can capture the physical observations correctly with Δt much larger than ε.

https://doi.org/10.1017/S0962492922000010 Published online by Cambridge University Press

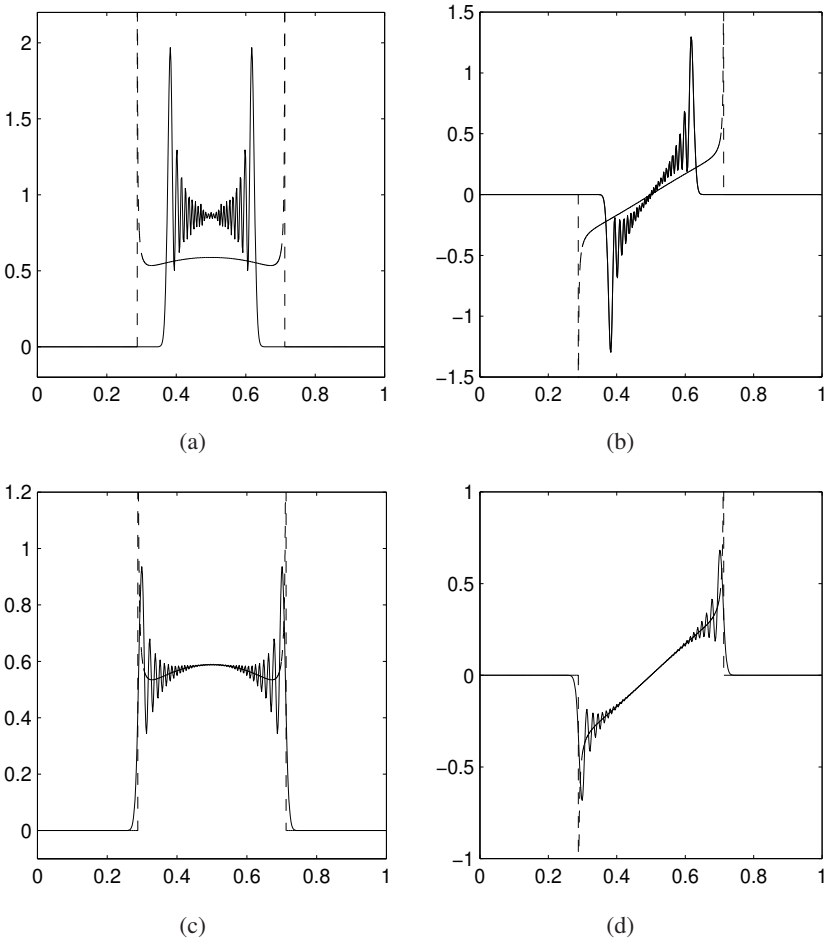

Figure 3.1. Example 3.3: numerical solutions at $t = 0.54$, for (a,b) CNSP with $k = 0.0001$, (c,d) TSSP2, (a,c) position density, (b,d) current density. Here $\varepsilon = 10^{-3}$, $V(x) = 10$, $h = 1/512$.

So far no numerical schemes are known to allow $\Delta x = o(1)$ for the Schrödinger equation (2.1). The best one can do is to allow $\Delta x = o(\sqrt{\varepsilon})$, by using the Gaussian beam or Gaussian wave packet methods; see Heller (2006), Hill (1990), Jin, Wu and Yang (2008), Leung and Qian (2009) and Russo and Smereka (2013). For more recent results about Gaussian-type approximations see Jin *et al.* (2011) and Lasser and Lubich (2020).

3.4. Ehrenfest dynamics

The *ab initio* methods have played indispensable roles in simulating large systems of quantum molecular dynamics. There the forces acting on the nuclei are computed

https://doi.org/10.1017/S0962492922000010 Published online by Cambridge University Press

from electronic structures, a procedure known as the 'on-the-fly' calculation in the chemistry literature; for detailed reviews, see *e.g.* Tully (1998) and Marx and Hutter (2009). The *Ehrenfest dynamics* is one popularly used method of this type. There we separate the quantum system into two subsystems: a fast varying quantum mechanical part for electrons and a slowly varying part for the nuclei. Due to the large mass difference between electrons and nuclei, the nucleonic system can be passed to the (semi-) classical limit, so the computational cost is significantly reduced.

Take $x \in \mathbb{R}^d$ as the electronic coordinate, $y \in \mathbb{R}^n$ as the nucleonic coordinate, with $d, n \in \mathbb{N}$, and let $\langle \cdot, \cdot \rangle_{L^2_x}$ and $\langle \cdot, \cdot \rangle_{L^2_y}$, respectively, denote the usual inner product in $L^2(\mathbb{R}^d_x)$ and $L^2(\mathbb{R}^n_y)$, that is,

$$\langle f, g \rangle_{L^2_z} \equiv \int_{\mathbb{R}^m} \overline{f}(z) g(z) \, \mathrm{d}z.$$

The total Hamiltonian of the system acting on $L^2(\mathbb{R}^{d+n})$ is assumed to be of the form

$$H = -\frac{\varepsilon^2}{2}\Delta_x - \frac{\delta^2}{2}\Delta_y + V(x, y), \tag{3.12}$$

where $V(x, y) \in \mathbb{R}$ is some real potential.

Consider the following mixed quantum-classical system (corresponding to the limit $\delta \to 0$) (Bisseling *et al.* 1987, Makri and Miller 1987, Jin, Sparber and Zhou 2017*b*):

$$\begin{cases} \mathrm{i}\varepsilon \partial_t \psi^\varepsilon = -\dfrac{\varepsilon^2}{2}\Delta_x \psi^\varepsilon + \Upsilon^\varepsilon(x, t)\psi^\varepsilon, \quad \psi^\varepsilon(0, x) = \psi^\varepsilon_{\mathrm{in}}(x), \\ \partial_t \mu^\varepsilon + \eta \cdot \nabla_y \mu^\varepsilon + F^\varepsilon(y, t) \cdot \nabla_\eta \mu^\varepsilon = 0, \quad \mu^\varepsilon(0, x, \eta) = \mu_{\mathrm{in}}(y, \eta). \end{cases} \tag{3.13}$$

Here $\mu^\varepsilon(\cdot, \cdot, t)$ denotes the phase space probability density for the slowly varying nuclei at time t, $F^\varepsilon = -\nabla_y V^\varepsilon_{\mathrm{E}}$ is the force obtained from the Ehrenfest potential

$$V^\varepsilon_{\mathrm{E}}(y, t) = \int_{\mathbb{R}^d} V(x, y) |\psi^\varepsilon(x, t)|^2 \, \mathrm{d}x,$$

and

$$\Upsilon^\varepsilon(x, t) = \iint_{\mathbb{R}^{2n}} V(x, y) \mu^\varepsilon(y, \eta, t) \, \mathrm{d}y \, \mathrm{d}\eta. \tag{3.14}$$

This system will be called the *Schrödinger–Liouville–Ehrenfest* (SLE) system. Note that the dependence of μ^ε on ε is purely from the forcing through the Ehrenfest potential V^ε_E appearing in the Liouville equation. In the case of a single particle distribution concentrated on the classical trajectories $(y(t), \eta(t))$, that is,

$$\mu(t, y, \eta) = \delta(y - y(t), \eta - \eta(t)),$$

(3.13) gives (Tully 1998, Drukker 1999, Schütte and Bornemann 1999, Szepessy

https://doi.org/10.1017/S0962492922000010 Published online by Cambridge University Press

2011)

$$\begin{cases} \mathrm{i}\varepsilon\partial_t\psi^\varepsilon = -\dfrac{\varepsilon^2}{2}\Delta_x\psi^\varepsilon + V(x, y(t))\psi^\varepsilon, \quad \psi^\varepsilon(0, x) = \psi_{\mathrm{in}}(x), \\ \dot{y}(t) = \eta(t), \quad y(0) = y_0, \\ \dot{\eta}(t) = -\nabla_y V_{\mathrm{E}}^\varepsilon(y(t)), \quad \eta(0) = \eta_0. \end{cases} \tag{3.15}$$

The iterated semiclassical limit ($\delta \to 0$, then $\varepsilon \to 0$) and the full classical limit ($\delta = \varepsilon \to 0$) were rigorously justified in Jin *et al.* (2017*b*).

Again, the main numerical difficulty for $\varepsilon \ll 1$ here is that we need to resolve oscillations of frequency of order $O(1/\varepsilon)$ in both time and space, as they are present in the solution ψ^ε. This requires us to use time steps of order $\Delta t = o(\varepsilon)$ as well as a spatial grid with $\Delta x = o(\varepsilon)$ to resolve the wave functions. As analysed in the preceding subsection, we may ask whether one can design a numerical method that allows the capturing of *physical observables* even for time steps much larger than $O(\varepsilon)$. For *non-linear* Schrödinger equations, in general, this is no longer true, as was demonstrated numerically by Bao, Jin and Markowich (2003). The SLE system (3.13) is a non-linearly coupled system, and we therefore expect the same type of problem at first glance. Nevertheless, Fang, Jin and Sparber (2018) introduced an efficient numerical method for the SLE system that allows large (compared with ε) computational mesh sizes in both y and η and a large time step for both the Schrödinger and the Liouville equations, but still *captures the physical observables correctly*. While large meshes in y and η do not seem so surprising, since they are coordinates of the nuclei, the possibility of large time steps for solving the Schrödinger equation for electrons is far from obvious, due to the non-linear nature of the SLE system.

3.4.1. A time-splitting scheme for the SLE system

Consider the case $d = n = 1$, and the domain $(x, y) \in [0, 1]^2$, with uniform mesh sizes $\Delta y, \Delta\eta$ applied to the classical part of the SLE (3.13). Set

$$J = \frac{1}{\Delta y}, \quad K = \frac{1}{\Delta\eta}, \quad M = \frac{1}{\Delta x}, \quad y_j = j\Delta y, \quad \eta_k = k\Delta\eta, \quad x_j = j\Delta x.$$

The time-splitting scheme, introduced in Fang *et al.* (2018), can then be described as follows. From time $t = t_n = n\Delta t$ to $t = t_{n+1} = (n + 1)\Delta t$, the SLE system is solved in two steps. First solve

$$\begin{cases} \mathrm{i}\varepsilon\partial_t\psi^\varepsilon = -\dfrac{\varepsilon^2}{2}\Delta_x\psi^\varepsilon, \\ \partial_t\mu^\varepsilon = -\eta\cdot\nabla_y\mu^\varepsilon - F^\varepsilon(y, t)\cdot\nabla_\eta\mu^\varepsilon, \end{cases} \tag{3.16}$$

from $t = t_n$ to an intermediate time $t_* = t_n + \Delta t$. Then solve

$$\begin{cases} \mathrm{i}h\partial_t\psi^h = \Upsilon^h(x, t)\psi^h, \\ \partial_t\mu^h = 0, \end{cases} \tag{3.17}$$

https://doi.org/10.1017/S0962492922000010 Published online by Cambridge University Press

with initial data computed from Step 1, to obtain the solution at time $t = t_{n+1}$.

In (3.16), the Schrödinger equation will be discretized in space by a spectral method using the fast Fourier transform, and integrated in Fourier space in time exactly. The Liouville equation can be solved either by a spectral method or by a finite difference (*e.g.* upwind) scheme in space, and then marching the corresponding ODE system forward in time. An advantage of this splitting method is that in the second step, $\Upsilon^h(x,t)$ defined in (3.14) is *independent* of time, since obviously μ^h is independent of time. Hence the time integration in (3.17) can also be solved *exactly* as

$$\psi_j^{\varepsilon,n+1} = \exp\left(-\frac{\mathrm{i}}{\varepsilon}\Upsilon^\varepsilon(x_j,t_*)\Delta t\right)\psi_j^{\varepsilon,*}.$$

As an example, consider an upwind spatial discretization of μ. In the first step, solve

$$\begin{cases} \mathrm{i}\varepsilon\partial_t\psi^\varepsilon = -\dfrac{\varepsilon^2}{2}\partial_{xx}\psi^\varepsilon, \\ \dfrac{\mathrm{d}}{\mathrm{d}t}\mu_{jk}^\varepsilon = -\eta_k(D_y\mu^\varepsilon)_{jk} - F_j^\varepsilon(D_\eta\mu^\varepsilon)_{jk}, \end{cases} \tag{3.18}$$

where both $D_y\mu^\varepsilon$ and $D_\eta\mu^\varepsilon$ represent the upwind discretization of the spatial derivatives. To solve the Liouville equation, apply the forward Euler scheme for the time discretization. Specifically,

$$\begin{cases} \psi_j^{\varepsilon,*} = \dfrac{1}{M}\displaystyle\sum_{\ell=-M/2}^{M/2-1} \mathrm{e}^{-\mathrm{i}\varepsilon\omega_\ell^2/2}\hat{\psi}_\ell^{\varepsilon,n}\,\mathrm{e}^{\mathrm{i}\omega_\ell x_j}, \quad j = 0,\dots,M-1, \\ \dfrac{\mu_{jk}^{\varepsilon,*} - \mu_{jk}^{\varepsilon,n}}{\Delta t} = -\eta_k(D_y\mu^{\varepsilon,n})_{jk} - F_j^{\varepsilon,n}(D_\eta\mu^{\varepsilon,n})_{jk}, \end{cases} \tag{3.19}$$

where $w_\ell = 2\pi\ell$.

The second step is then given by

$$\begin{cases} \mathrm{i}\varepsilon\partial_t\psi^\varepsilon = \Upsilon_d^\varepsilon(x,t)\psi^\varepsilon, \\ \dfrac{\mathrm{d}}{\mathrm{d}t}\mu_{jk}^\varepsilon = 0, \end{cases} \tag{3.20}$$

where $\Upsilon_d^\varepsilon(x,t)$ is the quadrature approximation of $\Upsilon^\varepsilon(x,t)$. Thus we explicitly get

$$\psi_j^{\varepsilon,n+1} = \exp(-\mathrm{i}\Upsilon_d^{\varepsilon,*}(x_j)\Delta t/\varepsilon)\psi_j^{\varepsilon,*}, \quad \mu_{jk}^{\varepsilon,n+1} = \mu_{jk}^{\varepsilon,*}, \tag{3.21}$$

where

$$\Upsilon_d^{\varepsilon,*}(x) = \sum_{j=0}^{J-1}\sum_{k=0}^{K-1} V(x,y_j)\mu_{jk}^{\varepsilon,*}\Delta y\Delta\eta = \sum_{j=0}^{J-1}\sum_{k=0}^{K-1} V(x,y_j)\mu_{jk}^{\varepsilon,n+1}\Delta y\Delta\eta,$$

which is the trapezoidal rule for μV with compact support.

https://doi.org/10.1017/S0962492922000010 Published online by Cambridge University Press

3.4.2. The spatial meshing strategy

We first show that one can take the limit $\varepsilon \to 0$, for fixed Δy and $\Delta\eta$. Consider a semidiscretized version of the SLE system (3.13) in one spatial dimension $d = n = 1$, where the Liouville equation is discretized by the upwind scheme:

$$\begin{cases} \mathrm{i}\varepsilon\partial_t\psi^\varepsilon = -\dfrac{\varepsilon^2}{2}\partial_{xx}\psi^\varepsilon + \Upsilon_d^\varepsilon(x,t)\psi^\varepsilon, \quad \psi^\varepsilon(0,x) = \psi_{\mathrm{in}}^\varepsilon(x), \\ \partial_t\mu^\varepsilon + \eta D_y\mu^\varepsilon + F^\varepsilon(y,t)D_\eta\mu^\varepsilon = 0, \quad \mu^\varepsilon(0,y,\eta) = \mu_{\mathrm{in}}^\varepsilon(y,\eta). \end{cases} \tag{3.22}$$

The following theorem is given in Fang *et al.* (2018).

Theorem 3.4. Under some suitable conditions for V and initial data, for any $T > 0$, the solution of semi-discretized SLE system (3.22) satisfies, up to extraction of subsequences,

$$w^\varepsilon[\psi^\varepsilon] \overset{\varepsilon\to 0_+}{\longrightarrow} \nu, \quad \mu_{jk}^\varepsilon \overset{\varepsilon\to 0_+}{\longrightarrow} \mu_{jk}^0,$$

in the w-$*$ topology, where $j = 0, \ldots, J-1$ and $k = 0, \ldots, K-1$. In addition, ν and μ_{jk} solve the semi-discretized Liouville system

$$\begin{cases} \partial_t\nu + \xi\partial_x\nu - \partial_x\Upsilon_d^0(x,t)\partial_\xi\nu = 0, \\ \dfrac{\mathrm{d}}{\mathrm{d}t}\mu_{jk}^0 + \eta_k D_y\mu_{jk}^0 + F_j^0 D_\eta\mu_{jk}^0 = 0. \end{cases}$$

The above result shows that the scheme is AP in y, η with respect to ε, namely one can use $\Delta y, \Delta\eta \sim O(1)$. This is the *first* such result for highly oscillatory problems in spatial variables, and more interestingly, the problem under study is *non-linear*!

Remark 3.5. Numerical experiments show that the same type of behaviour is true not only for mixed spectral-finite difference schemes but also for purely spectral schemes; see Fang *et al.* (2018). The proof, however, only works for the former case since it requires positivity of the energy. For spectral methods the theory is still lacking.

3.4.3. Time discretization

The time discretization of the splitting scheme can also be shown to be AP. Note that the semiclassical limit of SLE (3.13), as $\varepsilon \to 0$, is (Jin *et al.* 2017*b*)

$$\partial_t\mu + \eta\cdot\nabla_y\mu + F^0(y,t)\cdot\nabla_\eta\mu = 0, \tag{3.23}$$

$$\partial_t\nu + \xi\cdot\nabla_x\nu - \nabla_x\Upsilon^0(x,t)\cdot\nabla_\xi\nu = 0. \tag{3.24}$$

As $\varepsilon \to 0$, the splitting schemes (3.18) and (3.20), respectively, approach

$$\begin{cases} \partial_t\nu + \xi\partial_x\nu = 0, \\ \dfrac{\mathrm{d}}{\mathrm{d}t}\mu_{jk} + \eta_k(D_y\mu)_{jk} + F_j^0(D_\eta\mu)_{jk} = 0, \end{cases} \tag{3.25}$$

https://doi.org/10.1017/S0962492922000010 Published online by Cambridge University Press

and

$$\begin{cases} \partial_t \nu - \partial_x \Upsilon_d^0(x,t)\partial_\xi \nu = 0, \\ \dfrac{\mathrm{d}}{\mathrm{d}t}\mu_{jk} = 0. \end{cases} \tag{3.26}$$

This is the time-splitting scheme for (3.23)–(3.24), where ν is the limit of the Wigner transform of ψ^ε on the x variable. This shows that $\Delta t \sim O(1)$ can be chosen independent of the small parameter ε. In turn, this yields the convergence of the scheme towards the corresponding scheme of the limiting equation, as stated in (3.25) and (3.26), uniformly in Δt. Hence it is AP in t.

In summary, the scheme (3.18)–(3.20) is AP in t, y, η with respect to ε. We only need $\Delta x = O(\varepsilon)$.

3.4.4. Numerical experiments

We now present some numerical experiments from Fang *et al.* (2018). The interaction potential is given by

$$V(x,y) = \frac{(x+y)^2}{2}.$$

The one-dimensional SLE system is solved on the interval $x \in [-\pi, \pi]$ and $y, \eta \in [-2\pi, 2\pi]$ with periodic boundary conditions.

Example 3.6. The initial conditions for the SLE system (3.13) are

$$\psi_{\mathrm{in}}(x) = \exp(-25(x+0.2)^2)\exp\left(\frac{-\mathrm{i}\ln(2\cosh(5(x+0.2)))}{5\varepsilon}\right)$$

and

$$\mu_{\mathrm{in}}(y,\eta) = \begin{cases} C_{\mathrm{N}} \exp\left(-\dfrac{1}{1-y^2}\right)\exp\left(-\dfrac{1}{1-\eta^2}\right) & \text{for } |y|<1,\ |\eta|<1, \\ 0 & \text{otherwise.} \end{cases}$$

Here $C_{\mathrm{N}} > 0$ is the normalization factor such that $\iint_{\mathbb{R}^2} \mu_{\mathrm{in}} \mathrm{d}y\, \mathrm{d}\eta = 1$. The time-splitting method with a spectral-upwind scheme is used (*i.e.* with an upwind scheme for the Liouville equation). For $\varepsilon = 1/256, 1/1024, 1/4096$, $T = 0.5$, choose $\Delta x = 2\pi\varepsilon/16$, $\Delta y = \Delta\eta = 4\pi/128$. For each choice of ε, the SLE system is solved first with Δt independent of h and second with $\Delta t = o(\varepsilon)$; specifically, we compare the two cases where $\Delta t = 0.01$ and $\Delta t = \varepsilon/10$, for numerical values of μ (denoted by μ_1 and μ_2 respectively). As shown in Table 3.1, the error is insensitive in ε, showing a uniform-in-ε convergence in $\Delta t, \Delta\eta$ and Δy.

Example 3.7. In this example we choose the same initial data for μ_{in} as in Example 3.6, but

$$\psi_{\mathrm{in}}(x) = \exp(-5(x+0.1)^2)\exp\left(\frac{\mathrm{i}\sin x}{h}\right).$$

https://doi.org/10.1017/S0962492922000010 Published online by Cambridge University Press

Table 3.1. Example 3.6: relative ℓ^2-difference $\|\mu_1 - \mu_2\|_{\ell^2}/\|\mu_2\|_{\ell^2}$ for various ε.

ε	1/256	1/1024	1/4096
$\dfrac{\|\mu_1 - \mu_2\|_{\ell^2}}{\|\mu_2\|_{\ell^2}}$	1.65×10^{-3}	1.69×10^{-3}	1.70×10^{-3}

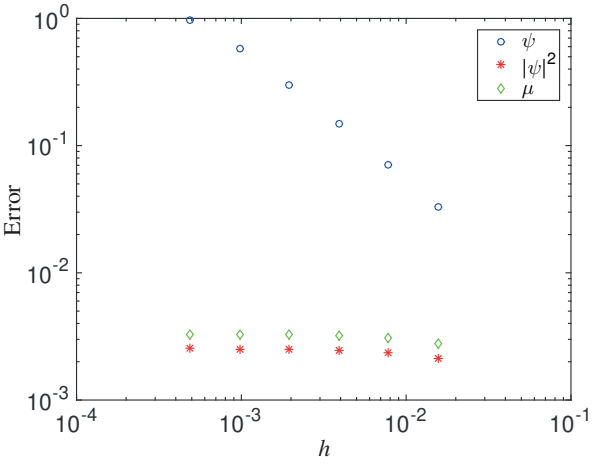

Figure 3.2. Example 3.7: ℓ^2-errors of the wave function ψ^ε, position density $|\psi^\varepsilon|^2$ and μ for various ε. Fix $\Delta t = 0.01$. For $h = 1/64, 1/128, 1/256, 1/512, 1/1024, 1/2048$, choose $\Delta x = 2\pi\varepsilon/16$. The reference solution is computed with $\Delta t = \varepsilon/10$.

Now fix $\Delta t = 0.01$, a stopping time $T = 0.4$, and $\Delta y = \Delta\eta = 4\pi/128$, while $\Delta x = 2\pi\varepsilon/16$, for $\varepsilon = 1/64, 1/128, 1/256, 1/512, 1/1024, 1/2048$. The reference solution is computed with $\Delta t = h/10$. From the ℓ^2-error plotted in Figure 3.2, one can see that although the error in the wave function increases as ε decreases, the error for the position density $|\psi^\varepsilon|^2$, as well as for the macroscopic quantity μ, does not change noticeably. This shows that ε-independent $\Delta t, \Delta y$ and $\Delta\eta$ can be taken to accurately obtain physical observables, but not the wave function ψ^ε itself.

4. Numerical passages from classical mechanics to kinetic equations

4.1. The random batch methods

Consider the second-order interacting particle systems described by

$$\begin{aligned} \mathrm{d}r_i &= v_i\,\mathrm{d}t, \\ \mathrm{d}v_i &= \left[b(r_i) + \alpha_N \sum_{j:j\neq i} K(r_i - r_j) - \gamma v_i\right]\mathrm{d}t + \sigma\,\mathrm{d}W_i, \end{aligned} \tag{4.1}$$

https://doi.org/10.1017/S0962492922000010 Published online by Cambridge University Press

and the first-order system described by

$$\mathrm{d}r_i = b(r_i)\,\mathrm{d}t + \alpha_N \sum_{j:j\neq i} K_1(r_i - r_j)\,\mathrm{d}t + \sigma\,\mathrm{d}W_i, \quad i = 1, 2, \ldots, N. \tag{4.2}$$

The main difficulty for the numerical simulations of particle system (4.1) or (4.2) is that for larger N, the computational cost per time step is $O(N^2)$. The fast multipole method (FMM) (Rokhlin 1985) reduces the complexity to $O(N)$ if the interaction decays sufficiently rapidly. However, the implementation of the FMM is quite delicate. A simple random algorithm, called the random batch method (RBM), has been proposed in Jin, Li and Liu (2020*a*) to reduce the computation cost per time step from $O(N^2)$ to $O(N)$. The key idea of the RBM is to use a randomly chosen 'mini-batch' in the summation term in (4.2) and (4.1). Such an idea has its origin in the stochastic gradient descent (SGD) method. The idea was also used for the computation of the mean-field flocking model (Albi and Pareschi 2013, Carrillo, Pareschi and Zanella 2019).

Let $T > 0$ be the simulation time, and we choose a time step $\Delta t > 0$. Pick a batch size $2 \le p \ll N$ that divides N. Consider the discrete time grids $t_k := k\Delta t$, $k \in \mathbb{N}$. For each sub-interval $[t_{k-1}, t_k)$, the method has two substeps: (1) at t_{k-1}, randomly group the N particles into $n := N/p$ subgroups (batches); (2) particles only interact with those in the same batch. This is given in Algorithm 1.

Algorithm 1 (RBM for (4.1))

for m in $1 : [T/\Delta t]$ **do**
  Divide $\{1, 2, \ldots, N = pn\}$ into n batches $\mathcal{C}_q$, $1 \le q \le n$ randomly.
  for each batch $\mathcal{C}_q$ **do**
    Update r_i, v_i $(i \in \mathcal{C}_q)$ by solving the following for $t \in [t_{m-1}, t_m)$:

$$\begin{aligned} \mathrm{d}r_i &= v_i\,\mathrm{d}t, \\ \mathrm{d}v_i &= \left[b(r_i) + \frac{\alpha_N(N-1)}{p-1} \sum_{j\in\mathcal{C}_q, j\neq i} K(r_i - r_j) - \gamma v_i \right] \mathrm{d}t + \sigma\,\mathrm{d}W_i. \end{aligned} \tag{4.3}$$

  end for
end for

The RBM uses the random permutation, and each particle belongs to one and only one batch. An alternative approach, which allows replacement, is Algorithm 2.

Unlike Algorithm 1, in Algorithm 2, for one iteration of k, some particles may not be updated while some may be drawn more than once.

The random division into n batches of equal size can be implemented using random permutation, which can be realized in $O(N)$ operations by Durstenfeld's modern revision of Fisher–Yates shuffle algorithm (Durstenfeld 1964) (in MATLAB, one can use 'randperm(N)'). The ODE solver per particle per time step in

https://doi.org/10.1017/S0962492922000010 Published online by Cambridge University Press

Algorithm 2 (RBM-r)

for m in $1:[T/\Delta t]$ **do**
  for k from 1 to N/p **do**
    Pick a set $\mathcal{C}_k$ of size p randomly with replacement.
    Update r_i $(i \in \mathcal{C}_k)$ by solving the following SDE for time Δt:

$$\begin{cases} \mathrm{d}x_i = u_i\,\mathrm{d}t, \\ \mathrm{d}u_i = \left[b(x_i) + \dfrac{\alpha_N(N-1)}{p-1} \displaystyle\sum_{j\in\mathcal{C}_k, j\neq i} K(x_i - x_j) - \gamma u_i \right] \mathrm{d}t + \sigma\,\mathrm{d}W_i. \\ x_i(0) = r_i, \quad u_i(0) = v_i, \end{cases} \tag{4.4}$$

    i.e. solve (4.4) with initial values $x_i(0) = r_i, u_i(0) = v_i$, and set $r_i \leftarrow x_i(\Delta t)$, $v_i \leftarrow u_i(\Delta t)$.
  end for
end for

(4.3) or (4.4) requires merely $O(p)$ operations, thus for all particles, each time step costs only $O(pN)$. Since $p \ll N$ the overall cost per time step is significantly reduced from $O(N^2)$ to basically $O(N)$.

For the RBM to really gain significant efficiency, we need Δt to be *independent* of N. We state an error estimate on the RBM for the second-order systems (4.1) in the mean-field regime (*i.e.* $\alpha_N = 1/(N-1)$) from Jin, Li and Sun (2020*b*), which was built upon the argument for the first-order system in Jin *et al.* (2020*a*).

Let $(\tilde{r}_i, \tilde{v}_i)$ denote the solutions to the random batch process (4.3) with the Brownian motion used being $\tilde{W}_i$. Consider the synchronization coupling

$$r_i(0) = \tilde{r}_i(0) \sim \mu_0, \quad W_i = \tilde{W}_i. \tag{4.5}$$

Let $\mathbb{E}$ denote the expected value, namely integration on Ω with respect to the probability measure $\mathbb{P}$, and consider the $L^2(\cdot)$-norm of a random variable

$$\|\zeta\| = \sqrt{\mathbb{E}|\zeta|^2}. \tag{4.6}$$

For finite time intervals, the error of the RBM is given by the following theorem.

Theorem 4.1. Let $b(\cdot)$ be Lipschitz-continuous, and assume that $|\nabla^2 b|$ has polynomial growth, and the interaction kernel K is Lipschitz-continuous. Then

$$\sup_{t\in[0,T]} \sqrt{\mathbb{E}|\tilde{r}_i(t) - r_i(t)|^2 + \mathbb{E}|\tilde{v}_i(t) - v_i(t)|^2} \le C(T)\sqrt{\frac{\Delta t}{p-1} + (\Delta t)^2}, \tag{4.7}$$

where $C(T)$ is independent of N.

The RBM has also been proposed for interacting particle systems used as a sampling method for the invariant measure of (4.1) (Li *et al.* 2020*a*, Li, Xu and Zhao 2020*b*, Jin and Li 2020). In these applications, the long-time behaviour, and

https://doi.org/10.1017/S0962492922000010 Published online by Cambridge University Press

in particular the convergence to the invariant measure, is of interest. For such an analysis some additional contraction assumptions are needed.

Assumption 1. Assume $b = -\nabla V$ for some $V \in C^2(\mathbb{R}^d)$ that is bounded from below (*i.e.* $\inf_x V(x) > -\infty$), and there exist $\lambda_M \geq \lambda_m > 0$ such that the eigenvalues of $H := \nabla^2 V$ satisfy

$$\lambda_m \leq \lambda_i(x) \leq \lambda_M \quad \text{for all } 1 \leq i \leq d,\ x \in \mathbb{R}^d.$$

The interaction kernel K is bounded and Lipschitz-continuous. Moreover, the friction γ and the Lipschitz constant L of $K(\cdot)$ satisfy

$$\gamma > \sqrt{\lambda_M + 2L}, \quad \lambda_m > 2L. \tag{4.8}$$

Then the following uniform strong convergence estimate holds (Jin *et al.* 2020*b*).

Theorem 4.2. Under Assumption 1 and the coupling (4.5), the solutions to (4.1) and (4.3) satisfy

$$\sup_{t\geq 0} \sqrt{\mathbb{E}|\tilde{r}_i(t) - r_i(t)|^2 + \mathbb{E}|\tilde{v}_i(t) - v_i(t)|^2} \leq C\sqrt{\frac{\Delta t}{p-1} + (\Delta t)^2}, \tag{4.9}$$

where the constant C does not depend on p and N.

The RBM error and (4.9) are independent of N, in the mean-field regime, so the RBM is AP in particle number N in this regime.

4.1.1. An illustration: Dyson Brownian motion

The following example is from Jin *et al.* (2020*a*). Consider a typical example in random matrix theory, where we are interested in solving the following system of SDEs ($1 \leq j \leq N$), called the Dyson Brownian motion:

$$\mathrm{d}\lambda_j(t) = -\beta\lambda_j(t)\,\mathrm{d}t + \frac{1}{N}\sum_{k:k\neq j}\frac{1}{\lambda_j - \lambda_k}\,\mathrm{d}t + \frac{1}{\sqrt{N}}\,\mathrm{d}W_j, \tag{4.10}$$

where the $\{W_j\}$ are independent standard Brownian motions. The system can be used to find the eigenvalues of a Hermitian-valued Ornstein–Uhlenbeck process. The Brownian motion effect is small when N is large. The limiting equation for $N \to \infty$ is given by

$$\partial_t \rho(x,t) + \partial_x(\rho(u - \beta x)) = 0, \quad u(x,t) = \pi(H\rho)(x,t), \tag{4.11}$$

where ρ is the density for λ as $N \to \infty$, $H(\cdot)$ is the Hilbert transform on $\mathbb{R}$, and $\pi = 3.14\ldots$ is the circumference ratio.

For $\beta = 1$, it can be shown that the corresponding limiting equation (4.11) has an invariant measure, given by the semicircle law:

$$\rho(x) = \frac{1}{\pi}\sqrt{2 - x^2}. \tag{4.12}$$

https://doi.org/10.1017/S0962492922000010 Published online by Cambridge University Press

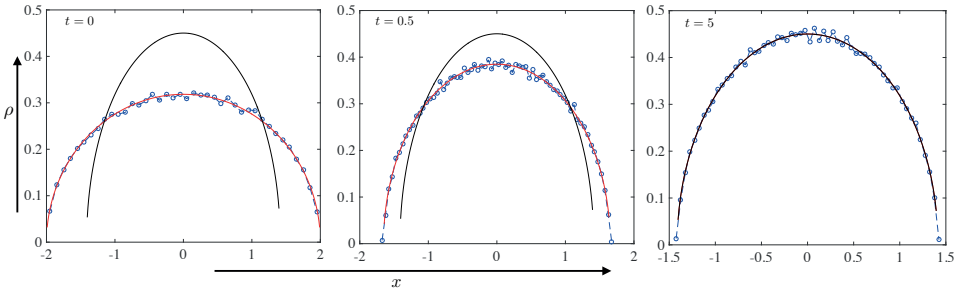

Figure 4.1. RBM solution (circles) of the Dyson Brownian motion. The empirical densities at various times are plotted. The red curve is the density distribution predicted by the analytic solution (4.13). The black curve is the equilibrium semicircle law (4.12).

To test the behaviour of the RBM numerically, note an analytic solution to the limiting equation (4.11):

$$\rho(x,t) = \frac{\sqrt{2\sigma(t) - x^2}}{\sigma(t)\pi}, \quad \sigma(t) = 1 + \mathrm{e}^{-2t}. \tag{4.13}$$

For each iteration, the force is singular and a splitting strategy is adopted. Specifically, define

$$X^{ij} := X^i - X^j. \tag{4.14}$$

The RBM is implemented as follows:

$$Y_m^i = \frac{1}{2}(X_{m-1}^i + X_{m-1}^j) + \mathrm{sgn}(X_{m-1}^{ij})\sqrt{|X_{m-1}^{ij}|^2 + 4\Delta t},$$
$$Y_m^j = \frac{1}{2}(X_{m-1}^i + X_{m-1}^j) - \mathrm{sgn}(X_{m-1}^{ij})\sqrt{|X_{m-1}^{ij}|^2 + 4\Delta t}$$

and

$$X_m^i = Y_m^i - \Delta t Y_m^i + \sqrt{\frac{\Delta t}{N}} z^i, \quad X_m^j = Y^j(t_m) - \Delta t Y_m^j + \sqrt{\frac{\Delta t}{N}} z^j.$$

Here $z^i, z^j \sim \mathcal{N}(0,1)$.

Figure 4.1 shows that the RBM captures the evolution of distribution and the equilibrium semicircle law (4.12), as desired. RBM-r also has similar behaviour.

4.1.2. The mean-field limit of the RBM

To further understand the behaviour of the RBM, when N is large, it will be interesting to investigate its mean-field limit. To this end, consider the RBM for the first-order system (4.2) with $\alpha_N = 1/(N-1)$.

Intuitively, when $N \gg 1$, the probability that two chosen particles are correlated is very small. Hence, in the $N \to \infty$ limit, two chosen particles will be independent

https://doi.org/10.1017/S0962492922000010 Published online by Cambridge University Press

with probability 1. Due to the exchangeability, the marginal distributions of the particles will be identical. Based on this observation, Jin and Li (2022*a*) derived and proved the mean-field limit given in Algorithm 3.

Algorithm 3 (mean-field dynamics of the RBM for the first-order system (4.2))

1: $\tilde{\mu}(\cdot, t_0) = \mu_0$.
2: **for** $k \geq 0$ **do**
3: Let $\rho^{(p)}(\ldots, 0) = \tilde{\mu}(\cdot, t_k)^{\otimes p}$ be a probability measure on $(\mathbb{R}^d)^p \cong \mathbb{R}^{pd}$.
4: Evolve the measure $\rho^{(p)}$ to find $\rho^{(p)}(\ldots, \Delta t)$ via the following Fokker–Planck equation:

$$\partial_t \rho^{(p)} = -\sum_{i=1}^{p} \nabla_{x_i} \cdot \left(\left[b(x_i) + \frac{1}{p-1} \sum_{j=1, j\neq i}^{p} K_1(x_i - x_j) \right] \rho^{(p)} \right) + \frac{1}{2}\sigma^2 \sum_{i=1}^{p} \Delta_{x_i} \rho^{(p)}. \tag{4.15}$$

5: Set

$$\tilde{\mu}(\cdot, t_{k+1}) := \int_{(\mathbb{R}^d)^{\otimes(p-1)}} \rho^{(p)}(\cdot, \mathrm{d}y_2, \ldots, \mathrm{d}y_p, \Delta t). \tag{4.16}$$

6: **end for**

The dynamics in Algorithm 3 naturally gives a non-linear operator $\mathcal{G}_\infty : \mathbf{P}(\mathbb{R}^d) \to \mathbf{P}(\mathbb{R}^d)$ as

$$\tilde{\mu}(\cdot, t_{k+1}) =: \mathcal{G}_\infty(\tilde{\mu}(\cdot, t_k)). \tag{4.17}$$

Corresponding to this is the following SDE system for $t \in [t_k, t_{k+1})$:

$$\mathrm{d}mx_i = b(mx_i)\,\mathrm{d}t + \frac{1}{p-1} \sum_{j=1, j\neq i}^{p} K_1(mx_i - mx_j)\,\mathrm{d}t + \sigma\,\mathrm{d}mW_i, \quad i = 1, \ldots, p, \tag{4.18}$$

with $\{mx_i(t_k)\}$ drawn i.i.d. from $\tilde{\mu}(\cdot, t_k)$.

Hence, in the mean-field limit of the RBM, we start with a configuration in molecular chaos, then the p particles evolve by interacting with each other. We take the first marginal of this new p-particle distribution, and at the starting point of the next time interval, we impose the molecular chaos condition so that the particles are independent again.

Furthermore, Jin and Li (2022*a*) proved that this mean-field limit is $O(\Delta t)$ distant (in the Wasserstein-1 sense) from the mean-field limit of the original particle system (2.30), thus completing the AP diagram in Figure 1.2.

4.2. Molecular dynamics

One of the most important interacting particle systems is molecular dynamics (MD), which simulates the dynamics or equilibrium properties of a large system of atoms and molecules using Newton's second law. It has a wide range of applications, such

https://doi.org/10.1017/S0962492922000010 Published online by Cambridge University Press

as chemical physics, soft materials and biophysics (Ciccotti, Frenkel and McDonald 1987, Frenkel and Smit 2001). Here we review an interesting application of the RBM to MD simulation, called random batch Ewald (Jin, Li, Xu and Zhao 2021*a*), which achieves $O(N)$ complexity with high parallel efficiency (Liang *et al.* 2022).

The equations of motion governing N 'molecules' with masses m_i are given by

$$\begin{aligned} \mathrm{d}r_i &= v_i \,\mathrm{d}t, \\ m_i \,\mathrm{d}v_i &= \left[-\sum_{j:j\neq i} \nabla\phi(r_i - r_j) \right] \mathrm{d}t + \sigma_i \,\mathrm{d}W_i. \end{aligned} \tag{4.19}$$

Here the W_i are noise or other external forcing terms, and $\phi(\cdot)$ is the Coulomb potential

$$\phi(x) = \frac{q_i q_j}{r},$$

where q_i is the charge for the ith particle and $r = |x|$. Another popular potential often used is the Lennard-Jones potential (Frenkel and Smit 2001):

$$\phi(x) = 4\left(\frac{1}{r^{12}} - \frac{1}{r^6} \right). \tag{4.20}$$

Between ions, both types of potential exist, and between charge-neutral molecules, the Lennard-Jones potential might be the main force.

4.2.1. RBM with kernel splitting

Due to the singularity at $x = 0$ of the Lennard-Jones potential (4.20), a direct application of the RBM could give poor results. One effective strategy is to decompose the K into two parts (Martin, Chen and Siepmann 1998, Hetenyi, Bernacki and Berne 2002),

$$K(x) = K_1(x) + K_2(x). \tag{4.21}$$

Here K_1 has a short range that decays quickly, so it can be ignored for $|x| \geq r_0$, for some r_0 chosen to be comparable to the mean distance of the particles. $K_2(x)$ is a bounded smooth function. We then apply the RBM to the K_2 part only (Li *et al.* 2020*b*).

4.2.2. Random batch Ewald: importance sampling

The Coulomb interaction is a long-range interaction, which decays slowly as $1/r$ and in the meantime contains a singularity at $r = 0$. The bottleneck in MD simulation lies in the expensive simulation of the Coulomb interaction, which has computational complexity $O(N^2)$. Some popular methods include particle–particle particle–mesh Ewald (PPPM) (Luty, Davis, Tironi and Van Gunsteren 1994, Deserno and Holm 1998), and multipole-type methods such as treecode (Barnes and Hut 1986, Duan and Krasny 2000) and fast multipole methods (FMM) (Greengard and Rokhlin 1987, Ying, Biros and Zorin 2004). These methods can

https://doi.org/10.1017/S0962492922000010 Published online by Cambridge University Press

reduce the complexity per time step from $O(N^2)$ to $O(N \log N)$ or even $O(N)$, and have achieved great success in practice. However, some issues still remain to be resolved; for example, the prefactor in the linear scaling can be large, or the implementation can be non-trivial, or the scalability for parallel computing is not high.

The RBE method is based on the Ewald splitting for the Coulomb kernel with a random 'mini-batch' technique applied in the Fourier series for the long-range part.

Solids or fluids with large volume are usually modelled in a box with length L, with periodic conditions. Consider N particles with net charge q_i $(1 \le i \le N)$ under the electroneutrality condition

$$\sum_{i=1}^{N} q_i = 0. \tag{4.22}$$

The forces are computed using $F_i = -\nabla_{r_i} U$, where U is the Coulomb potential energy, with periodic boundary condition, given by

$$U = \frac{1}{2} \sum_{n}{}' \sum_{i,j=1}^{N} q_i q_j \frac{1}{|r_{ij} + nL|}, \tag{4.23}$$

where $n \in \mathbb{Z}^3$. $\sum'$ is defined such that $n = 0$ is not included when $i = j$.

The classical Ewald summation decomposes $1/r$ into long-range smooth parts and short-range singular parts:

$$\frac{1}{r} = \frac{\operatorname{erf}(\sqrt{\alpha} r)}{r} + \frac{\operatorname{erfc}(\sqrt{\alpha} r)}{r}, \tag{4.24}$$

where

$$\operatorname{erf}(x) := \frac{2}{\sqrt{\pi}} \int_0^x \exp(-u^2)\, \mathrm{d}u$$

is the error function and $\operatorname{erfc} = 1 - \operatorname{erf}$. Correspondingly, $U = U_1 + U_2$ with

$$\begin{aligned} U_1 &= \frac{1}{2} \sum_{n}{}' \sum_{i,j} q_i q_j \frac{\operatorname{erf}(\sqrt{\alpha}|r_{ij} + nL|)}{|r_{ij} + nL|}, \\ U_2 &= \frac{1}{2} \sum_{n}{}' \sum_{i,j} q_i q_j \frac{\operatorname{erfc}(\sqrt{\alpha}|r_{ij} + nL|)}{|r_{ij} + nL|}, \end{aligned} \tag{4.25}$$

where U_2 corresponds to the short-range forces, which is inexpensive, while U_1 is the long-range part that will be put into the Fourier space

$$U_1 = \frac{2\pi}{V} \sum_{k \neq 0} \frac{1}{k^2} |\rho(k)|^2 \, \mathrm{e}^{-k^2/4\alpha} - \sqrt{\frac{\alpha}{\pi}} \sum_{i=1}^{N} q_i^2, \tag{4.26}$$

https://doi.org/10.1017/S0962492922000010 Published online by Cambridge University Press

where $\rho(k) := \sum_{i=1}^{N} q_i \, \mathrm{e}^{\mathrm{i}k\cdot r_i}$. Then

$$F_{i,1} = -\nabla_{r_i} U_1 = -\sum_{k\neq 0} \frac{4\pi q_i k}{Vk^2} \, \mathrm{e}^{-k^2/(4\alpha)} \, \mathrm{Im}(\mathrm{e}^{-\mathrm{i}k\cdot r_i} \rho(k)), \tag{4.27}$$

where $r_{ij} = r_j - r_i$, is bounded for small k. The key idea of RBE is to do *importance sampling* according to the discrete Gaussian distribution $\mathrm{e}^{-k^2/(4\alpha)}$. Denote

$$S := \sum_{k\neq 0} \mathrm{e}^{-k^2/(4\alpha)} = H^3 - 1, \tag{4.28}$$

where

$$H := \sum_{m\in\mathbb{Z}} \mathrm{e}^{-\pi^2 m^2/(\alpha L^2)} = \sqrt{\frac{\alpha L^2}{\pi}} \sum_{m=-\infty}^{\infty} \mathrm{e}^{-\alpha m^2 L^2} \approx \sqrt{\frac{\alpha L^2}{\pi}} (1 + 2\,\mathrm{e}^{-\alpha L^2}), \tag{4.29}$$

since often $\alpha L^2 \gg 1$. Hence S is the sum for all three-dimensional vectors k except 0. Then we can regard the sum as an expectation over the probability distribution

$$\mathscr{P}_k := S^{-1} \, \mathrm{e}^{-k^2/(4\alpha)}, \tag{4.30}$$

which, with $k \neq 0$, is a discrete Gaussian distribution that can be sampled efficiently *offline*. Once the time evolution starts, we just need to randomly draw a few ($O(p)$) samples for each time step from this pre-sampled Gaussian sequence.

Ultimately, the force $F_{i,1}$ in (4.27) will be calculated by the following mini-batch random variable:

$$F_{i,1} \approx F_{i,1}^{*} := -\sum_{\ell=1}^{p} \frac{S}{p} \frac{4\pi k_\ell q_i}{Vk_\ell^2} \mathrm{Im}(\mathrm{e}^{-\mathrm{i}k_\ell \cdot r_i} \rho(k_\ell)). \tag{4.31}$$

The PPPM method uses the fast Fourier transform, while RBE uses random mini-batch to speed up the computation in the Fourier space. The complexity of RBE for the real space part is $O(N)$. By choosing the *same batch* of frequencies for all forces (4.31) (*i.e.* using the same k_ℓ, $1 \leq \ell \leq p$ for all $F_{i,1}^{*}$, $1 \leq i \leq N$) in the same time step, the complexity per iteration for the frequency part is reduced to $O(pN)$. Therefore the RBE method has linear complexity per time step if we choose $p = O(1)$.

Another advantage of RBE is that there are few particle interactions at each iteration. This significantly reduces the amount of message passing when many CPUs are used for parallel computing, so we achieve remarkable scalability (Liang *et al.* 2022).

To illustrate the performance of the RBE method, consider an electrolyte with monovalent binary ions (first example in Jin *et al.* 2021*a*). In the reduced units (Frenkel and Smit 2001, section 3.2), the dielectric constant is taken as $\varepsilon = 1/4\pi$ so that the potential of a charge is $\phi(r) = q/r$ and the temperature is $T = \beta^{-1} = 1$. Under the Debye–Hückel (DH) theory (linearized Poisson–Boltzmann equation),

https://doi.org/10.1017/S0962492922000010 Published online by Cambridge University Press

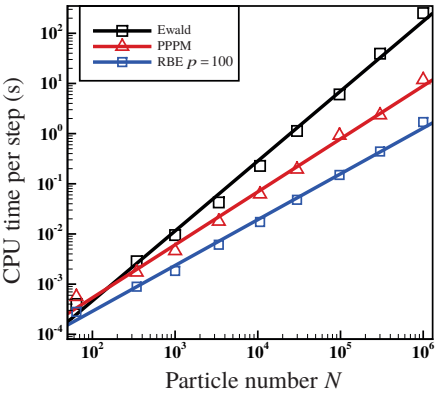

Figure 4.2. Comparison of the Ewald sum, PPPM and RBE methods.

the charge potential outside one ion is given by

$$-\varepsilon\Delta\phi = \begin{cases} 0 & r < a, \\ q\rho_{\infty,+}\, \mathrm{e}^{-\beta q\phi} - q\rho_{\infty,-}\, \mathrm{e}^{\beta q\phi} \approx \beta q^2 \rho_r \phi & r > a, \end{cases}$$

where $\rho_{\infty,+} = \rho_{\infty,-} = N/(2V)$ are the densities of the positive and negative ions at infinity, both being $\rho_r/2$. The parameter a is the effective diameter of the ions, which is related to the setting of the Lennard-Jones potential. In the simulations, $a = 0.2$ and the setting of Lennard-Jones potential can be found in Jin *et al.* (2021*a*). This approximation gives the net charge density $\rho = -\varepsilon\Delta\phi$ for $r \gg a$,

$$\ln(r\rho(r)) \approx -1.941r - 1.144.$$

Figure 4.2 shows the CPU time consumed for different particle numbers inside the box with the same side length $L = 10$. Both the PPPM and RBE methods scale linearly with the particle numbers. However, even for batch size $p = 100$, the RBE method consumes much less time. Clearly the RBE method has the same level of accuracy compared with the PPPM method for the densities considered.

Next, Figure 4.3 shows the parallel efficiency of the PPPM and RBE methods from Liang *et al.* (2022) for the all-atom simulation of pure water systems. As can be seen, due to the reduction of communications for the particles, the RBE method gains better parallel efficiency. This parallel efficiency is more obvious when the number of particles is larger. In Liang *et al.* (2022), the simulation results of pure water systems also indicate that RBE-type methods are not only able to sample from the equilibrium distribution but can also compute the dynamical properties of pure water systems accurately.

For a comprehensive review of the RBM and its extensions and applications, see the recent review by Jin and Li (2022*b*).

https://doi.org/10.1017/S0962492922000010 Published online by Cambridge University Press

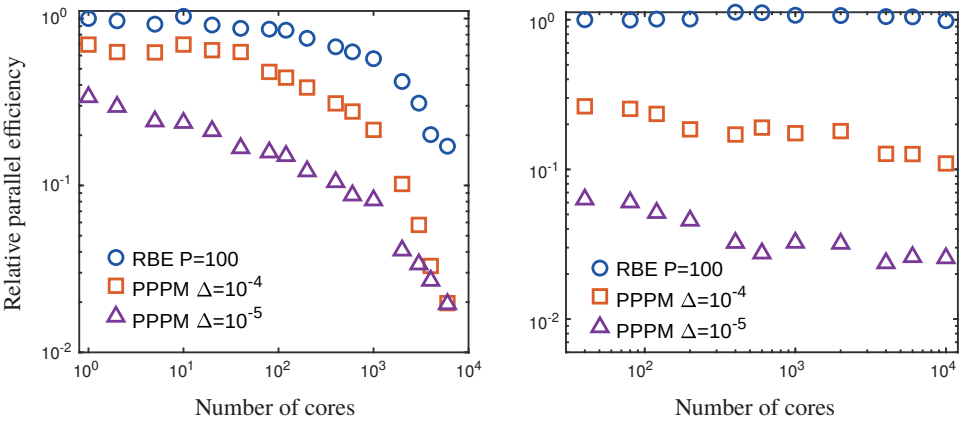

Figure 4.3. Parallel efficiency of the PPPM and RBE methods for all-atom simulation of pure water systems: (a) 3×10^5 atoms, (b) 3×10^7 atoms.

5. Numerical passages from kinetic equations to hydrodynamic equations

The multiscale problems that involve both kinetic and hydrodynamic scales occur in many physical settings. For example, in a nuclear reactor, neutrons may conduct a significant amount of scattering in the diffusive regime. In the space shuttle re-entry problem, the mean-free path could vary from $O(1)$ m to $O(10^{-8})$ m when the vehicle passes from the free-streaming regime to the rarefied gas regime (described by the Boltzmann equation) and then to the transition regimes and eventually to the hydrodynamic regime (described by the Euler or Navier–Stokes equations) (Rivell 2006). It is also known that in hypersonic flows (Mach number larger than 1.4), the shock profile of the Navier–Stokes equations does not give an accurate shock width, so we need to use the Boltzmann equation in the shock region (Foch 1973, Agarwal, Yun and Balakrishnan 1999). In plasma physics, the Debye length might be small, and we need to deal with quasi-neutral regimes (Fornberg 1996, Degond and Deluzet 2017). In all these kinetic problems we need to deal with multiple time and space scales.

Kinetic theory is the area in which the concept of AP was first introduced, and also most successfully and extensively used. Earlier efforts in this direction concentrated on time-independent transport equations that have diffusive behaviour (Larsen *et al.* 1987, Larsen and Morel 1989). However, for multiscale kinetic equations the main challenges lie in time discretizations, due to the stiffness, non-locality and nonlinearity of the collision operators.

The term 'asymptotic-preserving' was first coined in Jin (1999). An AP scheme typically possesses the following key features for multiscale kinetic equations.

https://doi.org/10.1017/S0962492922000010 Published online by Cambridge University Press

- Implicit time discretization that can be either explicitly or easily implemented: for example, it at least avoids complicated non-linear algebraic system solvers such as Newton's iteration.
- When the Knudsen number $\varepsilon \to 0$, the scheme for the kinetic equations automatically becomes a good scheme for the limiting hydrodynamic equations.

AP schemes are also related to the development of kinetic schemes for compressible Euler equations, which was based on discretizing a linear kinetic equation thanks to its linear convection, followed by a projection to the local Maxwellian (Deshpande 1986, Perthame 1990, Prendergast and Xu 1993). It is also relevant to the lattice Boltzmann approximation to incompressible Navier–Stokes equations (Chen, Chen and Matthaeus 1992, Chen and Doolen 1998, Qian, d'Humières and Lallemand 1992, He and Luo 1997). Relaxation schemes for non-linear hyperbolic systems also share a similar spirit (Jin and Xin 1995). Below we review a few representative AP schemes.

5.1. *The BGK penalization method*

We are mainly interested in dealing with the numerical difficulties when the Knudsen number $\varepsilon \ll 1$. The first challenge is numerical stiffness, which puts severe constraints on Δt. In order to allow $\Delta t \gg \varepsilon$, we need some implicit treatment for the non-local, non-linear collision operator, which is numerically non-trivial.

The *penalization method*, introduced by Filbet and Jin (2010), was the first AP scheme for the non-linear Boltzmann equation that overcomes the stiffness issue of the collision operator. The idea is to penalize $\mathcal{Q}(f)$ by the BGK operator $\beta(\mathcal{M} - f)$:

$$\partial_t f + v \cdot \nabla_x f = \underbrace{\frac{\mathcal{Q}(f) - \beta(\mathcal{M} - f)}{\varepsilon}}_{\text{less stiff, explicit}} + \underbrace{\frac{\beta(\mathcal{M} - f)}{\varepsilon}}_{\text{stiff, explicit}}, \tag{5.1}$$

where β is some constant suitably chosen to approximate the Fréchet derivative of $\mathcal{Q}(f)$ around $\mathcal{M}$, such that terms in the first brace become less stiff or non-stiff and can be treated explicitly. The other part is a BGK operator, which can be inverted *explicitly* (Coron and Perthame 1991), thanks to the conservation properties of the collision terms on the right-hand side of (5.1).

A first-order IMEX (implicit–explicit) discretization of (5.1) can be written as

$$\frac{f^{n+1} - f^n}{\Delta t} + v \cdot \nabla_x f^n = \frac{\mathcal{Q}(f^n) - \beta(\mathcal{M}^n - f^n)}{\varepsilon} + \frac{\beta(\mathcal{M}^{n+1} - f^{n+1})}{\varepsilon}. \tag{5.2}$$

Taking the moments $\int_{\mathbb{R}^d} \cdot \phi(v)\, \mathrm{d}v$, with $\phi(v)$ defined in (2.36) on both sides of (5.2), and using the properties (2.36), we get

$$\frac{\langle f \rangle^{n+1} - \langle f \rangle^n}{\Delta t} + \nabla_x \cdot \langle v f \rangle^n = 0, \tag{5.3}$$

https://doi.org/10.1017/S0962492922000010 Published online by Cambridge University Press

where $\langle\cdot\rangle = \int \phi(v)\cdot \mathrm{d}v$ means the moments. From (5.3) we can solve for the moments ρ, u and T at $t = t^{n+1}$, so $\mathcal{M}^{n+1}$ is obtained. Then f^{n+1} can be obtained from (5.2) explicitly. Note that the entire process is *explicit*!

In practice, β can be roughly estimated as

$$\beta = \sup_v |\mathcal{Q}^-(f)|,$$

where $\mathcal{Q}^-$ is the loss part of the collision operator defined such that $\mathcal{Q}(f) = \mathcal{Q}^+(f) - f\mathcal{Q}^-(f)$. β can also be made time- and space-dependent for better numerical accuracy (Yan and Jin 2013).

To capture the compressible Euler limit, a necessary condition is that, as $\varepsilon \to 0$,

$$f^n = \mathcal{M}^n, \quad \text{for any } n, \quad \text{with } \Delta t, \Delta x \text{ fixed.}$$

Filbet and Jin (2010) showed formally that

$$\text{for } \varepsilon \ll 1, \quad \text{if } f^n = \mathcal{M}^n + O(\varepsilon), \quad \text{then } f^{n+1} = \mathcal{M}^{n+1} + O(\varepsilon).$$

Numerical experiments in Filbet and Jin (2010) show that, regardless of the initial condition f^0, there exists an integer $N > 0$ such that

$$f^n = \mathcal{M}^n + O(\varepsilon) \quad \text{for any } n \geq N. \tag{5.4}$$

Substituting (5.4) into (5.2) and taking the moments, we have

$$\frac{\langle f\rangle^{n+1} - \langle f\rangle^n}{\Delta t} + \nabla_x \cdot \int_{\mathbb{R}^d} v\phi(v)\,\mathcal{M}^n\,\mathrm{d}v = O(\varepsilon) \quad \text{for any } n \geq N,$$

which is a consistent discretization to the limiting Euler system (2.38). This means the scheme is AP after an initial transient time.

Remark 5.1. One possible way to remove the initial layer problem and hence achieve AP in one time step was suggested in Yan and Jin (2013), where the idea is to perform the penalization in two successive steps:

$$\begin{cases} \dfrac{f^* - f^n}{\Delta t} + v\cdot\nabla_x f^n = \dfrac{\mathcal{Q}(f^n) - \beta(\mathcal{M}^n - f^n)}{\varepsilon} + \dfrac{\beta(\mathcal{M}^* - f^*)}{2\varepsilon}, \\ \dfrac{f^{n+1} - f^*}{\Delta t} = \dfrac{\beta(\mathcal{M}^{n+1} - f^{n+1})}{2\varepsilon}. \end{cases}$$

The idea of using a linear or simpler operator to penalize the non-linear or complicated operator turns out to be a generic approach. For specific problems, we need to seek an appropriate penalization operator. For example, consider the non-linear Fokker–Planck–Landau equation, whose collision operator is given by

$$\mathcal{Q}(f)(v) = \nabla_v \cdot \int_{\mathbb{R}^d} A(v - v_*)\big[f(v_*)\nabla_v f(v) - f(v)\nabla_{v_*} f(v_*)\big]\,\mathrm{d}v_*, \tag{5.5}$$

where A is a semi-positive definite matrix. This equation is relevant to the study

https://doi.org/10.1017/S0962492922000010 Published online by Cambridge University Press

of Coulomb interactions. The diffusive nature of the collision operator introduces more stiffness. An explicit scheme would require $\Delta t = O(\varepsilon(\Delta v)^2)$, where Δv is the mesh size in v, which is even more restrictive than the Boltzmann collision operator. Jin and Yan (2011) proposed the following Fokker–Planck operator as a penalization:

$$\mathcal{P}_{\mathrm{FP}}(f) = \nabla_v \cdot \left(\mathcal{M} \nabla_v \left(\frac{f}{\mathcal{M}} \right) \right).$$

Similar approaches, with variant penalties, have been proposed for the quantum Boltzmann equation (Filbet, Hu and Jin 2012), the quantum Fokker–Planck–Landau equation (Hu, Jin and Yan 2012) and the multi-species Boltzmann equation (Jin and Li 2013).

Another AP scheme for the Boltzmann equation, developed later in Liu, Xu, Sun and Cai (2016), relies on the integral representation of the BGK model. The final form of the scheme also ends up with a linear combination of the Boltzmann collision operator and the BGK operator, with a slightly different combination of coefficients.

5.2. *Exponential integration*

Another class of asymptotic-preserving methods is the *exponential integration method*. This method is based on a reformulation of the equation into an exponential form, with the Maxwellian embedded. This makes it easier to capture the asymptotic limit and other physical properties such as positivity.

For the space-homogeneous Boltzmann equation,

$$\partial_t f = \frac{1}{\varepsilon} \mathcal{Q}(f), \tag{5.6}$$

Dimarco and Pareschi (2011) introduced the following reformulation:

$$\partial_t \left[(f - \mathcal{M}) \, \mathrm{e}^{\beta t/\varepsilon} \right] = \partial_t f \, \mathrm{e}^{\beta t/\varepsilon} + \frac{\beta(f - \mathcal{M})}{\varepsilon} \mathrm{e}^{\beta t/\varepsilon} = \frac{\mathcal{Q} - \beta(\mathcal{M} - f)}{\varepsilon} \mathrm{e}^{\beta t/\varepsilon}. \tag{5.7}$$

Here β is an auxiliary parameter and, as in the penalization method, $\beta(\mathcal{M} - f)$ is used to approximate the Fréchet derivative of $\mathcal{Q}$; β is chosen to be the smallest value that preserves the positivity of f.

Equation (5.7) is fully equivalent to the original problem (5.6). However, it updates the difference between f and $\mathcal{M}$, and the exponential term $\exp(-\beta t/\varepsilon)$ removes the stiffness and numerically forces the convergence between f and $\mathcal{M}$, an essential mechanism for the AP property. It can be easily extended to all explicit Runge–Kutta methods, which are not only of high order but also satisfy the AP property automatically.

The need to convect $\mathcal{M}$ makes it difficult to extend the scheme to the non-homogeneous case. Li and Pareschi (2014) use an evolving Maxwellian function

https://doi.org/10.1017/S0962492922000010 Published online by Cambridge University Press

within each time step. They reformulate the Boltzmann equation as

$$\partial_t[(f-\mathcal{M})\exp(\beta t/\varepsilon)] = \left(\frac{\mathcal{P}-\beta\mathcal{M}}{\varepsilon} - v\cdot\nabla_x f - \partial_t\mathcal{M}\right)\exp(\beta t/\varepsilon), \tag{5.8}$$

while the moment equations are obtained after taking the moments of the original Boltzmann equation (2.31):

$$\partial_t\langle f\rangle + \nabla_x\cdot\langle\phi v f\rangle = 0. \tag{5.9}$$

To compute $\partial_t\mathcal{M}$, note that

$$\partial_t\mathcal{M} = \partial_\rho\mathcal{M}\partial_t\rho + \nabla_u\mathcal{M}\cdot\partial_t u + \partial_T\mathcal{M}\partial_t T, \tag{5.10}$$

where $\partial_\rho\mathcal{M}$, $\nabla_u\mathcal{M}$ can be expressed analytically and $\partial_T\mathcal{M}$ are all explicit. The time derivatives of the other three macroscopic quantities ρ, u, T can be obtained from (5.9).

With this formulation, we can just use the Runge–Kutta time discretization.

This method preserves positivity, high-order accuracy and strong AP properties.

5.3. *Micro–macro decomposition*

The 'micro–macro' decomposition decomposes the density distribution function into the local Maxwellian, plus the deviation

$$f = \mathcal{M} + \varepsilon g, \quad \text{with} \quad \int \phi[f-\mathcal{M}]\,\mathrm{d}v = 0. \tag{5.11}$$

One early approach of using such a decomposition to design an AP scheme for the radiative heat transfer equations was used by Klar and Schmeiser (2001), and it was also used by Liu and Yu (2004) to analyse the shock propagation of the Euler equations in passing the fluid limit of the Boltzmann equation. Its application to the non-linear Boltzmann equation started with the work of Bennoune, Lemou and Mieussens (2008).

Define the linearized collision operator around $\mathcal{M}$ as

$$\mathcal{L}_{\mathcal{M}}g = \mathcal{Q}[\mathcal{M}, g] + \mathcal{Q}[g, \mathcal{M}].$$

With some calculation, we get

$$\begin{cases} \partial_t g + (\mathrm{I}-\Pi_{\mathcal{M}})(v\cdot\nabla_x g) - \mathcal{Q}[g,g] = \dfrac{1}{\varepsilon}[\mathcal{L}_{\mathcal{M}}g - (\mathrm{I}-\Pi_{\mathcal{M}})(v\cdot\nabla_x\mathcal{M})], \\ \partial_t\displaystyle\int\phi\mathcal{M}\,\mathrm{d}v + \int\phi v\cdot\nabla_x\mathcal{M}\,\mathrm{d}v + \varepsilon\nabla_x\cdot\langle v\phi g\rangle = 0. \end{cases} \tag{5.12}$$

Here $\Pi_{\mathcal{M}}$ is the projection operator that maps an arbitrary $\mathcal{M}$-weighted L_2-function into the null space of $\mathcal{L}_{\mathcal{M}}$, namely, for any $\psi \in L_2(\mathcal{M}\,\mathrm{d}v)$,

$$\Pi_{\mathcal{M}}(\psi) \in \mathrm{Null}\mathcal{L}_{\mathcal{M}} = \mathrm{Span}\{\mathcal{M}, v\mathcal{M}, |v|^2\mathcal{M}\}. \tag{5.13}$$

https://doi.org/10.1017/S0962492922000010 Published online by Cambridge University Press

For the Boltzmann equation, the projection operator can be written explicitly as

$$\Pi_{\mathcal{M}}(\psi) = \frac{1}{\rho}\left[\langle\psi\rangle + \frac{(v-u)\cdot\langle(v-u)\psi\rangle}{T} + \left(\frac{|v-u|^2}{2T} - \frac{d}{2}\right)\frac{2}{d}\left\langle\left(\frac{|v-u|^2}{2T} - \frac{d}{2}\right)\psi\right\rangle\right]\mathcal{M}, \tag{5.14}$$

where $\langle\cdot\rangle$ is the integration over v.

In the original Boltzmann equation, the stiff term $\mathcal{Q}[f,f]$ is quadratic in f, hence difficult to invert. The two stiff terms here are both linear, so their implicit discretization can be inverted more easily. Bennoune *et al.* (2008) took the following discretization:

$$\begin{cases} \dfrac{g^{n+1}-g^n}{\Delta t} + (\mathrm{I}-\Pi_{\mathcal{M}^n})(v\cdot\nabla_x g^n) - \mathcal{Q}[g^n,g^n] = \dfrac{1}{\varepsilon}\big[\mathcal{L}_{\mathcal{M}^n} g^{n+1} \\ \qquad -(\mathrm{I}-\Pi_{\mathcal{M}^n})(v\cdot\nabla_x\mathcal{M}^n)\big], \\ \displaystyle\int \phi\mathcal{M}^{n+1}\,\mathrm{d}v + \Delta t\varepsilon\int \phi v\cdot\nabla_x g^{n+1}\,\mathrm{d}v = \int \phi\mathcal{M}^n\,\mathrm{d}v - \Delta t\int \phi v\cdot\nabla_x\mathcal{M}^n\,\mathrm{d}v. \end{cases} \tag{5.15}$$

The only term that needs to be inverted is $\mathrm{I} - (\Delta t/\varepsilon)\mathcal{L}_{\mathcal{M}}$ in the first equation. It is a linear operator, and the negative spectrum of $\mathcal{L}$ guarantees the invertibility. The quadratic operator $\mathcal{Q}[f,f]$ is no longer stiff and is thus treated explicitly.

The following AP property was proved in Bennoune *et al.* (2008).

Theorem 5.2. The scheme is AP, specifically as follows.

(i) The time discretization (5.15) of the Boltzmann equation (5.12) gives, in the limit $\varepsilon \to 0$, a scheme consistent with the compressible Euler system (2.38).

(ii) For small ε, scheme (5.15) is asymptotically equivalent, up to $O(\varepsilon^2)$, to an explicit time discretization of the Navier–Stokes equations (2.39).

Gamba, Jin and Liu (2019) used the BGK penalization method in the micro–macro decomposition framework to further avoid the inversion of the linearized collision operator $\mathcal{L}$.

5.4. Linear transport equations

5.4.1. AP schemes based on parity equations

We now consider the linear transport equation in the diffusive regime (2.40). Let

$$\mathcal{L}(f) = \int b(v,w)\{M(v)f(w) - M(w)f(v)\}\,\mathrm{d}w.$$

Split (2.40) into two equations, one for v and one for $-v$:

$$\begin{aligned} \varepsilon\,\partial_t f(v) + v\cdot\nabla_x f(v) &= \frac{1}{\varepsilon}\mathcal{L}(f)(v), \\ \varepsilon\,\partial_t f(-v) - v\cdot\nabla_x f(-v) &= \frac{1}{\varepsilon}\mathcal{L}(f)(-v). \end{aligned} \tag{5.16}$$

https://doi.org/10.1017/S0962492922000010 Published online by Cambridge University Press

Define the even and odd parities as

$$r(t,x,v) = \frac{1}{2}\left[f(t,x,v) + f(t,x,-v)\right],$$
$$j(t,x,v) = \frac{1}{2\varepsilon}\left[f(t,x,v) - f(t,x,-v)\right]. \tag{5.17}$$

Adding and subtracting the two equations in (5.16) leads to

$$\partial_t r + v\cdot\nabla_x j = \frac{1}{\varepsilon^2}\mathcal{L}(r), \tag{5.18}$$

$$\partial_t j + \frac{1}{\varepsilon^2} v\cdot\nabla_x r = -\frac{1}{\varepsilon^2}\lambda j, \tag{5.19}$$

where we used the property that

$$\int b(v,w) j(w)\,\mathrm{d}w = 0$$

since $j(w)$ is an odd function in w.

Remark 5.3. If $b(v,w) = b(|v|,|w|)$, then it is possible to use the even and odd parities only for the positive components of v and w, hence reducing the computational domain, as is the case for neutron transport equations (Lewis and Miller 1984).

Since now the convection term is also stiff, the idea of Jin, Pareschi and Toscani (2000) was to rewrite (5.18) and (5.19) in the following form:

$$\partial_t r + v\cdot\nabla_x j = \frac{1}{\varepsilon^2}\mathcal{L}(r), \tag{5.20}$$

$$\partial_t j + v\cdot\nabla_x r = -\frac{1}{\varepsilon^2}\left[\lambda j + (1-\varepsilon^2\psi) v\cdot\nabla_x r\right], \tag{5.21}$$

where $\psi = \psi(\varepsilon)$ is a free parameter satisfying $0 \le \psi \le 1/\varepsilon^2$. Hence the characteristic speeds on the right-hand side are now independent of ε. The simplest choice of ψ is

$$\psi(\varepsilon) = \min\left\{1, \frac{1}{\varepsilon^2}\right\}.$$

(A related approach in Klar (1998) moves all the stiff terms in (5.19) to the right-hand side.)

One can easily derive the diffusion equation from (5.20) and (5.21). As $\varepsilon \to 0$, they give

$$\mathcal{L}(r) = 0, \tag{5.22}$$

$$\lambda j = -v\cdot\nabla_x r. \tag{5.23}$$

Solving (5.22) gives

$$r = \rho(x,t) M(v), \tag{5.24}$$

https://doi.org/10.1017/S0962492922000010 Published online by Cambridge University Press

where

$$\rho(x,t) = \langle f(x,\cdot,t)\rangle = \langle r(x,\cdot,t)\rangle.$$

With (5.24), equation (5.23) gives

$$j = \frac{M(v)}{\lambda(v)}[-v\cdot\nabla_x\rho]. \tag{5.25}$$

Applying (5.24) and (5.25) in (5.20), and integrating over v, we get the diffusion equation (2.41) with (2.42). Thus (5.20) and (5.21) set the foundation for AP schemes. We can split the stiff relaxation step

$$\partial_t r = \frac{1}{\varepsilon^2}\mathcal{L}(r), \tag{5.26}$$

$$\partial_t j = \frac{1}{\varepsilon^2}[-\lambda j - (1-\varepsilon^2\phi)(v\cdot\nabla_x r)], \tag{5.27}$$

from the non-stiff transport step

$$\begin{aligned} &\partial_t r + v\cdot\nabla_x j = 0,\\ &\partial_t j + v\cdot\nabla_x r = 0. \end{aligned} \tag{5.28}$$

Equations (5.28) can be solved using an explicit scheme, whereas for step (5.26)–(5.27) we use an implicit scheme.

The key is how to solve the collision step (5.26) implicitly in an efficient way. In the case of neutron transport, where $L(r) = \rho - r$, the implicit term can be integrated explicitly (Jin *et al.* 2000). Otherwise we can use the penalty method of Filbet and Jin (2010); see Deng (2012).

As far as spatial discretization is concerned, we can use any upwind-type scheme for convection terms in (5.28), while on the right-hand side of (5.27), Jin *et al.* (2000) suggested using centre difference for the gradient of r. When $\varepsilon \to 0$, these spatial discretizations become consistent and stable discretizations of (2.41) and are thus AP spatially. However, the limiting discrete diffusion equation is not compact. In one dimension it is a five-point rather than a three-point discretization of the diffusion equation. This problem can be fixed by using a staggered grid for r and j, as pointed out in Jin and Pareschi (2001) and then extended to two space dimensions in Küpper, Frank and Jin (2016).

One AP scheme developed in Sun, Jiang and Xu (2015) allows us to get a compact three-point scheme in the limit.

5.4.2. AP schemes based on micro–macro decomposition

The micro–macro decomposition approach, proposed by Lemou and Mieussens (2008), begins with the decomposition

$$f = \rho M + \varepsilon g. \tag{5.29}$$

Clearly $\langle g\rangle = 0$. Applying (5.29) in (2.40) gives

$$\varepsilon M\partial_t\rho + \varepsilon^2\partial_t g + v\cdot M\nabla_x\rho + \varepsilon v\cdot\nabla_x g = \mathcal{L}g. \tag{5.30}$$

https://doi.org/10.1017/S0962492922000010 Published online by Cambridge University Press

Integrating this equation with respect to v gives the following continuity equation:

$$\partial_t \rho + \nabla_x \cdot \langle v g \rangle = 0. \tag{5.31}$$

Define operator $\Pi\colon \Pi(\cdot)(v) := M\langle \cdot \rangle$, and I the identity operator. Applying the orthogonal projection $I - \Pi$ to (5.30) gives the equation for g:

$$\varepsilon^2 \partial_t g + \varepsilon (I - \Pi)(v \cdot \nabla_x g) + v \cdot M \nabla_x \rho = \mathcal{L} g. \tag{5.32}$$

Equations (5.31) and (5.32) constitute the micro–macro formulation of (2.40).

We first consider the time discretization. The following was used in Lemou and Mieussens (2008):

$$\frac{g^{n+1} - g^n}{\Delta t} + \frac{1}{\varepsilon}(I - \Pi)(v \cdot \nabla_x g^n) = \frac{1}{\varepsilon^2}\mathcal{L} g^{n+1} - \frac{1}{\varepsilon^2} v \cdot M \nabla_x \rho^n. \tag{5.33}$$

In the continuity equation (5.31) there is no stiff term, but to recover the correct diffusion limit, the flux of g is taken at t_{n+1}, which gives

$$\frac{\rho^{n+1} - \rho^n}{\Delta t} + \nabla_x \cdot \langle v g^{n+1} \rangle = 0. \tag{5.34}$$

As $\varepsilon \to 0$, (5.33) gives

$$\mathcal{L} g^{n+1} = v \cdot M \nabla_x \rho^n,$$

which implies

$$g^{n+1}(v) = \mathcal{L}^{-1}(vM) \cdot \nabla_x \rho^n = \frac{M(v)}{\lambda(v)} \left[\int b(v, w) g^{n+1}(w)\, \mathrm{d}w - v \cdot \nabla_x \rho^n \right].$$

Applying this to (5.34), and using the rotational invariance of σ, yield the following time-explicit discretization of the diffusion equation (2.41):

$$\frac{\rho^{n+1} - \rho^n}{\Delta t} + \nabla_x \cdot \langle D \nabla \rho^n \rangle = 0.$$

Thus this time discretization is AP.

Now consider the case of one space dimension. A staggered grid can be used. Define $x_{i+1/2} = (i + 1/2)\Delta x$. Now the macroscopic density ρ will be defined at grid point x_i, while g is defined at $x_{i+1/2}$. Using upwind discretization for the space derivative, we arrive at

$$\frac{\rho_i^{n+1} - \rho_i^n}{\Delta t} + \left\langle v \frac{g_{i+1/2}^{n+1} - g_{i-1/2}^{n+1}}{\Delta x} \right\rangle = 0, \tag{5.35}$$

$$\frac{g_{i+1/2}^{n+1} - g_{i+1/2}^n}{\Delta x} + \frac{1}{\varepsilon \Delta x}(I - \Pi)\Big(v^+ \big(g_{i+1/2}^n - g_{i-1/2}^n \big) + v^- \big(g_{i+3/2}^n - g_{i+1/2}^n \big) \Big)$$
$$= \frac{1}{\varepsilon^2}\mathcal{L} g_{i+1/2}^{n+1} - \frac{1}{\varepsilon^2} v M \frac{\rho_{i+1}^n - \rho_i^n}{\Delta x}, \tag{5.36}$$

where $v^{\pm} = (v \pm |v|)/2$.

https://doi.org/10.1017/S0962492922000010 Published online by Cambridge University Press

As $\varepsilon \to 0$, (5.36) gives

$$g_{i+1/2}^{n+1} = \mathcal{L}^{-1}(\nu M)\frac{\rho_{i+1}^n - \rho_i^n}{\Delta x},$$

which when applied to (5.35) gives the following scheme:

$$\frac{\rho^{n+1} - \rho^n}{\Delta t} + D\frac{\rho_{i+1}^n - 2\rho_i^n + \rho_{i-1}^n}{(\Delta x)^2} = 0.$$

This is the classical three-point explicit discretization of the diffusion equation (2.41) and (2.42).

The uniform stability condition ($\Delta t \le C(\Delta x)^2$, uniformly in ε) of this method was proved in Liu and Mieussens (2010).

Among all the above approaches, in the limit $\varepsilon \to 0$, the time discretization is explicit for the limiting diffusion equation. This imposes a numerical stability condition such as $\Delta t = O((\Delta x)^2)$. Consider the case of $\mathcal{L} = r - \rho$, hence $\lambda = 1$, in the parity formulation (5.18) and (5.19). Boscarino, Pareschi and Russo (2013) proposed reformulating the system into

$$\partial_t r = \underbrace{-\nu\partial_x\left(j + \frac{\nu(\varepsilon)\nu\partial_x r}{\sigma}\right)}_{\text{explicit}} \underbrace{-\frac{\sigma}{\varepsilon^2}(r-\rho) + \nu(\varepsilon)\nu^2\frac{\partial_{xx} r}{\sigma}}_{\text{implicit}}, \tag{5.37}$$

$$\partial_t j = \underbrace{-\frac{1}{\varepsilon^2}\left(j + \frac{\nu\partial_x r}{\sigma}\right)}_{\text{implicit}}, \tag{5.38}$$

where $\mu(\varepsilon) \in [0,1]$ is a free parameter such that $\mu(0) = 1$; $\mu = 1$ guarantees the largest stability region. When $\varepsilon \to 0$, we get an *implicit* discretization of the diffusion equation, enabling a stability condition such as $\Delta t = O(\Delta x)$.

5.5. *Stochastic AP schemes for linear transport equation with uncertainties*

Kinetic models usually have *uncertainties* that can arise in collision kernels, scattering coefficients, initial or boundary data, geometry, source or forcing terms (Bird 1994, Berman, Haverkort and Woerdman 1986, Koura and Matsumoto 1991). Understanding the impact of these uncertainties, and quantifying and even controlling them, in the sense of uncertainty quantification (UQ), is crucial to the simulations of the complex kinetic systems in order to verify, validate and improve these models, and to conduct risk management.

The uncertainty is usually modelled by a random vector $z \in \mathbb{R}^n$ in a properly defined probability space $(\Sigma, \mathcal{A}, \mathbb{P})$, whose event space is Σ and equipped with σ-algebra $\mathcal{A}$ and probability measure $\mathbb{P}$. We also assume the components of z are mutually independent random variables with known probability $\omega(z)\colon I_z \longrightarrow \mathbb{R}^+$, obtained already through some dimension reduction technique, *e.g.* Karhunen–Loève (KL) expansion (Loève 1977).

https://doi.org/10.1017/S0962492922000010 Published online by Cambridge University Press

5.5.1. The linear transport equation with isotropic scattering

Consider the linear transport equation in one-dimensional slab geometry with random input:

$$\varepsilon\delta_t f + v\delta_x f = \frac{\sigma}{\varepsilon}\mathcal{L}f, \quad t > 0,\ x \in [0,1],\ v \in [-1,1],\ z \in I_z, \tag{5.39}$$

$$\mathcal{L}f(t,x,v,z) = \frac{1}{2}\int_{-1}^{1} f(t,x,v',z)\,\mathrm{d}v' - f(t,x,v,z), \tag{5.40}$$

with the initial condition

$$f(0,x,v,z) = f^0(x,v,z). \tag{5.41}$$

This equation arises in neutron transport, radiative transfer, *etc.,* and describes particle transport (*e.g.* neutrons) in a background medium (*e.g.* nuclei). Here $v = \Omega \cdot e_x = \cos\theta$, where θ is the angle between the moving direction and the x-axis. Assume

$$\sigma(x,z) \geq \sigma_{\min} > 0. \tag{5.42}$$

Let

$$\langle\phi\rangle = \frac{1}{2}\int_{-1}^{1} \phi(v)\,\mathrm{d}v \tag{5.43}$$

denote the average of a velocity-dependent function ϕ.

Let $\rho = \langle f\rangle$. For each fixed z, as $\varepsilon \to 0$, ρ solves the following diffusion equation:

$$\partial_t\rho = \partial_x\left(\frac{1}{3}\sigma(x,z)^{-1}\partial_x\rho\right). \tag{5.44}$$

In order to understand the property of numerical methods for uncertain kinetic equations, it is important to study the regularity and long-time behaviour in the random space of the linear transport equation (5.39)–(5.41). Consider the Hilbert space of the random variable,

$$H(I_z;\ \omega\,\mathrm{d}z) = \left\{f\colon I_z \to \mathbb{R}^+,\ \int_{I_z} f^2(z)\omega(z)\,\mathrm{d}z < +\infty\right\}, \tag{5.45}$$

equipped with the inner product and norm defined as

$$\langle f,g\rangle_\omega = \int_{I_z} fg\,\omega(z)\,\mathrm{d}z, \quad \|f\|_\omega^2 = \langle f,f\rangle_\omega. \tag{5.46}$$

Define the kth-order differential operator with respect to z as

$$D^k f(t,x,v,z) := \partial_z^k f(t,x,v,z), \tag{5.47}$$

and the Sobolev norm in z as

$$\|f(t,x,v,\cdot)\|_{H^k}^2 := \sum_{\alpha\leq k} \|D^\alpha f(t,x,v,\cdot)\|_\omega^2. \tag{5.48}$$

https://doi.org/10.1017/S0962492922000010 Published online by Cambridge University Press

Finally, introduce norms in space and velocity as follows:

$$\|f(t,\cdot,\cdot,\cdot)\|_\Gamma^2 := \int_Q \|f(t,x,v,\cdot)\|_\omega^2 \,\mathrm{d}x\,\mathrm{d}v, \quad t \geq 0, \tag{5.49}$$

where $Q = [0,1]\times[-1,1]$ denotes the domain in phase space. The following results were established in Jin, Liu and Ma (2017*a*).

Theorem 5.4 (uniform regularity). If, for some integer $m \geq 0$,

$$\|D^k\sigma(z)\|_{L^\infty} \leq C_\sigma, \quad \|D^k f_0\|_\Gamma \leq C_0, \quad k = 0,\dots,m, \tag{5.50}$$

then the solution f to the linear transport equation (5.39)–(5.41), with periodic boundary condition in x, satisfies

$$\|D^k f(t,\cdot,\cdot,\cdot)\|_\Gamma \leq C, \quad k = 0,\dots,m, \quad \text{for all } t > 0, \tag{5.51}$$

where C_σ, C_0 and C are constants independent of ε.

The above theorem shows that, under some smoothness assumption on σ, the regularity of the initial data is preserved in time and the Sobolev norm of the solution is bounded uniformly in ε.

5.5.2. Stochastic Galerkin approximation

An interesting and important scenario is when the uncertainty and small scaling are both present in the equation. Among various UQ methods (Xiu 2010, Gunzburger, Webster and Zhang 2014), we consider the stochastic Galerkin (SG) method, which is suitable for our AP analysis thanks to its Galerkin formulation.

Let $\{\phi_i(z), i = 0,1,\dots,\}$ denote the complete orthogonal polynomial basis in the Hilbert space $H(I_z;\omega(z)\,\mathrm{d}z)$ corresponding to the weight $\omega(z)$, where $\phi_i(z)$ is a polynomial of degree i and satisfies the orthonormality condition:

$$\langle\phi_i,\phi_j\rangle_\omega = \int \phi_i(z)\phi_j(z)\omega(z)\,\mathrm{d}z = \delta_{ij}.$$

Here $\phi_0(z) = 1$, and δ_{ij} is the Kronecker delta function. Since the solution $f(t,\cdot,\cdot,\cdot)$ is defined in $L^2([0,1]\times[-1,1]\times\mathbb{I}_z;\,\mathrm{d}\mu)$, we have the generalized polynomial chaos expansion (Xiu and Karniadakis 2002)

$$f(t,x,v,z) = \sum_{i=0}^{\infty} f_i(t,x,v)\,\phi_i(z), \quad \hat{f} = (f_i)_{i=0}^\infty := \left(\bar{f},\hat{f}_1\right).$$

The mean and variance of f can be obtained from the expansion coefficients as

$$\bar{f} = E(f) = \int_{I_z} f\omega(z)\,\mathrm{d}z = f_0, \quad \mathrm{var}(f) = |\hat{f}_1|^2.$$

Denote the SG solution by

$$f^K = \sum_{i=0}^{K} f_i\,\phi_i, \quad \hat{f}^K = (f_i)_{i=0}^K := \left(\bar{f},\hat{f}_1^K\right), \tag{5.52}$$

https://doi.org/10.1017/S0962492922000010 Published online by Cambridge University Press

from which we can extract the mean and variance of f^K from the expansion coefficients as

$$E(f^K) = \bar{f}, \quad \text{var}(f^K) = |\hat{f}_1^K|^2.$$

Furthermore, define

$$\begin{aligned} \sigma_{ij} &= \langle \phi_i, \sigma \phi_j \rangle_\omega, \qquad \Sigma = (\sigma_{ij})_{M+1,M+1}, \\ \sigma_{ij}^a &= \langle \phi_i, \sigma^a \phi_j \rangle_\omega, \quad \Sigma^a = (\sigma_{ij}^a)_{M+1,M+1}, \end{aligned} \tag{5.53}$$

for $0 \le i, j \le M$. Let I be the $(K+1)\times(K+1)$ identity matrix. Σ, Σ^a are symmetric positive definite matrices satisfying

$$\Sigma \ge \sigma_{\min} I.$$

If we apply the polynomial chaos ansatz (5.52) to the transport equation (5.39) and conduct the Galerkin projection, we obtain

$$\varepsilon \partial_t \hat{f} + v \partial_x \hat{f} = -\frac{1}{\varepsilon}(I - [\cdot])\Sigma \hat{f}. \tag{5.54}$$

Note that the SG method makes the random transport equations into deterministic systems (5.54) that are vector analogues of the original scalar deterministic transport equations. Therefore we can naturally utilize the deterministic AP machinery to solve the SG system to achieve the desired AP goals, and hence minimize 'intrusion' to the legacy deterministic codes. To this end, Jin, Xiu and Zhu (2015) introduced the notion of *stochastic asymptotic-preserving (sAP)*. A scheme is sAP if an SG method for the random kinetic equation becomes an SG approximation for the limiting macroscopic, random (hydrodynamic or diffusion) equation as $\varepsilon \to 0$, with K, mesh size and time step all held fixed. Such schemes guarantee that for $\varepsilon \to 0$, *all* numerical parameters, including K, can be chosen only for accuracy requirements, but *independent* of ε.

We now use the micro–macro decomposition

$$\hat{f}(t, x, v, z) = \hat{\rho}(t, x, z) + \varepsilon \hat{g}(t, x, v, z), \tag{5.55}$$

where $\hat{\rho} = [\hat{f}]$ and $[\hat{g}] = 0$, in (5.54) to get

$$\partial_t \hat{\rho} + \partial_x \langle v \hat{g} \rangle = -\Sigma^a \hat{\rho} + \hat{S}, \tag{5.56a}$$

$$\partial_t \hat{g} + \frac{1}{\varepsilon}(I - \langle . \rangle)(v \partial_x \hat{g}) = -\frac{1}{\varepsilon^2}\Sigma \hat{g} - \Sigma^a \hat{g} - \frac{1}{\varepsilon^2} v \partial_x \hat{\rho}, \tag{5.56b}$$

with initial data

$$\hat{\rho}(0, x, z) = \hat{\rho}_0(x, z), \quad \hat{g}(0, x, v, z) = \hat{g}_0(x, v, z).$$

As $\varepsilon \to 0$, system (5.56) formally approaches the diffusion limit

$$\partial_t \hat{\rho} = \partial_x \left(\frac{1}{3} \Sigma^{-1} \partial_x \hat{\rho} \right). \tag{5.57}$$

https://doi.org/10.1017/S0962492922000010 Published online by Cambridge University Press

This is the SG approximation to the random diffusion equation (5.44). Thus the SG approximation is sAP in the sense of Jin *et al.* (2015).

The following result was proved in Jin *et al.* (2017*a*).

Theorem 5.5. If, for some integer $m \geq 0$,

$$\|\sigma(z)\|_{H^k} \leq C_\sigma, \quad \|D^k f_0\|_\Gamma \leq C_0, \quad \|D^k(\partial_x f_0)\|_\Gamma \leq C_x, \quad k = 0, \ldots, m, \tag{5.58}$$

then for $t \leq T$, the error of the SG method is

$$\|f - f^K\|_\Gamma \leq \frac{C(T)}{K^k}, \tag{5.59}$$

where $C(T)$ is a constant independent of ε.

Theorem 5.5 gives a uniform-in-ε spectral convergence rate, so we can choose K independent of ε, a very strong sAP property. Such a result is also obtained with the anisotropic scattering case, for the linear semiconductor Boltzmann equation (Jin and Liu 2017).

5.5.3. A full discretization

Here we adopt the micro–macro decomposition fully discrete scheme for the SG system (5.56).

Corresponding to (5.35) and (5.36), we have

$$\frac{\hat\rho_i^{n+1} - \hat\rho_i^n}{\Delta t} + \left\langle v \frac{\hat g_{i+1/2}^{n+1} - \hat g_{i-1/2}^{n+1}}{\Delta x} \right\rangle = 0, \tag{5.60a}$$

$$\frac{\hat g_{i+1/2}^{n+1} - \hat g_{i+1/2}^n}{\Delta t} + \frac{1}{\varepsilon \Delta x}(I - \langle \Pi \rangle)\left(v^+(\hat g_{i+1/2}^n - \hat g_{i-1/2}^n) + v^-(\hat g_{i+3/2}^n - \hat g_{i+1/2}^n)\right)$$
$$= -\frac{1}{\varepsilon^2}\Sigma_i \hat g_{i+1/2}^{n+1} - \frac{1}{\varepsilon^2} v \frac{\hat\rho_{i+1}^n - \hat\rho_i^n}{\Delta x}. \tag{5.60b}$$

Its formal limit, when $\varepsilon \to 0$, is given by

$$\frac{\hat\rho_i^{n+1} - \hat\rho_i^n}{\partial_t} - \frac{1}{3}\Sigma^{-1} \frac{\hat\rho_{i+1}^n - 2\hat\rho_i^n + \hat\rho_{i-1}^n}{\Delta x^2} = 0. \tag{5.61}$$

This is the fully discrete SG scheme for (5.57). Thus the fully discrete scheme is sAP.

One important property for an AP scheme is to have a stability condition independent of ε, so we can take $\Delta t \gg O(\varepsilon)$. The next theorem from Jin *et al.* (2017*a*) confirms this.

Theorem 5.6. If Δt satisfies the CFL condition

$$\Delta t \leq \frac{\sigma_{\min}}{3}(\Delta x)^2 + \frac{2\varepsilon}{3}\Delta x, \tag{5.62}$$

https://doi.org/10.1017/S0962492922000010 Published online by Cambridge University Press

then the solution obtained by scheme (5.60) satisfies the energy estimate

$$\sum_{i=0}^{N-1}\left((\hat{\rho}^{n+})^2+\frac{\varepsilon^2}{2}\int_{-1}^{1}(\hat{g}^n_{i+1/2})^2\,\mathrm{d}v\right)\le\sum_{i=0}^{N-1}\left((\hat{\rho}^0_i)^2+\frac{\varepsilon^2}{2}\int_{-1}^{1}(\hat{g}^0_{i+\frac{1}{2}})^2\,\mathrm{d}v\right)$$

for every n, and hence the scheme (5.60) is stable.

Since the right-hand side of (5.62) has a lower bound, which is essentially a stability condition of the discrete diffusion equation (5.61)), when $\varepsilon\to 0$, the scheme is asymptotically stable and Δt remains finite even if $\varepsilon\to 0$.

Next we consider a numerical example from Jin *et al.* (2017*a*). Consider a random coefficient with one-dimensional random parameter:

$$\sigma(z)=2+z,\quad z \text{ is uniformly distributed in } (-1,1).$$

The limiting random diffusion equation is

$$\partial_t\rho=\frac{1}{3\sigma(z)}\partial_{xx}\rho, \tag{5.63}$$

with initial condition and boundary conditions

$$\rho(t,0,z)=1,\quad \rho(t,1,z)=0,\quad \rho(0,x,z)=0.$$

The analytical solution for (5.63) with the given initial and boundary conditions is

$$\rho(t,x,z)=1-\mathrm{erf}\left(\frac{x}{\sqrt{\frac{4}{3\sigma(z)}t}}\right). \tag{5.64}$$

When ε is small, this can be used as the reference solution. For large ε or if we cannot get an analytic solution, we will use the collocation method (see Gunzburger *et al.* 2014) with the same time and spatial discretization to the micro–macro system (5.60) as a comparison in the following examples. In addition, the standard 30-point Gauss–Legendre quadrature set is used for the velocity space to compute ρ.

To examine the accuracy, two error norms are used, namely the differences in the mean solutions and in the corresponding standard deviation, with ℓ^2-norm in x:

$$e_{\mathrm{mean}}(t)=\|\mathbb{E}[u^h]-\mathbb{E}[u]\|_{\ell^2},$$
$$e_{\mathrm{std}}(t)=\|\sigma[u^h]-\sigma[u]\|_{\ell^2},$$

where u^h and u, respectively, are the numerical solutions and the reference solutions.

In Figure 5.1 we plot the errors in mean and standard deviation of the SG solutions at $t=0.01$ with different K. Three sets of results are included: solutions with $\Delta x=0.04$, $\Delta x=0.02$ and $\Delta x=0.01$, with $\Delta t=0.0002/3$ always used. One can see that the errors become smaller with a finer mesh, and the solutions decay rapidly in K and then saturate where spatial discretization error dominates.

https://doi.org/10.1017/S0962492922000010 Published online by Cambridge University Press

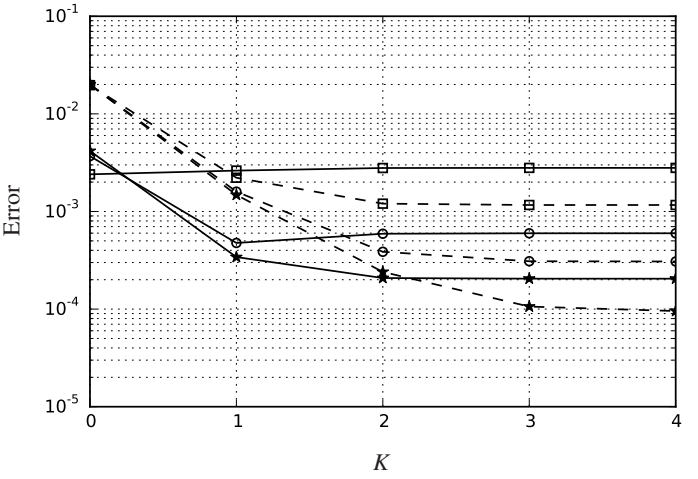

Figure 5.1. Solutions to (5.63)–(5.64) from Jin *et al.* (2017*a*): errors of the mean (solid line) and standard deviation (dashed line) of ρ with respect to the polynomial chaos order K at $\varepsilon = 10^{-8}$, for $\Delta x = 0.04$ (squares), $\Delta x = 0.02$ (circles), $\Delta x = 0.01$ (stars).

In Figure 5.2 we examine the difference between the solution $t = 0.01$ obtained by SG with $K = 4$, $\Delta x = 0.01$, $\Delta t = \Delta x^2/12$ and the limiting analytical solution (5.64). One can observe that the differences become smaller as ε is smaller in a quadratic fashion, before the numerical errors become dominant. Therefore the method works for all ranges of ε.

A discontinuous Galerkin method sAP scheme for the same problem was developed by Chen, Liu and Mu (2017), who also proved uniform stability and a rigorous sAP property.

5.6. *Stochastic Galerkin methods for general non-linear kinetic equations with uncertainties*

Consider a general non-linear kinetic equation with multi-dimensional uncertainties:

$$\begin{cases} \varepsilon^{\alpha}\partial_t f + v\cdot\nabla_x f - \nabla_{\mathbf{x}}\phi\cdot\nabla_v f = \dfrac{1}{\varepsilon}\mathcal{Q}(f), \quad t>0,\ x\in\Omega,\ v\in\mathbb{R}^d,\ z\in\mathbb{R}^n, \\ f(0,x,v) = f^0(x,v). \end{cases} \tag{5.65}$$

Here $\alpha = 0$ and 1, respectively, correspond to the Euler (acoustic) and incompressible Navier–Stokes scalings (Bardos, Golse and Levermore 1991).

We again use the generalized polynomial chaos approximation

$$f(t,x,v,z) \approx \sum_{|k|=0}^{K} f_k(t,x,v)\Phi_k(z) := f^K(t,x,v,z), \tag{5.66}$$

https://doi.org/10.1017/S0962492922000010 Published online by Cambridge University Press

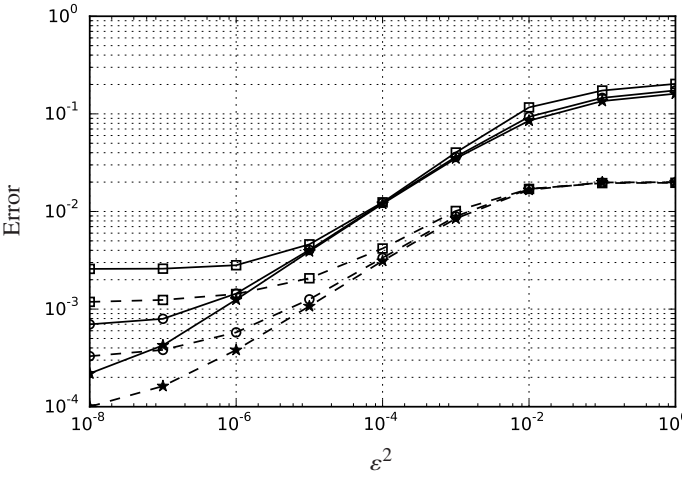

Figure 5.2. Solutions to (5.63)–(5.64) from Jin *et al.* (2017*a*): differences in the mean (solid line) and standard deviation (dashed line) of ρ with respect to ε^2, between the limiting analytical solution (5.64) and the SG solution with $K = 4$, for $\Delta x = 0.04$ (squares), $\Delta x = 0.02$ (circles), $\Delta x = 0.01$ (stars).

where $k = (k_1, \ldots, k_n)$ is a multi-index with $|k| = k_1 + \cdots + k_n$. The $\{\Phi_k(z)\}$ are orthonormal polynomials from $\mathbb{P}_K^n$, the set of all n-variate polynomials of degree up to M, and satisfy

$$\langle \Phi_k, \Phi_j \rangle_\omega = \int_{I_z} \Phi_k(z)\Phi_j(z)\omega(z)\,\mathrm{d}z = \delta_{kj}, \quad 0 \le |k|,\ |j| \le K.$$

Here δ_{kj} is the Kronecker delta function.

Now we insert (5.66) into (5.65). Upon a standard Galerkin projection, we obtain, for each $0 \le k \le M$,

$$\begin{cases} \varepsilon^\alpha \partial_t f_k + v \cdot \nabla_x f_k - \displaystyle\sum_{|j|=0}^{K} \nabla_x \phi_{kj} \cdot \nabla_v f_j = \frac{1}{\varepsilon} \mathcal{Q}_k(f^K), \\ f_k(0, x, v) = f_k^0(x, v), \end{cases} \tag{5.67}$$

with

$$\mathcal{Q}_k(f^K) := \int_{I_z} \mathcal{Q}(f^K)(t, x, v, z)\Phi_k(z)\omega(z)\,\mathrm{d}z,$$

$$\phi_{kj} := \int_{I_z} \phi(t, x, z)\Phi_k(z)\Phi_j(z)\omega(z)\,\mathrm{d}z,$$

$$f_k^0 := \int_{I_z} f^0(x, v, z)\Phi_k(z)\omega(z)\,\mathrm{d}z.$$

https://doi.org/10.1017/S0962492922000010 Published online by Cambridge University Press

We also assume that the potential $\phi(t, x, z)$ is given *a priori* for simplicity; the case when it is coupled to a Poisson equation can be treated similarly (Zhu and Jin 2017).

5.6.1. Hypocoercivity estimate of the SG system

The hypocoercivity theory (Villani 2009) can be used to study the properties of the SG methods. For general linear transport with uncertainty, see Li and Wang (2017). For non-linear problems we need to consider the perturbative form (Jin and Zhu 2018, Liu and Jin 2018)

$$f_k = \mathcal{M} + \varepsilon M h_k, \tag{5.68}$$

where h_k is the coefficient of the following generalized polynomial chaos expansion:

$$h(t, x, v, z) \approx \sum_{|k|=0}^{M} h_k(t, x, v)\Phi_k(z) := h^K(t, x, v, z). \tag{5.69}$$

Inserting ansatz (5.68) and (5.69) into (5.67) and conducting a standard Galerkin projection, we obtain the SG system for h_k (consider the case of $\phi = 0$) (Hu and Jin 2016):

$$\begin{cases} \partial_t h_k + \dfrac{1}{\varepsilon^\alpha} v \cdot \nabla_x h_k = \dfrac{1}{\varepsilon^{1+\alpha}} \mathcal{L}_k(h^K) + \dfrac{1}{\varepsilon^\alpha} \mathcal{F}_k(h^K, h^K), \\ h_k(0, x, v) = h_k^0(x, v), \quad x \in \Omega \subset \mathbb{T}^d,\ v \in \mathbb{R}^d, \end{cases} \tag{5.70}$$

for each $1 \le |k| \le K$, with initial data given by

$$h_k^0 := \int_{I_z} h^0(x, v, z)\psi_k(z)\,\pi(z)\,\mathrm{d}z.$$

For the Boltzmann equation, the collision parts are given by

$$\begin{aligned} \mathcal{L}_k(h^K) &= \mathcal{L}_k^+(h^K) \\ &= \sum_{|i|=1}^{K} \int_{\mathbb{R}^d \times \mathbb{S}^{d-1}} \widetilde{S}_{ki}\, \phi(|v - v_*|)\,(h_i(v')M(v_*') \\ &\quad + h_i(v_*')M(v'))\,M(v_*)\,\mathrm{d}v_*\,\mathrm{d}\sigma \\ &\quad - M(v) \sum_{|i|=1}^{K} \int_{\mathbb{R}^d \times \mathbb{S}^{d-1}} \widetilde{S}_{ki}\, \phi(|v - v_*|)\, h_i(v_*)M(v_*)\,\mathrm{d}v_*\,\mathrm{d}\sigma - \sum_{|i|=1}^{K} \nu_{ki} h_i, \end{aligned}$$

$$\begin{aligned} \mathcal{F}_k(h^K, h^K)(t, x, v) = &\sum_{|i|,|j|=1}^{K} \int_{\mathbb{R}^d \times \mathbb{S}^{d-1}} S_{kij}\, \phi(|v - v_*|)\, M(v_*) \\ &\times (h_i(v')h_j(v_*') - h_i(v)h_j(v_*))\,\mathrm{d}v_*\,\mathrm{d}\sigma, \end{aligned}$$

https://doi.org/10.1017/S0962492922000010 Published online by Cambridge University Press

with

$$\widetilde{S}_{ki} := \int_{I_z} b(\cos\theta, z)\,\psi_k(z)\psi_i(z)\,\pi(z)\,\mathrm{d}z,$$
$$\widetilde{\nu}_{ki} := \int_{\mathbb{R}^d\times\mathbb{S}^{d-1}} \widetilde{S}_{ki}\,\phi(|v-v_*|)\,\mathcal{M}(v_*)\,\mathrm{d}v_*\,\mathrm{d}\sigma,$$
$$S_{kij} := \int_{I_z} b(\cos\theta, z)\,\psi_k(z)\psi_i(z)\psi_j(z)\,\pi(z)\,\mathrm{d}z.$$

For technical reasons we assume $z \in I_z$ is one-dimensional and I_z has finite support $|z| \le C_z$ (which is the case, for example, for the uniform and Beta distribution). Define

$$\|h\|^2_{H^s_{x,v}} = \sum_{|j|+|l|\le s} \|\partial_l^j h\|^2_{L^2_{x,v}}, \quad \|h\|^2_{H^s_z} = \int_{I_z} \|h\|^2_{H^s_{x,v}}\pi(z)\,\mathrm{d}z.$$

Liu and Jin (2018) and Daus, Jin and Liu (2019) give the following results, under some suitable assumption on b.

Theorem 5.7. Assume the collision kernel B is given by

$$B(|v-v_*|), \cos\theta, z) = \phi(|v-v_*|)b(\cos\theta, z),$$

where $\phi(\xi) = C_\phi \xi^\gamma$ with $\gamma \in [0,1]$, $C_\phi > 0$ for all $\eta \in [-1,1]$. Further, we assume

$$|\partial_\eta b(\eta, z)| \le C_b, \quad |\partial_z^k b(\eta, z)| \le C_b^*$$

for all $0 \le k \le r$, where b is linear in z, given in the form

$$b(\cos\theta, z) = b_0(\cos\theta) + b_1(\cos\theta)z. \tag{5.71}$$

Assume some upper and positive lower boundedness on b and its derivatives. In addition, assume (Jin and Shu 2017)

$$\|\psi_k\|_{L^\infty} \le Ck^p \quad \text{for all } k, \tag{5.72}$$

with a parameter $p > 0$. Let $q > p + 2$, and define the energy E^K by

$$E^K(t) = E^K_{s,q}(t) = \sum_{k=1}^K \|k^q h_k\|^2_{H^s_{x,v}}, \tag{5.73}$$

with the initial data satisfying $E^K(0) \le \eta$. Then, for all $s \ge s_0$, $0 \le \varepsilon_d \le 1$, such that for $0 \le \varepsilon \le \varepsilon_d$, if h^K is an SG solution (5.70) in $H^s_{x,v}$, the following hold.

(i) Under the incompressible Navier–Stokes scaling ($\alpha = 1$),

$$E^K(t) \le \eta\,\mathrm{e}^{-\tau t}.$$

(ii) Under the acoustic scaling ($\alpha = 0$),

$$E^K(t) \le \eta\,\mathrm{e}^{-\varepsilon\tau t},$$

https://doi.org/10.1017/S0962492922000010 Published online by Cambridge University Press

where η, τ are all positive constants that only depend on s and q, independent of K and z.

From here, we also conclude that $\|h^K\|_{H^s_{x,v}L^\infty_z}$ decays exponentially in time, with the same rate as $E^K(t)$, namely

$$\|h^K\|_{H^s_{x,v}L^\infty_z} \leq \eta\, \mathrm{e}^{-\tau t} \tag{5.74}$$

in the incompressible Navier–Stokes scaling, and

$$\|h^K\|_{H^s_{x,v}L^\infty_z} \leq \eta\, \mathrm{e}^{-\varepsilon\tau t}$$

in the acoustic scaling.

Liu and Jin (2018) also give the following error estimates on the SG method.

Theorem 5.8. Suppose the assumptions on the collision kernel and basis functions in Theorem 5.7 are satisfied, and the initial data are the same as those in Theorem 5.7. Then the following hold.

(i) Under the incompressible Navier–Stokes scaling,

$$\|h - h^K\|_{H^s_z} \leq C_e\, \frac{\mathrm{e}^{-\lambda t}}{K^r}, \tag{5.75}$$

(ii) Under the acoustic scaling,

$$\|h - h^K\|_{H^s_z} \leq C_e\, \frac{\mathrm{e}^{-\varepsilon\lambda t}}{K^r}, \tag{5.76}$$

with the constants C_e, $\lambda > 0$ independent of K and ε.

The above results show that the regularity of the SG solutions is the same as the initial data. Furthermore, the numerical fluctuation h^K converges to h with spectral accuracy, and the numerical error will decay exponentially in time in the random space.

5.7. Asymptotic-preserving neural network approximation

Kinetic equations have the curse of dimensionality since this solves equations in phase space. While this survey mainly concentrates on dealing with multiscale issues, it will be interesting to also deal with the issue of high dimensionality together with multiple scales. To this end, deep neural networks (DNNs) offer a possible direction, since there have been examples in which DNNs offer some advantages for high-dimensional PDEs (E and Yu 2018, Raissi, Perdikaris and Karniadakis 2019, Lu *et al.* 2021*a*, Li *et al.* 2021).

Unlike classical numerical schemes, a neural network uses a non-polynomial approximation to approximate the training data via optimization of an empirical loss/risk. For multiscale kinetic equations it is essential to construct a neural network that is AP (referred to as an APNN) (Li and Yang 2021).

https://doi.org/10.1017/S0962492922000010 Published online by Cambridge University Press

We first introduce conventional notations for deep neural networks (DNNs). An L-layer feed-forward neural network is defined recursively as

$$\begin{aligned} f_\theta^{[0]}(x) &= x, \\ f_\theta^{[l]}(x) &= \sigma \circ (W^{[l-1]} f_\theta^{[l-1]}(x) + b^{[l-1]}), \quad 1 \le l \le L-1, \\ f_\theta(x) &= f_\theta^{[L]}(x) = W^{[L-1]} f_\theta^{[L-1]}(x) + b^{[L-1]}, \end{aligned} \tag{5.77}$$

where $W^{[l]} \in \mathbb{R}^{m_{l+1} \times m_l}$, $b^l \in \mathbb{R}^{m_{l+1}}$, $m_0 = d_{\text{in}} = d$ is the input dimension, $m_L = d_0$ is the output dimension, σ is a scalar function and '$\circ$' means entry-wise operation. We denote the set of parameters by θ. The layers are denoted by a list, *i.e.* $[m_0, \dots, m_L]$.

Consider the linear transport equation with initial and boundary conditions over a bounded domain $\mathcal{T} \times \mathcal{D} \times \Omega$:

$$\begin{cases} \varepsilon \partial_t f + v \cdot \nabla_x f = \dfrac{1}{\varepsilon} \mathcal{L} f, & (t, x, v) \in \mathcal{T} \times \mathcal{D} \times \Omega, \\ \mathcal{B} f = F_{\text{B}}, & (t, x, v) \in \mathcal{T} \times \partial\mathcal{D} \times \Omega, \\ \mathcal{I} f = f_0, & (t, x, v) \in \{t = 0\} \times \mathcal{D} \times \Omega, \end{cases} \tag{5.78}$$

where F_{B}, f_0 are given functions, $\partial\mathcal{D}$ is the boundary of $\mathcal{D}$, and $\mathcal{B}$ and $\mathcal{I}$, respectively, are initial and boundary operators. Here $\mathcal{L} = \sigma(\rho - f)$.

5.7.1. The failure of PINNs to resolve small scales

PINNs (physics-informed neural networks) are standard neural networks to solve PDEs. There the density function $f(t, x, v)$ is approximated by a neural network

$$\text{NN}_\theta(t, x, v) \approx f(t, x, v). \tag{5.79}$$

The inputs of a DNN are (t, x, v), *i.e.* $m_0 = 3, 5$ for one and two dimensions, respectively. The output is a scalar which represents the value of f at (t, x, v). Since f is always non-negative, we put an exponential function at the last output layer of the DNN:

$$f_\theta^{\text{NN}}(t, x, v) := \exp(-\tilde{f}_\theta^{\text{NN}}(t, x, v)) \approx f(t, x, v) \tag{5.80}$$

to represent the numerical solution of f. Then the mean square of the residual of the original transport equation (5.78) is used as the target loss function, together with boundary and initial conditions as penalty terms:

$$\begin{aligned} \mathcal{R}_{\text{PINN}}^{\varepsilon} = & \frac{1}{|\mathcal{T} \times \mathcal{D} \times \Omega|} \int_{\mathcal{T}} \int_{\mathcal{D}} \int_{\Omega} |\varepsilon^2 \partial_t f_\theta^{\text{NN}} + \varepsilon v \cdot \nabla_x f_\theta^{\text{NN}} - \mathcal{L} f_\theta^{\text{NN}}|^2 \, \mathrm{d}v \, \mathrm{d}x \, \mathrm{d}t \\ & + \frac{\lambda_1}{|\mathcal{T} \times \partial\mathcal{D} \times \Omega|} \int_{\mathcal{T}} \int_{\partial\mathcal{D}} \int_{\Omega} |\mathcal{B} f_\theta^{\text{NN}} - F_{\text{B}}|^2 \, \mathrm{d}v \, \mathrm{d}x \, \mathrm{d}t \\ & + \frac{\lambda_2}{|\mathcal{D} \times \Omega|} \int_{\mathcal{D}} \int_{\Omega} |\mathcal{I} f_\theta^{\text{NN}} - f_0|^2 \, \mathrm{d}v \, \mathrm{d}x, \end{aligned} \tag{5.81}$$

https://doi.org/10.1017/S0962492922000010 Published online by Cambridge University Press

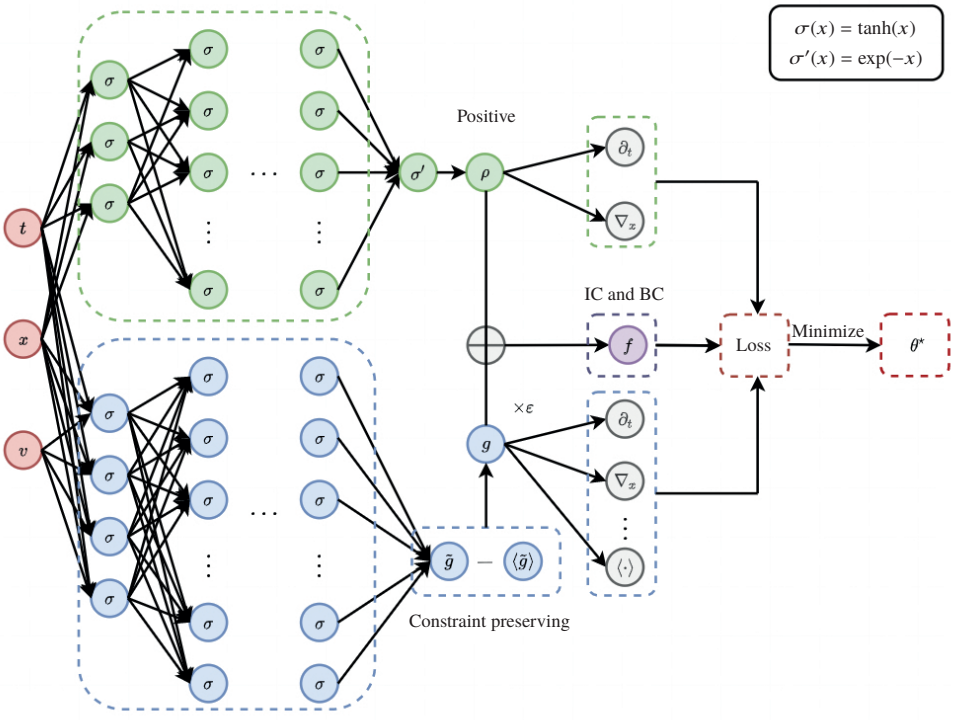

Figure 5.3. Schematic of APNNs for solving the linear transport equation with initial and boundary conditions.

where λ_1 and λ_2 are the penalty weights to be tuned. Then a standard stochastic gradient descent (SGD) method or Adam optimizer is used to find the global minimum of this loss.

Now let us check whether this PINN method is AP. We only need to focus on the first term of (5.81):

$$\mathcal{R}^{\varepsilon}_{\text{PINN, residual}} := \frac{1}{|\mathcal{T}\times\mathcal{D}\times\Omega|}\int_{\mathcal{T}}\int_{\mathcal{D}}\int_{\Omega}|\varepsilon^2\partial_t f_\theta^{\text{NN}} + \varepsilon v\cdot\nabla_x f_\theta^{\text{NN}} - \mathcal{L}f_\theta^{\text{NN}}|^2\,\mathrm{d}v\,\mathrm{d}x\,\mathrm{d}t. \tag{5.82}$$

Taking $\varepsilon \to 0$, formally this will lead to

$$\mathcal{R}_{\text{PINN, residual}} := \frac{1}{|\mathcal{T}\times\mathcal{D}\times\Omega|}\int_{\mathcal{T}}\int_{\mathcal{D}}\int_{\Omega}|-\mathcal{L}f_\theta^{\text{NN}}|^2\,\mathrm{d}v\,\mathrm{d}x\,\mathrm{d}t, \tag{5.83}$$

which can be viewed as the PINN loss of the equilibrium equation

$$\mathcal{L}f = 0. \tag{5.84}$$

This shows that when ε is very small, to leading order we are solving equation $\mathcal{L}f = 0$, which gives $f = \rho$. This does not give the desired diffusion equation (2.41). This explains why the PINN will fail when ε is small.

https://doi.org/10.1017/S0962492922000010 Published online by Cambridge University Press

The APNN, introduced in Jin, Ma and Wu (2021*b*), puts the micro–macro system (5.31) or (5.32) into the loss, instead of the original equation (5.78).

First the DNN needs to parametrize two functions $\rho(x, v)$ and $g(t, x, v)$. So here two networks are used. First,

$$\rho_\theta^{\mathrm{NN}}(t, x) := \exp(-\tilde{\rho}_\theta^{\mathrm{NN}}(t, x)) \approx \rho(t, x). \tag{5.85}$$

Notice here that ρ is non-negative. Second,

$$g_\theta^{\mathrm{NN}}(t, x, v) := \tilde{g}_\theta^{\mathrm{NN}}(t, x, v) - \langle \tilde{g}_\theta^{\mathrm{NN}} \rangle(t, x) \approx g(t, x, v). \tag{5.86}$$

Here $\tilde{\rho}$ and $\tilde{g}$ are both fully connected neural networks. Notice that by choosing $g_\theta^{\mathrm{NN}}(t, x, v)$ as in (5.86) it will automatically satisfy the constraint

$$\langle g \rangle = 0, \tag{5.87}$$

because

$$\langle g_\theta^{\mathrm{NN}} \rangle = \langle \tilde{g}_\theta^{\mathrm{NN}} \rangle - \langle \tilde{g}_\theta^{\mathrm{NN}} \rangle = 0 \quad \text{for all } t, x. \tag{5.88}$$

Then the APNN loss is defined as

$$\begin{aligned}
\mathcal{R}_{\mathrm{APNN}}^{\varepsilon} = & \frac{1}{|\mathcal{T} \times \mathcal{D}|} \int_{\mathcal{T}} \int_{\mathcal{D}} |\partial_t \rho_\theta^{\mathrm{NN}} + \nabla_x \cdot \langle v g_\theta^{\mathrm{NN}} \rangle|^2 \, \mathrm{d}x \, \mathrm{d}t \\
& + \frac{1}{|\mathcal{T} \times \mathcal{D} \times \Omega|} \int_{\mathcal{T}} \int_{\mathcal{D}} \int_{\Omega} |\varepsilon^2 \partial_t g_\theta^{\mathrm{NN}} + \varepsilon (I - \Pi)(v \cdot \nabla_x g_\theta^{\mathrm{NN}}) \\
& \quad + v \cdot \nabla_x \rho_\theta^{\mathrm{NN}} - \mathcal{L} g_\theta^{\mathrm{NN}}|^2 \, \mathrm{d}v \, \mathrm{d}x \, \mathrm{d}t \\
& + \frac{\lambda_1}{\mathcal{T} \times \partial \mathcal{D} \times \Omega|} \int_{\mathcal{T}} \int_{\partial \mathcal{D}} \int_{\Omega} |\mathcal{B}(\rho_\theta^{\mathrm{NN}} + \varepsilon g_\theta^{\mathrm{NN}}) - F_{\mathrm{B}}|^2 \, \mathrm{d}v \, \mathrm{d}x \, \mathrm{d}t \\
& + \frac{\lambda_2}{|\mathcal{D} \times \Omega|} \int_{\mathcal{D}} \int_{\Omega} |\mathcal{I}(\rho_\theta^{\mathrm{NN}} + \varepsilon g_\theta^{\mathrm{NN}}) - f_0|^2 \, \mathrm{d}v \, \mathrm{d}x.
\end{aligned} \tag{5.89}$$

A schematic plot of the method is given in Figure 5.3.

To show the AP property of this loss formally, we only need to focus on the first two terms of (5.89):

$$\begin{aligned}
\mathcal{R}_{\mathrm{APNN,\,residual}}^{\varepsilon} = & \frac{1}{|\mathcal{T} \times \mathcal{D}|} \int_{\mathcal{T}} \int_{\mathcal{D}} |\partial_t \rho_\theta^{\mathrm{NN}} + \nabla_x \cdot \langle v g_\theta^{\mathrm{NN}} \rangle - Q|^2 \, \mathrm{d}x \, \mathrm{d}t \\
& + \frac{1}{|\mathcal{T} \times \mathcal{D} \times \Omega|} \int_{\mathcal{T}} \int_{\mathcal{D}} \int_{\Omega} |\varepsilon^2 \partial_t g_\theta^{\mathrm{NN}} + \varepsilon (I - \Pi)(v \cdot \nabla_x g_\theta^{\mathrm{NN}}) \\
& \quad + v \cdot \nabla_x \rho_\theta^{\mathrm{NN}} - \mathcal{L} g_\theta^{\mathrm{NN}} - (I - \Pi) \varepsilon Q|^2 \, \mathrm{d}v \, \mathrm{d}x \, \mathrm{d}t.
\end{aligned} \tag{5.90}$$

Taking $\varepsilon \to 0$, formally this will lead to

$$\begin{aligned}
\mathcal{R}_{\mathrm{APNN,\,residual}} = & \frac{1}{|\mathcal{T} \times \mathcal{D}|} \int_{\mathcal{T}} \int_{\mathcal{D}} |\partial_t \rho_\theta^{\mathrm{NN}} + \nabla_x \cdot \langle v g_\theta^{\mathrm{NN}} \rangle - Q|^2 \, \mathrm{d}x \, \mathrm{d}t \\
& + \frac{1}{|\mathcal{T} \times \mathcal{D} \times \Omega|} \int_{\mathcal{T}} \int_{\mathcal{D}} \int_{\Omega} |v \cdot \nabla_x \rho_\theta^{\mathrm{NN}} - \mathcal{L} g_\theta^{\mathrm{NN}}|^2 \, \mathrm{d}v \, \mathrm{d}x \, \mathrm{d}t,
\end{aligned} \tag{5.91}$$

https://doi.org/10.1017/S0962492922000010 Published online by Cambridge University Press

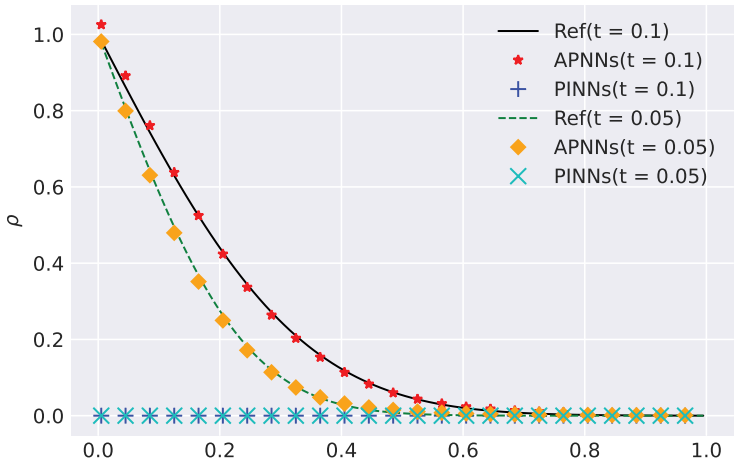

Figure 5.4. Example 5.9: $\varepsilon = 10^{-8}$. Plots of density ρ at $t = 0.05, 0.1$ by PINN, APNN and reference solutions. The neural networks are $[2, 128, 128, 128, 128, 1]$ for ρ and $[3, 256, 256, 256, 256, 1]$ for g, f. The batch size is 1000 in the domain, 400×2 with penalty $\lambda_1 = 10$ for the boundary condition and 1000 with penalty $\lambda_2 = 10$ for the initial condition; the number of quadrature points is 30. The relative ℓ^2-errors of PINNs and APNNs are 9.40×10^{-1} and 2.76×10^{-3} respectively.

which is the mean-square loss of equations

$$\begin{cases} \partial_t \rho + \nabla_x \cdot \langle v g \rangle = Q, \\ v \cdot \nabla_x \rho = \mathcal{L} g. \end{cases} \tag{5.92}$$

The second equation above yields $g = \mathcal{L}^{-1}(v \cdot \nabla_x \rho)$, which, when plugging into the first equation and integrating over v, gives the diffusion equation (2.41). Hence this proposed method is an APNN method.

Example 5.9. We present a numerical example from Jin *et al.* (2021*b*). Let $\sigma = 1$. Consider the initial data

$$f_0(x, v) = \frac{\rho(x)}{\sqrt{2\pi}} \mathrm{e}^{-v^2/2}, \tag{5.93}$$

where

$$\rho(x) = 1 + \cos(4\pi x), \tag{5.94}$$

and the isotropic in-flow boundary conditions

$$F_L(v) = 1, \quad F_R(-v) = 0, \quad \text{for } v > 0. \tag{5.95}$$

The results are shown in Figure 5.4. Clearly the PINN fails to conserve the mass, and for small ε does not give accurate results, while the APNN gives quite accurate results even when ε is very small.

https://doi.org/10.1017/S0962492922000010 Published online by Cambridge University Press

Remark 5.10. Not all AP schemes yield an APNN method when put into the loss. For example, Jin *et al.* (2021*b*) showed that the parity formulation (5.18)–(5.19) does not give an APNN network.

A similar loss function also based on micro–macro decomposition, but with a constraint (5.87) as a penalty, was proposed in Lu, Wang and Xu (2021*b*) for the stationary problem.

6. Other related multiscale problems

6.1. Non-linear hyperbolic systems with stiff source terms

Numerical methods for non-linear hyperbolic systems with stiff relaxation terms were among the earliest AP schemes for time-dependent problems. A prototype equation is given by

$$\begin{cases} \partial_t u + \partial_x g(u, v) = 0, \\ \partial_t v + \partial_x h(u, v) = \dfrac{1}{\varepsilon} R(u, v), \end{cases} \tag{6.1}$$

where the term R is dissipative, $\partial_v R \le 0$, and possesses a unique local equilibrium, $R(u, v) = 0$, which implies $v = f(u)$. Then, when $\varepsilon \to 0$, we have the macroscopic limit

$$\partial_t u + \partial_x g(u, f(u)) = 0.$$

This is an analogy of the Euler limit of the Boltzmann equation. If we use the Chapman–Enskog expansion to the $O(\varepsilon)$-term, then (6.1) can be approximated by a parabolic equation

$$\partial_t u + \partial_x g(u, f(u)) = \varepsilon \partial_x [h(u) \partial_x u]. \tag{6.2}$$

Here we need $h(u) > 0$, which requires the characteristic speeds of the original systems (6.1) to intertwine with that of the limiting equation (6.1). This condition is called the *subcharacteristic condition* (Chen, Levermore and Liu 1994). Equation (6.2) is an analogy of the Navier–Stokes approximation to the Boltzmann equation.

The numerical study of systems of the type (6.1) began in the works by Jin and Levermore (1996), Jin (1995) and Caflisch, Jin and Russo (1997), where the AP principle was used to design numerical schemes to handle the stiff relaxation term. High-order IMEX-type schemes were developed by Pareschi and Russo (2005) and Dumbser, Enaux and Toro (2008). Combining AP and the positivity-preserving property was done in Hu and Shu (2019). The relation between AP and a well-balanced scheme is revealed in Gosse and Toscani (2002). For AP schemes for gas dynamics with external force and frictions, see Bouchut, Ounaissa and Perthame (2007) and Chalons *et al.* (2010). A rigorous uniform accuracy proof of AP schemes for linear problems was recently made in Hu and Shu (2021).

https://doi.org/10.1017/S0962492922000010 Published online by Cambridge University Press

6.2. *Quasi-neutral limit in plasma*

In many plasma applications one can disregard charge separations, and then the quasi-neutral approximation can be used. However, near the plasma boundary, electrostatic sheathes may appear, and then we need to consider more complex models (Degond and Deluzet 2017).

Consider the one-species rescaled Euler–Poisson (EP) equations for charged particles:

$$\partial_t n + \nabla \cdot q = 0, \tag{6.3}$$

$$\partial_t q + \nabla \cdot \left(\frac{q \otimes q}{n} \right) + \nabla p(n) = n \nabla \phi, \tag{6.4}$$

$$\varepsilon^2 \Delta \phi = n - 1, \tag{6.5}$$

where $n = n(x,t)$ is the particle number density, $q = q(x,t) = nu$ is the momentum (u is the average velocity), $p(n) = n^\gamma$ is the pressure law with $\gamma \geq 1$, and $\phi = \phi(x,t)$ is the electric potential. Here negatively charged electrons with scaled charge equal to -1 are considered, with a uniform ion background density equal to 1. The dimensionless parameter $\varepsilon = \lambda_D / L$ is the scaled Debye length, *i.e.* the ratio of the actual Debye length λ_D to the macroscopic length scale L. In the quasineutral regime, $\varepsilon \ll 1$. Letting $\varepsilon \to 0$ in (6.5), we have $n = 1$, and the following limiting equations arise (Brenier 2000):

$$\nabla \cdot q = 0, \tag{6.6}$$

$$\partial_t q + \nabla \cdot (q \otimes q) = \nabla \phi. \tag{6.7}$$

These are the incompressible Euler equations.

A typical stable time discretization of the Euler–Poisson system requires $\Delta t \leq \varepsilon$, which is quite restrictive.

The main difficulty here is that when $\varepsilon \to 0$, the Poisson equation (6.5) becomes degenerate, hence a naive discretization would lead to poor numerical performance for small ε. A key idea introduced by Crispel, Degond and Vignal (2005) is to reformulate the system to a new one that remains *uniformly elliptic*. Taking ∂_t on (6.3), $\nabla\cdot$ on (6.4) and ∂_{tt} on (6.5) gives

$$\partial_{tt} n + \nabla \cdot \partial_t q = 0, \tag{6.8}$$

$$\nabla \cdot \partial_t q + \nabla^2 : \left(\frac{q \otimes q}{n} + p(n) \mathrm{I} \right) = \nabla \cdot (n \nabla \phi), \tag{6.9}$$

$$\varepsilon^2 \Delta \partial_{tt} \phi = \partial_{tt} n. \tag{6.10}$$

Eliminating $\nabla \cdot \partial_t q$ by combining (6.8) and (6.9) and using (6.10), we get

$$-\nabla \cdot [(n + \varepsilon^2 \partial_{tt}) \nabla \phi] + \nabla^2 : \left[\frac{q \otimes q}{n} + p(n) \mathrm{I} \right] = 0. \tag{6.11}$$

Although this system is equivalent to the original Euler–Poisson system, equation

https://doi.org/10.1017/S0962492922000010 Published online by Cambridge University Press

(6.11) is now *uniformly elliptic* in ε, so discretizing it suitably in time will guarantee the asymptotic stability with respect to ε.

This framework is quite general, and has been generalized to the two-fluid model (Crispel, Degond and Vignal 2007), the particle-in-cell method for the Vlasov–Poisson system (Degond *et al.* 2010*b*), the Euler–Maxwell system (Degond, Deluzet and Savelief 2012*a*) and the Vlasov–Maxwell system (Degond, Deluzet and Doyen 2017), among other plasma models. See the comprehensive review by Degond and Deluzet (2017).

6.3. *High-field limits*

In kinetic equations there is often a strong external field, such as the electric or magnetic field, that balances the collision term, leading to the so-called high-field limit (Cercignani, Gamba and Levermore 1997).

6.3.1. *High electric field*

Consider for example the interaction between the electrons and a surrounding bath through Coulomb force in electrostatic plasma, where the electron density distribution $f(t, x, v)$ is governed by the Vlasov–Poisson–Fokker–Planck system:

$$\partial_t f + v \cdot \nabla_x f - \frac{1}{\varepsilon}\nabla_x \phi \cdot \nabla_v f = \frac{1}{\varepsilon}\nabla_v \cdot (vf + \nabla_v f), \tag{6.12}$$

$$-\Delta\phi = \rho - h, \tag{6.13}$$

where $\varepsilon = (l_e/\Lambda)^2$ is the ratio between the mean-free path and the Debye length. Let $\varepsilon \to 0$ in (6.12). We obtain the high-field limit (Nieto, Poupaud and Soler 2001, Goudon, Nieto, Poupaud and Soler 2005):

$$\partial_t \rho - \nabla_x \cdot (\rho \nabla_x \phi) = 0, \tag{6.14}$$

$$-\Delta\phi = \rho - h(x). \tag{6.15}$$

We can combine the force term with the Fokker–Planck term as

$$\partial_t f + v \cdot \nabla_x f = \frac{1}{\varepsilon}\nabla_v \cdot [M \nabla_v (Mf)], \tag{6.16}$$

where $M = \mathrm{e}^{-|v+\nabla_x\phi|^2/2}$. This form is convenient for designing AP schemes (Jin and Wang 2011, Crouseilles and Lemou 2011), based on which we can easily use other well-developed AP frameworks. For more general collision operators, *e.g.* the semiconductor Boltzmann collision operator, this trick does not apply and we need other ideas, *e.g.* BGK penalization (Jin and Wang 2013). A variational approach was recently proposed in Carrillo, Wang, Xu and Yan (2021), using the Wasserstein gradient structure, to get positivity and AP easily.

6.3.2. *High magnetic field*

Magnetized plasmas are encountered in a wide variety of astrophysical situations but also in magnetic fusion devices such as tokamaks, where a large external

https://doi.org/10.1017/S0962492922000010 Published online by Cambridge University Press

magnetic field needs to be applied in order to keep the particles on the desired tracks. The Vlasov equation for such problems takes the following form:

$$\varepsilon \partial_t f + v \cdot \nabla_x f + \left(E(t,x) + \frac{1}{\varepsilon} v \wedge B_{\text{ext}}(t,x) \right) \cdot \nabla_v f = 0.$$

Here, for simplicity, we set all physical constants to one and consider that $\varepsilon > 0$ is a small parameter related to the ratio between the reciprocal Larmor frequency and the advection time scale. We consider a constant magnetic field acting in the vertical z-direction, so it yields the two-dimensional Vlasov–Poisson system with an external strong force:

$$\begin{cases} \varepsilon \partial_t f + v \cdot \nabla_x f + \left(E(t,x) - \dfrac{b\, v^\perp}{\varepsilon} \right) \cdot \nabla_v f = 0, \\ E = -\nabla_x \phi, \quad -\Delta_x \phi = \rho^\varepsilon, \quad \rho = \displaystyle\int_{\mathbb{R}^2} f \, \mathrm{d}v, \end{cases}$$

where we use the notation $v^\perp = (-v_y, v_x)$.

Most of the numerical schemes for the Vlasov–Poisson system are based on particle methods, which consist in approximating the distribution function by a finite number of macro-particles. The trajectories of these particles are determined from the characteristic curves corresponding to the Vlasov equation

$$\begin{cases} \varepsilon \dfrac{\mathrm{d}X^\varepsilon}{\mathrm{d}t} = V^\varepsilon, \\ \varepsilon \dfrac{\mathrm{d}V^\varepsilon}{\mathrm{d}t} = -\dfrac{b\, V^{\varepsilon\perp}}{\varepsilon} + E^\varepsilon(t, X^\varepsilon), \end{cases} \tag{6.17}$$

where we use the conservation of f along the characteristic curves

$$f(t, X^\varepsilon(t), V^\varepsilon(t)) = f(t^0, X^0, V^0).$$

In the limit $\varepsilon \to 0$, we expect oscillations occurring on typical time scales $O(1/\varepsilon^2)$ to coexist with a slow dynamics evolving on a time scale $O(1)$. We now sketch how to identify a closed system describing the slow evolution to leading order. To begin with, note that from the second line of system (6.17) it follows that V^ε oscillates at order $1/\varepsilon^2$ and thus remains bounded and converges weakly to zero.[1] As we detail below, one may also combine both lines of the system to obtain

$$\frac{\mathrm{d}}{\mathrm{d}t} \left(X^\varepsilon - \varepsilon \frac{V^{\varepsilon\perp}}{b} \right) = -\frac{1}{b} E^\perp(t, X^\varepsilon).$$

This shows that X^ε evolves slowly but, as such, does not provide a closed asymptotic evolution in the limit $\varepsilon \to 0$ and the corresponding asymptotic model is an equation

[1] Although we do not want to be too precise here, let us mention that in the present discussion *weakly* and *strongly* refer to the weak-* and strong topologies of L^∞, and that the weak convergences that we encounter actually correspond to strong convergence in $W^{-1,\infty}$.

https://doi.org/10.1017/S0962492922000010 Published online by Cambridge University Press

for the density ρ:

$$\begin{cases} \partial_t \rho - \ b\, E^{\perp} \cdot \nabla_x \rho = 0, \\ E = -\nabla_x \phi, \quad -\Delta_x \phi = \rho. \end{cases}$$

When b is not constant, we also need to know what happens to expressions that are quadratic in V^ε, and this does not follow readily from the weak convergence of V^ε (Filbet and Rodrigues 2017).

One of the oldest of these strategies (Frénod, Salvarani and Sonnendrücker 2009) was directly inspired by theoretical results on two-scale convergence, and relies on the fact that at the limit $\varepsilon \to 0$ the τ-dependence ($\tau = t/\varepsilon$) may be explicitly filtered out. Its main drawback is probably that it computes only the leading-order term in the limit $\varepsilon \to 0$. In particular, it is only available when ε is very small.

This may be fixed by keeping, alongside the stiff term to which a two-scale treatment is applied, a non-stiff part that is smaller in the limit $\varepsilon \to 0$ but becomes important when ε is not small. Such a decomposition may be obtained by using a micro–macro approach as in Crouseilles, Frénod, Hirstoaga and Mouton (2013*a*) and some references therein. This allows us to switch from one regime to another without any treatment of the transition between them, but results in relatively heavy schemes.

Another approach with similar advantages, developed in Crouseilles, Lemou and Méhats (2013*b*) and Frénod, Hirstoaga, Lutz and Sonnendrücker (2015), consists in explicitly doubling time variables and seeking higher-dimensional partial differential equations and boundary conditions in variables (t, τ, x, v) that contain the original system at the ε-diagonal $(t, \tau) = (t, t/\varepsilon)$. While the corresponding methods are extremely good at capturing oscillations, their design requires a deep *a priori* understanding of the detailed structure of oscillations. Further, a class of semi-implicit schemes has been proposed (Filbet and Rodrigues 2016, 2017, Hairer, Lubich and Wang 2020, Ricketson and Chacón 2020) to capture accurately the non-stiff part of the evolution while allowing for coarse discretization parameters. It allows us to capture the asymptotic limit of the two-dimensional Vlasov–Poisson system with a *uniform* magnetic field (Filbet and Rodrigues 2016, Filbet, Rodrigues and Zakerzadeh 2021). In many respects these schemes are remarkably natural and simple, and can be adapted to toroidal geometry as in Filbet and Rodrigues (2020).

6.4. *Highly anisotropic diffusion*

In magnetized plasma simulations, the magnetic field confines the particles around the field lines, which leads to highly anisotropic problems. The model problem is given by

$$\begin{aligned} -\nabla \cdot (A \nabla u) &= f \quad \text{on } \Omega, \\ \mathbf{n} \cdot A \nabla u &= 0 \quad \text{on } \Gamma_N, \\ u &= g \quad \text{on } \Gamma_D, \end{aligned} \tag{6.18}$$

https://doi.org/10.1017/S0962492922000010 Published online by Cambridge University Press

where $\Omega \subset \mathbb{R}^2$ or $\Omega \subset \mathbb{R}^3$ is a bounded domain with boundary $\partial\Omega = \Gamma_D \cup \Gamma_N$ and outward normal $\mathbf{n}$. The direction of the anisotropy is given by a unit vector field $\mathbf{b}$ and the anisotropic diffusion matrix is then given by

$$A = \frac{1}{\varepsilon} A_{||} \mathbf{b} \otimes \mathbf{b} + (I - \mathbf{b} \otimes \mathbf{b}) A_{\perp} (I - \mathbf{b} \otimes \mathbf{b}), \tag{6.19}$$

where $A_{||} > 0$ is a scalar and $A_{\perp}$ is a symmetric positive definite matrix field, both of order one. The problem becomes highly anisotropic when $\epsilon \ll 1$. Let (ξ, η) be the aligned coordinate system; the formal limit of $\epsilon \to 0$ leads to

$$\begin{aligned} -\partial_\xi (A_{||} \partial_\xi u) &= f \quad \text{on } \Omega, \\ \partial_\xi u &= 0 \quad \text{on } \Gamma_N, \\ u &= g \quad \text{on } \Gamma_D. \end{aligned}$$

Any function that remains constant along the $\mathbf{b}$ field solves the above limit equation, which indicates that the limit model is not well-posed. Due to the existence of infinitely many solutions when $\epsilon \to 0$, standard numerical discretizations suffer from large condition numbers when ϵ is small and usually lose convergence when $\varepsilon \ll h$ (h is the mesh size).

To avoid the aforementioned problem, the common approach is to use magnetic field aligned coordinates, which may run into problems when there are magnetic reconnections or highly fluctuating field directions. The other approach is to design methods whose condition numbers do not scale with the anisotropy strength, and the convergence orders are uniform with respect to ε. The main idea is to construct new systems that remain well-posed when $\varepsilon \to 0$. In a series of papers (Degond, Deluzet and Negulescu 2010*a*, Degond, Lozinski, Narski and Negulescu 2012*c*, Degond *et al.* 2012*b*, Narski and Ottaviani 2014), Degond, Narski, Negulescu and co-workers have proposed various reformulations and discretization strategies based on macro–micro decomposition. Another idea is based on field line integration. By substituting (6.19) into (6.18), we get

$$\begin{aligned} -\partial_\xi \left(\frac{1}{\epsilon} A_{||} \partial_\xi u \right) - \nabla \cdot ((I - \mathbf{b} \otimes \mathbf{b}) A_{\perp} (I - \mathbf{b} \otimes \mathbf{b}) \nabla u) &= f \quad \text{on } \Omega, \\ \frac{1}{\epsilon} A_{||} \partial_\xi u + \mathbf{n} \cdot (I - \mathbf{b} \otimes \mathbf{b}) A_{\perp} (I - \mathbf{b} \otimes \mathbf{b}) \nabla u &= 0 \quad \text{on } \Gamma_N, \\ u &= g \quad \text{on } \Gamma_D, \end{aligned} \tag{6.20}$$

Taking the integration of the first equation in (6.20) along a field line and using the second equation of the Neumann boundary condition, we can get

$$\begin{aligned} &\int_0^L (\nabla \cdot ((I - \mathbf{b} \otimes \mathbf{b}) A_{\perp} (I - \mathbf{b} \otimes \mathbf{b}) \nabla u) + f) \mathrm{d}\xi \\ &\quad = (\mathbf{n} \cdot (I - \mathbf{b} \otimes \mathbf{b}) A_{\perp} (I - \mathbf{b} \otimes \mathbf{b}) \nabla u) \big|_0^L, \end{aligned} \tag{6.21}$$

https://doi.org/10.1017/S0962492922000010 Published online by Cambridge University Press

where 0 and L are the two end-points of a field line. Equation (6.21) is independent of ϵ and provides information on how to determine the limit solution. A similar idea can be extended to more complex models such as the closed field line (Wang, Ying and Tang 2018, Narski and Ottaviani 2014) and high-order differential operators arising in plasma physics (Yang, Deluzet and Narski 2019).

6.5. *Low Mach number limit of compressible flows*

Recently there has been increasing research activity in developing Mach number uniform fluid solvers. Consider the case of isentropic Navier–Stokes equations:

$$\partial_t \rho + \nabla_x \cdot (\rho u) = 0, \tag{6.22}$$

$$\partial_t (\rho u) + \nabla_x \cdot (\rho u \otimes u) + \frac{1}{\varepsilon^2} \nabla_x p = \frac{1}{\mathrm{Re}} \Delta u. \tag{6.23}$$

Here ρ is the density, u the velocity and $p = \rho^\gamma$ the pressure, ε being the Mach number and Re the Reynolds number. When $\varepsilon \ll 1$, we seek the asymptotic expansion $\rho = \rho^{(0)} + \varepsilon^2 \rho^{(2)} + \cdots$ and $p = p^{(0)} + \varepsilon^2 p^{(2)} + \cdots$, which then yields (Klainerman and Majda 1981)

$$\nabla \cdot u^{(0)} = 0, \tag{6.24}$$

$$\partial_t u^{(0)} + (u^{(0)} \cdot \nabla) u^{(0)} + \frac{1}{\rho^{(0)}} \nabla p^{(2)} = \frac{1}{\mathrm{Re}} \Delta u^{(0)}. \tag{6.25}$$

The characteristic speeds of system (6.22) are of $O(1/\varepsilon)$, corresponding to fast acoustic waves. One would think the low Mach number problem is mainly a numerically stiff problem and hence a small time step of $O(\varepsilon)$ is needed if an explicit method is used. In fact the constraints are more severe. For shock-capturing methods, the numerical viscosity – a necessary ingredient to suppress artificial oscillations – is inversely proportional to the speed of sound, and hence $\Delta x = O(\varepsilon)$ is needed to reduce numerical dissipation (Guillard and Viozat 1999, Dellacherie 2010). We then need $\Delta t = O(\varepsilon \Delta x)$ for numerical stability in an explicit scheme.

In developing a numerical scheme that is efficient for all Mach numbers, ideally we hope to use mesh size and time step *independent* of ε, namely the scheme is AP. This is usually achieved by splitting the flux into a rapidly moving part (corresponding to the acoustic waves) and a slowly moving part. An earlier attempt in this direction is a splitting by Klein (1995), which was further improved by Noelle *et al.* (2014). Here we mention an approach introduced in Haack, Jin and Liu (2012) (see a related approach in Degond and Tang 2011 and Cordier, Degond and Kumbaro 2012), which takes the following splitting:

$$\begin{cases} \partial_t \rho + \alpha \nabla \cdot (\rho u) + (1 - \alpha) \nabla \cdot (\rho u) = 0, \\ \partial_t (\rho u) + \nabla \cdot (\rho u \otimes u) + \nabla \left(\dfrac{p(\rho) - a(t)\rho}{\varepsilon^2} \right) + \dfrac{a(t)}{\varepsilon^2} \nabla \rho = \dfrac{1}{\mathrm{Re}} \Delta u, \end{cases} \tag{6.26}$$

https://doi.org/10.1017/S0962492922000010 Published online by Cambridge University Press

where α and $a(t)$ are artificial parameters. By choosing $a(t)$ well approximating $p'(\rho)$, the third term in the second equation is non-stiff and will thus be treated explicitly. An implicit treatment of the $\nabla\rho$ term is necessary, but thanks to its linearity this can be done easily, since only Poisson solvers are needed. The scheme is shock-capturing in the high Mach number regime, and reduces to a projection method – a popular method for incompressible Navier–Stokes equations (Temam 1969, Chorin 1968) when $\varepsilon \to 0$, so the AP property for $\varepsilon \to 0$ is justified.

This direction is still rapidly evolving. One can find other techniques such as a Lagrange projection scheme (Chalons, Girardin and Kokh 2016, Zakerzadeh 2017), a modification of the Roe solver (Miczek, Röpke and Edelmann 2015, Barsukow *et al.* 2017) with applications to astrophysics problems, careful choice of numerical viscosity (Dimarco, Loubère and Vignal 2017) and error estimates on AP schemes for low Mach number flows (Feireisl *et al.* 2018).

Acknowledgements

Many of the presented works were partially supported by the NSF Division of Mathematical Sciences Focused Research Group: 'Collaborative Research on Kinetic Description of Multiscale Phenomena: Modeling, Theory and Computation' (2008–2011), and the NSF Division of Mathematical Sciences Research Network 'KI-Net: Kinetic description of emerging challenges in multiscale problems of natural sciences' (2012–2019). The author thanks Eitan Tadmor for his tireless effort in making these projects successful, and for his long-time support.

The author also thanks Francis Filbet for contributing to Section 6.3, and Min Tang for contributing to Section 6.4.

References

A. Abdulle, W. E, B. Engquist and E. Vanden-Eijnden (2012), The heterogeneous multiscale method, in *Acta Numerica*, Vol. 21, Cambridge University Press, pp. 1–87.

R. Agarwal, K.-Y. Yun and R. Balakrishnan (1999), Beyond Navier Stokes–Burnett equations for flow simulations in continuum-transition regime, in *30th Fluid Dynamics Conference*. Available at doi:10.2514/6.1999-3580.

G. Albi and L. Pareschi (2013), Binary interaction algorithms for the simulation of flocking and swarming dynamics, *Multiscale Model. Simul.* **11**, 1–29.

G. Albi, N. Bellomo, L. Fermo, S.-Y. Ha, J. Kim, L. Pareschi, D. Poyato and J. Soler (2019), Vehicular traffic, crowds, and swarms: From kinetic theory and multiscale methods to applications and research perspectives, *Math. Models Methods Appl. Sci.* **29**, 1901–2005.

W. Bao and J. Shen (2005), A fourth-order time-splitting Laguerre–Hermite pseudospectral method for Bose–Einstein condensates, *SIAM J. Sci. Comput.* **26**, 2010–2028.

W. Bao, S. Jin and P. A. Markowich (2002), On time-splitting spectral approximations for the Schrödinger equation in the semiclassical regime, *J. Comput. Phys.* **175**, 487–524.

W. Bao, S. Jin and P. A. Markowich (2003), Numerical study of time-splitting spectral discretizations of nonlinear Schrödinger equations in the semiclassical regimes, *SIAM J. Sci. Comput.* **25**, 27–64.

C. Bardos, F. Golse and D. Levermore (1991), Fluid dynamic limits of kinetic equations, I: Formal derivations, *J. Statist. Phys.* **63**, 323–344.

C. Bardos, R. Santos and R. Sentis (1984), Diffusion approximation and computation of the critical size, *Trans. Amer. Math. Soc.* **284**, 617–649.

J. Barnes and P. Hut (1986), A hierarchical $O(N \log N)$ force-calculation algorithm, *Nature* **324**, 446–449.

W. Barsukow, P. V. F. Edelmann, C. Klingenberg, F. Miczek and F. K. Röpke (2017), A numerical scheme for the compressible low-Mach number regime of ideal fluid dynamics, *J. Sci. Comput.* **72**, 623–646.

M. Bennoune, M. Lemou and L. Mieussens (2008), Uniformly stable numerical schemes for the Boltzmann equation preserving the compressible Navier–Stokes asymptotics, *J. Comput. Phys.* **227**, 3781–3803.

P. R. Berman, J. E. M. Haverkort and J. P. Woerdman (1986), Collision kernels and transport coefficients, *Phys. Rev. A* **34**, 4647–4656.

G. A. Bird (1994), *Molecular Gas Dynamics and the Direct Simulation of Gas Flows*, Clarendon Press, Oxford.

R. H. Bisseling, R. Kosloff, R. B. Gerber, M. A. Ratner, L. Gibson and C. Cerjan (1987), Exact time-dependent quantum mechanical dissociation dynamics of I2He: Comparison of exact time-dependent quantum calculation with the quantum time-dependent self-consistent field (TDSCF) approximation, *J. Chem. Phys.* **87**, 2760–2765.

S. Boscarino, L. Pareschi and G. Russo (2013), Implicit–explicit Runge–Kutta schemes for hyperbolic systems and kinetic equations in the diffusion limit, *SIAM J. Sci. Comput.* **35**, A22–A51.

F. Bouchut, F. Golse and M. Pulvirenti (2000), *Kinetic Equations and Asymptotic Theory*, Vol. 4 of Series in Applied Mathematics (Paris), Elsevier.

F. Bouchut, H. Ounaissa and B. Perthame (2007), Upwinding of the source term at interfaces for Euler equations with high friction, *Comput. Math. Appl.* **53**, 361–375.

J. F. Bourgat, P. Le Tallec, B. Perthame and Y. Qiu (1994), Coupling Boltzmann and Euler equations without overlapping, *Contemp. Math.* **157**, 377–377.

Y. Brenier (2000), Convergence of the Vlasov–Poisson system to the incompressible Euler equations, *Commun. Partial Differ. Equations* **25**, 737–754.

R. E. Caflisch, S. Jin and G. Russo (1997), Uniformly accurate schemes for hyperbolic systems with relaxation, *SIAM J. Numer. Anal.* **34**, 246–281.

J. A. Carrillo, L. Pareschi and M. Zanella (2019), Particle based gPC methods for mean-field models of swarming with uncertainty, *Commun. Comput. Phys.* **25**, 508–531.

J. A. Carrillo, L. Wang, W. Xu and M. Yan (2021), Variational asymptotic preserving scheme for the Vlasov–Poisson–Fokker–Planck system, *Multiscale Model. Simul.* **19**, 478–505.

C. Cercignani (1988), *The Boltzmann Equation and its Applications*, Vol. 67 of Applied Mathematical Sciences, Springer.

C. Cercignani, I. M. Gamba and C. D. Levermore (1997), High field approximations to a Boltzmann–Poisson system and boundary conditions in a semiconductor, *Appl. Math. Lett.* **10**, 111–117.

C. Chalons, F. Coquel, E. Godlewski, P.-A. Raviart and N. Seguin (2010), Godunov-type schemes for hyperbolic systems with parameter-dependent source: The case of Euler system with friction, *Math. Models Methods Appl. Sci.* **20**, 2109–2166.

C. Chalons, M. Girardin and S. Kokh (2016), An all-regime Lagrange-projection like scheme for the gas dynamics equations on unstructured meshes, *Commun. Comput. Phys.* **20**, 188–233.

G.-Q. Chen, C. D. Levermore and T.-P. Liu (1994), Hyperbolic conservation laws with stiff relaxation terms and entropy, *Commun. Pure Appl. Math.* **47**, 787–830.

H. Chen, S. Chen and W. H. Matthaeus (1992), Recovery of the Navier–Stokes equations using a lattice-gas Boltzmann method, *Phys. Rev. A* **45**, R5339.

S. Chen and G. D. Doolen (1998), Lattice Boltzmann method for fluid flows, *Annu. Rev. Fluid Mech.* **30**, 329–364.

Z. Chen, L. Liu and L. Mu (2017), DG-IMEX stochastic Galerkin schemes for linear transport equation with random inputs and diffusive scalings, *J. Sci. Comput.* **73**, 566–592.

A. J. Chorin (1968), Numerical solution of the Navier–Stokes equations, *Math. Comp.* **22**, 745–762.

G. Ciccotti, D. Frenkel and I. R. McDonald (1987), *Simulation of Liquids and Solids: Molecular Dynamics and Monte Carlo Methods in Statistical Mechanics*, North-Holland.

F. Cordier, P. Degond and A. Kumbaro (2012), An asymptotic-preserving all-speed scheme for the Euler and Navier–Stokes equations, *J. Comput. Phys.* **231**, 5685–5704.

F. Coron and B. Perthame (1991), Numerical passage from kinetic to fluid equations, *SIAM J. Numer. Anal.* **28**, 26–42.

L. Corry (2004), *David Hilbert and the Axiomatization of Physics (1898–1918): From Grundlagen der Geometrie to Grundlagen der Physik*, Vol. 10 of Archimedes, Springer.

M. G. Crandall and P.-L. Lions (1983), Viscosity solutions of Hamilton–Jacobi equations, *Trans. Amer. Math. Soc.* **277**, 1–42.

P. Crispel, P. Degond and M.-H. Vignal (2005), An asymptotically stable discretization for the Euler–Poisson system in the quasi-neutral limit, *C. R. Math. Acad. Sci. Paris* **341**, 323–328.

P. Crispel, P. Degond and M.-H. Vignal (2007), An asymptotic preserving scheme for the two-fluid Euler–Poisson model in the quasineutral limit, *J. Comput. Phys.* **223**, 208–234.

N. Crouseilles and M. Lemou (2011), An asymptotic preserving scheme based on a micro–macro decomposition for collisional Vlasov equations: Diffusion and high-field scaling limits, *Kinet. Relat. Models* **4**, 441.

N. Crouseilles, E. Frénod, S. A. Hirstoaga and A. Mouton (2013*a*), Two-scale macro–micro decomposition of the Vlasov equation with a strong magnetic field, *Math. Models Methods Appl. Sci.* **23**, 1527–1559.

N. Crouseilles, M. Lemou and F. Méhats (2013*b*), Asymptotic preserving schemes for highly oscillatory Vlasov–Poisson equations, *J. Comput. Phys.* **248**, 287–308.

F. Cucker and S. Smale (2007), Emergent behavior in flocks, *IEEE Trans. Automat. Control* **52**, 852–862.

E. S. Daus, S. Jin and L. Liu (2019), Spectral convergence of the stochastic Galerkin approximation to the Boltzmann equation with multiple scales and large random perturbation in the collision kernel, *Kinet. Relat. Models* **12**, 909–922.

P. Degond and F. Deluzet (2017), Asymptotic-preserving methods and multiscale models for plasma physics, *J. Comput. Phys.* **336**, 429–457.

P. Degond and M. Tang (2011), All speed scheme for the low Mach number limit of the isentropic Euler equations, *Commun. Comput. Phys.* **10**, 1–31.

P. Degond, F. Deluzet and D. Doyen (2017), Asymptotic-preserving particle-in-cell methods for the Vlasov–Maxwell system in the quasi-neutral limit, *J. Comput. Phys.* **330**, 467–492.

P. Degond, F. Deluzet and C. Negulescu (2010*a*), An asymptotic preserving scheme for strongly anisotropic elliptic problems, *Multiscale Model. Simul.* **8**, 645–666.

P. Degond, F. Deluzet and D. Savelief (2012*a*), Numerical approximation of the Euler–Maxwell model in the quasineutral limit, *J. Comput. Phys.* **231**, 1917–1946.

P. Degond, F. Deluzet, A. Lozinski, J. Narski and C. Negulescu (2012*b*), Duality-based asymptotic-preserving method for highly anisotropic diffusion equations, *Commun. Math. Sci.* **10**, 1–31.

P. Degond, F. Deluzet, L. Navoret, A.-B. Sun and M.-H. Vignal (2010*b*), Asymptotic-preserving particle-in-cell method for the Vlasov–Poisson system near quasineutrality, *J. Comput. Phys.* **229**, 5630–5652.

P. Degond, S. Jin and L. Mieussens (2005), A smooth transition model between kinetic and hydrodynamic equations, *J. Comput. Phys.* **209**, 665–694.

P. Degond, A. Lozinski, J. Narski and C. Negulescu (2012*c*), An asymptotic-preserving method for highly anisotropic elliptic equations based on a micro–macro decomposition, *J. Comput. Phys.* **231**, 2724–2740.

S. Dellacherie (2010), Analysis of Godunov type schemes applied to the compressible Euler system at low Mach number, *J. Comput. Phys.* **229**, 978–1016.

J. Deng (2012), Asymptotic preserving schemes for semiconductor Boltzmann equation in the diffusive regime, *Numer. Math. Theory Methods Appl.* **5**, 278–296.

M. Deserno and C. Holm (1998), How to mesh up Ewald sums, II: An accurate error estimate for the particle–particle particle–mesh algorithm, *J. Chem. Phys.* **109**, 7694–7701.

S. Deshpande (1986), Kinetic theory based new upwind methods for inviscid compressible flows, in *24th Aerospace Sciences Meeting*. Available at doi:10.2514/6.1986-275.

G. Dimarco and L. Pareschi (2011), Exponential Runge–Kutta methods for stiff kinetic equations, *SIAM J. Numer. Anal.* **49**, 2057–2077.

G. Dimarco, R. Loubère and M.-H. Vignal (2017), Study of a new asymptotic preserving scheme for the Euler system in the low Mach number limit, *SIAM J. Sci. Comput.* **39**, A2099–A2128.

K. Drukker (1999), Basics of surface hopping in mixed quantum/classical simulations, *J. Comput. Phys.* **153**, 225–272.

Z. H. Duan and R. Krasny (2000), An Ewald summation based multipole method, *J. Chem. Phys.* **113**, 3492–3495.

M. Dumbser, C. Enaux and E. F. Toro (2008), Finite volume schemes of very high order of accuracy for stiff hyperbolic balance laws, *J. Comput. Phys.* **227**, 3971–4001.

R. Durstenfeld (1964), Algorithm 235: Random permutation, *Commun. Assoc. Comput. Mach.* **7**, 420.

W. E and B. Engquist (2003), The heterogeneous multiscale methods, *Commun. Math. Sci.* **1**, 87–132.

W. E and B. Yu (2018), The deep Ritz method: A deep learning-based numerical algorithm for solving variational problems, *Commun. Math. Statist.* **6**, 1–12.

D. Fang, S. Jin and C. Sparber (2018), An efficient time-splitting method for the Ehrenfest dynamics, *Multiscale Model. Simul.* **16**, 900–921.

E. Feireisl, M. Lukáčová-Medvidová, S. Nečasová, A. Novotný and B. She (2018), Asymptotic preserving error estimates for numerical solutions of compressible Navier–Stokes equations in the low Mach number regime, *Multiscale Model. Simul.* **16**, 150–183.

F. Filbet and S. Jin (2010), A class of asymptotic-preserving schemes for kinetic equations and related problems with stiff sources, *J. Comput. Phys.* **229**, 7625–7648.

F. Filbet and L. M. Rodrigues (2016), Asymptotically stable particle-in-cell methods for the Vlasov–Poisson system with a strong external magnetic field, *SIAM J. Numer. Anal.* **54**, 1120–1146.

F. Filbet and L. M. Rodrigues (2017), Asymptotically preserving particle-in-cell methods for inhomogeneous strongly magnetized plasmas, *SIAM J. Numer. Anal.* **55**, 2416–2443.

F. Filbet and L. M. Rodrigues (2020), Asymptotics of the three-dimensional Vlasov equation in the large magnetic field limit, *J. Éc. Polytech. Math.* **7**, 1009–1067.

F. Filbet, J. Hu and S. Jin (2012), A numerical scheme for the quantum Boltzmann equation with stiff collision terms, *ESAIM Math. Model. Numer. Anal.* **46**, 443–463.

F. Filbet, L. M. Rodrigues and H. Zakerzadeh (2021), Convergence analysis of asymptotic preserving schemes for strongly magnetized plasmas, *Numer. Math.* **149**, 549–593.

J. D. Foch (1973), On higher order hydrodynamic theories of shock structure, in *The Boltzmann Equation* (E. G. D. Cohen and W. Thirring, eds), Springer, pp. 123–140.

B. Fornberg (1996), *A Practical Guide to Pseudospectral Methods*, Vol. 1 of Cambridge Monographs on Applied and Computational Mathematics, Cambridge University Press.

D. Frenkel and B. Smit (2001), *Understanding Molecular Simulation: From Algorithms to Applications*, Vol. 1 of Computational Science Series, Elsevier.

E. Frénod, S. A. Hirstoaga, M. Lutz and E. Sonnendrücker (2015), Long time behaviour of an exponential integrator for a Vlasov–Poisson system with strong magnetic field, *Commun. Comput. Phys.* **18**, 263–296.

E. Frénod, F. Salvarani and E. Sonnendrücker (2009), Long time simulation of a beam in a periodic focusing channel via a two-scale PIC-method, *Math. Models Methods Appl. Sci.* **19**, 175–197.

I. Gallagher, L. Saint-Raymond and B. Texier (2013), *From Newton to Boltzmann: Hard Spheres and Short-Range Potentials*, Zurich Lectures in Advanced Mathematics, European Mathematical Society (EMS), Zürich.

I. M. Gamba, S. Jin and L. Liu (2019), Micro–macro decomposition based asymptotic-preserving numerical schemes and numerical moments conservation for collisional nonlinear kinetic equations, *J. Comput. Phys.* **382**, 264–290.

A. Georges, G. Kotliar, W. Krauth and M. J. Rozenberg (1996), Dynamical mean-field theory of strongly correlated fermion systems and the limit of infinite dimensions, *Rev. Modern Phys.* **68**, 13.

P. Gérard, P. A. Markowich, N. J. Mauser and F. Poupaud (1997), Homogenization limits and Wigner transforms, *Commun. Pure Appl. Math.* **50**, 323–379.

F. Golse (2003), The mean-field limit for the dynamics of large particle systems, *Journées Équations aux Dérivées Partielles* **9**, 1–47.

F. Golse and T. Paul (2017), The Schrödinger equation in the mean-field and semiclassical regime, *Arch. Ration. Mech. Anal.* **223**, 57–94.

F. Golse, S. Jin and C. D. Levermore (1999), The convergence of numerical transfer schemes in diffusive regimes, I: Discrete-ordinate method, *SIAM J. Numer. Anal.* **36**, 1333–1369.

F. Golse, S. Jin and T. Paul (2021), On the convergence of time splitting methods for quantum dynamics in the semiclassical regime, *Found. Comput. Math.* **21**, 613–647.
L. Gosse and G. Toscani (2002), An asymptotic-preserving well-balanced scheme for the hyperbolic heat equations, *C. R. Math. Acad. Sci. Paris* **334**, 337–342.
T. Goudon, J. Nieto, F. Poupaud and J. Soler (2005), Multidimensional high-field limit of the electrostatic Vlasov–Poisson–Fokker–Planck system, *J. Differ. Equations* **213**, 418–442.
L. Greengard and V. Rokhlin (1987), A fast algorithm for particle simulations, *J. Comput. Phys.* **73**, 325–348.
H. Guillard and C. Viozat (1999), On the behaviour of upwind schemes in the low Mach number limit, *Comput. Fluids* **28**, 63–86.
M. D. Gunzburger, C. G. Webster and G. Zhang (2014), Stochastic finite element methods for partial differential equations with random input data, in *Acta Numerica*, Vol. 23, Cambridge University Press, pp. 521–650.
J. Haack, S. Jin and J.-G. Liu (2012), An all-speed asymptotic-preserving method for the isentropic Euler and Navier–Stokes equations, *Commun. Comput. Phys.* **12**, 955–980.
E. Hairer, C. Lubich and B. Wang (2020), A filtered Boris algorithm for charged-particle dynamics in a strong magnetic field, *Numer. Math.* **144**, 787–809.
X. He and L.-S. Luo (1997), Theory of the lattice Boltzmann method: From the Boltzmann equation to the lattice Boltzmann equation, *Phys. Rev. E* **56**, 6811.
E. J. Heller (2006), Guided Gaussian wave packets, *Acc. Chem. Res.* **39**, 127–134.
B. Hetenyi, K. Bernacki and B. J. Berne (2002), Multiple 'time step' Monte Carlo, *J. Chem. Phys.* **117**, 8203–8207.
N. R. Hill (1990), Gaussian beam migration, *Geophysics* **55**, 1416–1428.
J. Hu and S. Jin (2016), A stochastic Galerkin method for the Boltzmann equation with uncertainty, *J. Comput. Phys.* **315**, 150–168.
J. Hu and R. Shu (2019), A second-order asymptotic-preserving and positivity-preserving exponential Runge–Kutta method for a class of stiff kinetic equations, *Multiscale Model. Simul.* **17**, 1123–1146.
J. Hu and R. Shu (2021), On the uniform accuracy of implicit–explicit backward differentiation formulas (IMEX-BDF) for stiff hyperbolic relaxation systems and kinetic equations, *Math. Comp.* **90** , 641–670.
J. Hu, S. Jin and Q. Li (2017), Asymptotic-preserving schemes for multiscale hyperbolic and kinetic equations, in *Handbook of Numerical Analysis*, Vol. XVIII, Elsevier, pp. 103–129.
J. Hu, S. Jin and B. Yan (2012), A numerical scheme for the quantum Fokker–Planck–Landau equation efficient in the fluid regime, *Commun. Comput. Phys.* **12**, 1541–1561.
P.-E. Jabin and Z. Wang (2017), Mean field limit for stochastic particle systems, in *Active Particles*, Vol. 1, *Advances in Theory, Models, and Applications* (N. Bellomo *et al.*, eds), Springer, pp. 379–402.
S. Jin (1995), Runge–Kutta methods for hyperbolic conservation laws with stiff relaxation terms, *J. Comput. Phys.* **122**, 51–67.
S. Jin (1999), Efficient asymptotic-preserving (AP) schemes for some multiscale kinetic equations, *SIAM J. Sci. Comput.* **21**, 441–454.
S. Jin (2010), Asymptotic preserving (AP) schemes for multiscale kinetic and hyperbolic equations: A review, in *Lecture Notes for Summer School on Methods and Models of Kinetic Theory (M&MKT)*, pp. 177–216.

S. Jin and C. D. Levermore (1996), Numerical schemes for hyperbolic conservation laws with stiff relaxation terms, *J. Comput. Phys.* **126**, 449–467.
S. Jin and L. Li (2022*a*), On the mean field limit of the random batch method for interacting particle systems, *Sci. China Math.* **65**, 169–202.
S. Jin and L. Li (2022*b*), Random batch methods for classical and quantum interacting particle systems and statistical samplings. To appear in *Active Particles II* (N. Bellomo *et al.*, eds).
S. Jin and Q. Li (2013), A BGK-penalization-based asymptotic-preserving scheme for the multispecies Boltzmann equation, *Numer. Methods Partial Differ. Equations* **29**, 1056–1080.
S. Jin and X. Li (2020), Random batch algorithms for quantum Monte Carlo simulations, *Commun. Comput. Phys.* **28**, 1907–1936.
S. Jin and L. Liu (2017), An asymptotic-preserving stochastic Galerkin method for the semiconductor Boltzmann equation with random inputs and diffusive scalings, *Multiscale Model. Simul.* **15**, 157–183.
S. Jin and L. Pareschi (2001), Asymptotic-preserving (AP) schemes for multiscale kinetic equations: A unified approach, in *Hyperbolic Problems: Theory, Numerics, Applications* (H. Freistühler and G. Warnecke, eds), Vol. 141 of International Series of Numerical Mathematics, Birkhäuser, pp. 573–582.
S. Jin and R. Shu (2017), A stochastic asymptotic-preserving scheme for a kinetic-fluid model for disperse two-phase flows with uncertainty, *J. Comput. Phys.* **335**, 905–924.
S. Jin and L. Wang (2011), An asymptotic preserving scheme for the Vlasov–Poisson–Fokker–Planck system in the high field regime, *Acta Math. Sci.* **31**, 2219–2232.
S. Jin and L. Wang (2013), Asymptotic-preserving numerical schemes for the semiconductor Boltzmann equation efficient in the high field regime, *SIAM J. Sci. Comput.* **35**, B799–B819.
S. Jin and Z. Xin (1995), The relaxation schemes for systems of conservation laws in arbitrary space dimensions, *Commun. Pure Appl. Math.* **48**, 235–276.
S. Jin and B. Yan (2011), A class of asymptotic-preserving schemes for the Fokker–Planck–Landau equation, *J. Comput. Phys.* **230**, 6420–6437.
S. Jin and Z. Zhou (2013), A semi-Lagrangian time splitting method for the Schrödinger equation with vector potentials, *Commun. Inform. Syst.* **13**, 247–289.
S. Jin and Y. Zhu (2018), Hypocoercivity and uniform regularity for the Vlasov–Poisson–Fokker–Planck system with uncertainty and multiple scales, *SIAM J. Math. Anal.* **50**, 1790–1816.
S. Jin, C. D. Levermore and D. W. McLaughlin (1999), The semiclassical limit of the defocusing NLS hierarchy, *Commun. Pure Appl. Math.* **52**, 613–654.
S. Jin, L. Li and J.-G. Liu (2020*a*), Random batch methods (RBM) for interacting particle systems, *J. Comput. Phys.* **400**, 108877.
S. Jin, L. Li and Y. Sun (2020*b*), On the Random Batch Method for second order interacting particle systems. Available at arXiv:2011.10778 (to appear in *Multiscale Model. Simul.*).
S. Jin, L. Li, Z. Xu and Y. Zhao (2021*a*), A random batch Ewald method for particle systems with Coulomb interactions, *SIAM J. Sci. Comput.* **43**, B937–B960.
S. Jin, J.-G. Liu and Z. Ma (2017*a*), Uniform spectral convergence of the stochastic Galerkin method for the linear transport equations with random inputs in diffusive regime and a micro–macro decomposition-based asymptotic-preserving method, *Res. Math. Sci.* **4**, 1–25.

S. Jin, Z. Ma and K. Wu (2021*b*), Asymptotic-preserving neural networks for multiscale time-dependent linear transport equations. Available at arXiv:2111.02541.
S. Jin, P. Markowich and C. Sparber (2011), Mathematical and computational methods for semiclassical Schrödinger equations, in *Acta Numerica*, Vol. 20, Cambridge University Press, pp. 121–209.
S. Jin, L. Pareschi and G. Toscani (2000), Uniformly accurate diffusive relaxation schemes for multiscale transport equations, *SIAM J. Numer. Anal.* **38**, 913–936.
S. Jin, C. Sparber and Z. Zhou (2017*b*), On the classical limit of a time-dependent self-consistent field system: Analysis and computation, *Kinet. Relat. Models* **10**, 263–298.
S. Jin, H. Wu and X. Yang (2008), Gaussian beam methods for the Schrödinger equation in the semi-classical regime: Lagrangian and Eulerian formulations, *Commun. Math. Sci.* **6**, 995–1020.
S. Jin, D. Xiu and X. Zhu (2015), Asymptotic-preserving methods for hyperbolic and transport equations with random inputs and diffusive scalings, *J. Comput. Phys.* **289**, 35–52.
I. G. Kevrekidis, C. W. Gear and G. Hummer (2004), Equation-free: The computer-aided analysis of complex multiscale systems, *AIChE J.* **50**, 1346–1355.
S. Klainerman and A. Majda (1981), Singular limits of quasilinear hyperbolic systems with large parameters and the incompressible limit of compressible fluids, *Commun. Pure Appl. Math.* **34**, 481–524.
A. Klar (1998), An asymptotic-induced scheme for nonstationary transport equations in the diffusive limit, *SIAM J. Numer. Anal.* **35**, 1073–1094.
A. Klar and C. Schmeiser (2001), Numerical passage from radiative heat transfer to nonlinear diffusion models, *Math. Models Methods Appl. Sci.* **11**, 749–767.
A. Klar, H. Neunzert and J. Struckmeier (2000), Transition from kinetic theory to macroscopic fluid equations: A problem for domain decomposition and a source for new algorithms, *Transp. Theory Statist. Phys.* **29**, 93–106.
R. Klein (1995), Semi-implicit extension of a Godunov-type scheme based on low Mach number asymptotics, I: One-dimensional flow, *J. Comput. Phys.* **121**, 213–237.
K. Koura and H. Matsumoto (1991), Variable soft sphere molecular model for inverse-power-law or Lennard-Jones potential, *Phys. Fluids A* **3**, 2459–2465.
K. Küpper, M. Frank and S. Jin (2016), An asymptotic preserving two-dimensional staggered grid method for multiscale transport equations, *SIAM J. Numer. Anal.* **54**, 440–461.
O. E. Lanford, III (1975), Time evolution of large classical systems, in *Dynamical Systems, Theory and Applications (Rencontres, Battelle Res. Inst., Seattle, WA, 1974)*, Vol. 38 of Lecture Notes in Physics, Springer, pp. 1–111.
E. W. Larsen and J. E. Morel (1989), Asymptotic solutions of numerical transport problems in optically thick, diffusive regimes, II, *J. Comput. Phys.* **83**, 212–236.
E. W. Larsen, J. E. Morel and W. F. Miller Jr (1987), Asymptotic solutions of numerical transport problems in optically thick, diffusive regimes, *J. Comput. Phys.* **69**, 283–324.
C. Lasser and C. Lubich (2020), Computing quantum dynamics in the semiclassical regime, in *Acta Numerica*, Vol. 29, Cambridge University Press, pp. 229–401.
P. D. Lax and D. Levermore (1983), The small dispersion limit of the Korteweg–de Vries equation, I, *Commun. Pure Appl. Math.* **36**, 253–290.
T. Lelièvre and G. Stoltz (2016), Partial differential equations and stochastic methods in molecular dynamics, in *Acta Numerica*, Vol. 25, Cambridge University Press, pp. 681–880.

M. Lemou and L. Mieussens (2008), A new asymptotic preserving scheme based on micro–macro formulation for linear kinetic equations in the diffusion limit, *SIAM J. Sci. Comput.* **31**, 334–368.
S. Leung and J. Qian (2009), Eulerian Gaussian beams for Schrödinger equations in the semi-classical regime, *J. Comput. Phys.* **228**, 2951–2977.
E. E. Lewis and W. F. Miller (1984), *Computational Methods of Neutron Transport*, Wiley.
L. Li and C. Yang (2021), Asymptotic preserving scheme for anisotropic elliptic equations with deep neural network. Available at arXiv:2104.05337.
L. Li, Y. Li, J.-G. Liu, Z. Liu and J. Lu (2020*a*), A stochastic version of Stein variational gradient descent for efficient sampling, *Commun. Appl. Math. Comput. Sci.* **15**, 37–63.
L. Li, Z. Xu and Y. Zhao (2020*b*), A random-batch Monte Carlo method for many-body systems with singular kernels, *SIAM J. Sci. Comput.* **42**, A1486–A1509.
Q. Li and L. Pareschi (2014), Exponential Runge–Kutta for the inhomogeneous Boltzmann equations with high order of accuracy, *J. Comput. Phys.* **259**, 402–420.
Q. Li and L. Wang (2017), Uniform regularity for linear kinetic equations with random input based on hypocoercivity, *SIAM/ASA J. Uncertainty Quantif.* **5**, 1193–1219.
Z. Li, N. B. Kovachki, K. Azizzadenesheli, B. Liu, K. Bhattacharya, A. Stuart and A. Anandkumar (2021), Fourier neural operator for parametric partial differential equations, in *9th International Conference on Learning Representations (ICLR 2021)*. Available at open-review.net.
J. Liang, P. Tan, Y. Zhao, L. Li, S. Jin, L. Hong and Z. Xu (2022), Super-scalable molecular dynamics algorithm, *J. Chem. Phys.* **156**, 014114.
P.-L. Lions and T. Paul (1993), Sur les mesures de Wigner, *Rev. Mat. Iberoamer.* **9**, 553–618.
C. Liu, K. Xu, Q. Sun and Q. Cai (2016), A unified gas-kinetic scheme for continuum and rarefied flows, IV: Full Boltzmann and model equations, *J. Comput. Phys.* **314**, 305–340.
J.-G. Liu and L. Mieussens (2010), Analysis of an asymptotic preserving scheme for linear kinetic equations in the diffusion limit, *SIAM J. Numer. Anal.* **48**, 1474–1491.
L. Liu and S. Jin (2018), Hypocoercivity based sensitivity analysis and spectral convergence of the stochastic Galerkin approximation to collisional kinetic equations with multiple scales and random inputs, *Multiscale Model. Simul.* **16**, 1085–1114.
T.-P. Liu and S.-H. Yu (2004), Boltzmann equation: Micro–macro decompositions and positivity of shock profiles, *Commun. Math. Phys.* **246**, 133–179.
M. Loève (1977), *Probability Theory*, fourth edition, Springer.
L. Lu, P. Jin, G. Pang, Z. Zhang and G. E. Karniadakis (2021*a*), Learning nonlinear operators via DeepONet based on the universal approximation theorem of operators, *Nature Mach. Intell.* **3**, 218–229.
Y. Lu, L. Wang and W. Xu (2021*b*), Solving multiscale steady radiative transfer equation using neural networks with uniform stability. Available at arXiv:2110.07037.
B. A. Luty, M. E. Davis, I. G. Tironi and W. F. Van Gunsteren (1994), A comparison of particle–particle, particle–mesh and Ewald methods for calculating electrostatic interactions in periodic molecular systems, *Mol. Simul.* **14**, 11–20.
N. Makri and W. H. Miller (1987), Time-dependent self-consistent field (TDSCF) approximation for a reaction coordinate coupled to a harmonic bath: Single and multiple configuration treatments, *J. Chem. Phys.* **87**, 5781–5787.
P. A. Markowich, P. Pietra and C. Pohl (1999), Numerical approximation of quadratic observables of Schrödinger-type equations in the semi-classical limit, *Numer. Math.* **81**, 595–630.

P. A. Markowich, C. A. Ringhofer and C. Schmeiser (1990), *Semiconductor Equations*, Springer.

M. G. Martin, B. Chen and J. I. Siepmann (1998), A novel Monte Carlo algorithm for polarizable force fields: Application to a fluctuating charge model for water, *J. Chem. Phys.* **108**, 3383–3385.

D. Marx and J. Hutter (2009), *Ab Initio Molecular Dynamics: Basic Theory and Advanced Methods*, Cambridge University Press.

H. P. McKean (1967), Propagation of chaos for a class of non-linear parabolic equations, in *Stochastic Differential Equations (Lecture Series in Differential Equations, Session 7, Catholic Univ., 1967)*, pp. 41–57.

F. Miczek, F. K. Röpke and P. V. Edelmann (2015), New numerical solver for flows at various Mach numbers, *Astronom. Astrophys.* **576**, A50.

S. Motsch and E. Tadmor (2014), Heterophilious dynamics enhances consensus, *SIAM Rev.* **56**, 577–621.

J. Narski and M. Ottaviani (2014), Asymptotic preserving scheme for strongly anisotropic parabolic equations for arbitrary anisotropy direction, *Comput. Phys. Commun.* **185**, 3189–3203.

J. Nieto, F. Poupaud and J. Soler (2001), High-field limit for the Vlasov–Poisson–Fokker–Planck system, *Arch. Ration. Mech. Anal.* **158**, 29–59.

S. Noelle, G. Bispen, K. R. Arun, M. Lukáčová-Medvidová and C.-D. Munz (2014), A weakly asymptotic preserving low Mach number scheme for the Euler equations of gas dynamics, *SIAM J. Sci. Comput.* **36**, B989–B1024.

L. Pareschi and G. Russo (2005), Implicit–explicit Runge–Kutta schemes and applications to hyperbolic systems with relaxation, *J. Sci. Comput.* **25**, 129–155.

B. Perthame (1990), Boltzmann type schemes for gas dynamics and the entropy property, *SIAM J. Numer. Anal.* **27**, 1405–1421.

K. H. Prendergast and K. Xu (1993), Numerical hydrodynamics from gas-kinetic theory, *J. Comput. Phys.* **109**, 53–66.

Y.-H. Qian, D. d'Humières and P. Lallemand (1992), Lattice BGK models for Navier–Stokes equation, *EPL (Europhysics Letters)* **17**, 479.

M. Raissi, P. Perdikaris and G. E. Karniadakis (2019), Physics-informed neural networks: A deep learning framework for solving forward and inverse problems involving nonlinear partial differential equations, *J. Comput. Phys.* **378**, 686–707.

L. F. Ricketson and L. Chacón (2020), An energy-conserving and asymptotic-preserving charged-particle orbit implicit time integrator for arbitrary electromagnetic fields, *J. Comput. Phys.* **418**, 109639.

T. Rivell (2006), Notes on earth atmospheric entry for Mars sample return missions. Technical report TP-2006-213486, NASA Ames Research Center, Moffett Field, CA, USA.

V. Rokhlin (1985), Rapid solution of integral equations of classical potential theory, *J. Comput. Phys.* **60**, 187–207.

G. Russo and P. Smereka (2013), The Gaussian wave packet transform: Efficient computation of the semi-classical limit of the Schrödinger equation, 1: Formulation and the one dimensional case, *J. Comput. Phys.* **233**, 192–209.

C. Schütte and F. A. Bornemann (1999), On the singular limit of the quantum-classical molecular dynamics model, *SIAM J. Appl. Math.* **59**, 1208–1224.

C. Sparber, P. Markowich and N. Mauser (2003), Wigner functions versus WKB-methods in multivalued geometrical optics, *Asymptot. Anal.* **33**, 153–187.
H. E. Stanley (1971), *Phase Transitions and Critical Phenomena*, Clarendon Press, Oxford.
W. Sun, S. Jiang and K. Xu (2015), An asymptotic preserving unified gas kinetic scheme for gray radiative transfer equations, *J. Comput. Phys.* **285**, 265–279.
A. Szepessy (2011), Langevin molecular dynamics derived from Ehrenfest dynamics, *Math. Models Methods Appl. Sci.* **21**, 2289–2334.
D. C. Tan, T. Zhang, T. Chang and Y. X. Zheng (1994), Delta-shock waves as limits of vanishing viscosity for hyperbolic systems of conservation laws, *J. Differ. Equations* **112**, 1–32.
R. Temam (1969), Sur l'approximation de la solution des équations de Navier–Stokes par la méthode des pas fractionnaires (ii), *Arch. Ration. Mech. Anal.* **33**, 377–385.
J. C. Tully (1998), Mixed quantum–classical dynamics, *Faraday Discussions* **110**, 407–419.
T. Vicsek, A. Czirók, E. Ben-Jacob, I. Cohen and O. Shochet (1995), Novel type of phase transition in a system of self-driven particles, *Phys. Rev. Lett.* **75**, 1226.
C. Villani (2009), *Hypocoercivity*, Vol. 202 of Memoirs of the American Mathematical Society, American Mathematical Society.
Y. Wang, W. Ying and M. Tang (2018), Uniformly convergent scheme for strongly anisotropic diffusion equations with closed field lines, *SIAM J. Sci. Comput.* **40**, B1253–B1276.
E. P. Wigner (1932), On the quantum correction for thermodynamic equilibrium, *Phys. Rev.* **40**, 749–759.
D. Xiu (2010), *Numerical Methods for Stochastic Computations*, Princeton University Press.
D. Xiu and G. E. Karniadakis (2002), The Wiener–Askey polynomial chaos for stochastic differential equations, *SIAM J. Sci. Comput.* **24**, 619–644.
B. Yan and S. Jin (2013), A successive penalty-based asymptotic-preserving scheme for kinetic equations, *SIAM J. Sci. Comput.* **35**, A150–A172.
C. Yang, F. Deluzet and J. Narski (2019), On the numerical resolution of anisotropic equations with high order differential operators arising in plasma physics, *J. Comput. Phys.* **386**, 502–523.
L. Ying, G. Biros and D. Zorin (2004), A kernel-independent adaptive fast multipole algorithm in two and three dimensions, *J. Comput. Phys.* **196**, 591–626.
H. Zakerzadeh (2017), On the Mach-uniformity of the Lagrange-projection scheme, *ESAIM Math. Model. Numer. Anal.* **51**, 1343–1366.
Y. Zhu and S. Jin (2017), The Vlasov–Poisson–Fokker–Planck system with uncertainty and a one-dimensional asymptotic preserving method, *Multiscale Model. Simul.* **15**, 1502–1529.